Computational and wind tunnel studies of shelterbelts
for reduction of wind flow and wind-induced loads on low-rise buildings

by

Sarah Ruth Schmidt

A thesis submitted to the graduate faculty

in partial fulfillment of the requirements for the degree of

MASTER OF SCIENCE

Co-majors: Meteorology;

Engineering Mechanics

Program of Study Committee:
Eugene S. Takle, Co-major Professor
Partha P. Sarkar, Co-major Professor
Ron Nelson

Iowa State University

Ames, Iowa

2008

TABLE OF CONTENTS

LIST OF TABLES

LIST OF FIGURES

ACKNOWLEDGEMENTS

I would like to take this opportunity to express my thanks to those who helped me with various aspects of conducting research and the writing of this thesis. First my major professors, Dr. Eugene S. Takle and Dr. Partha P. Sarkar, for their guidance, patience and support throughout this research and the writing of this thesis. Their insights and words of encouragement often inspired me and renewed my hopes for completing my graduate education. I would also like to thank my other committee member for his efforts and contributions to this work: Dr. Ron Nelson. I would additionally like to thank Dan Rajewski for his help with the shelterbelt model and his patience with me trying to learn how to use it, Wei Zhang and Kevin Sehn for their help in teaching me how to do the experimental testing, and Bill Rickard who built everything so that I could actually do the experiments.

ABSTRACT

Numerical and experimental tests were done to determine the optimum design parameters of a shelterbelt for wind damage mitigation to structures behind the shelterbelt. The Wang and Takle shelterbelt numerical model was used to study the shelterbelt's cross-sectional shape, height, spacing/line tightness, density/density distribution, line width, number of lines, and wind speed parameters. The numerical model was also used to study the effectiveness of more realistically shaped shelterbelt tree lines, rather than using the traditional blocks to represent each line of trees in the shelterbelt. Finally, experiments were conducted in a wind tunnel to test the effects of wind-induced load reduction with the implementation of a shelterbelt screen, studying forces rather than flow fields. The parametric numerical studies determined the most effective shelterbelt configurations that consisted of multiple lines of tall, equal height, thin lines, with fairly dense elements, that are closely spaced. The tree parameterization studies found that tree arrangements of multiple lines of dense trees that included low vegetation provided the most protection from winds and turbulence. Having taller trees to the windward rather than the leeward side proved to give more shelter. The wind tunnel tests found that the presence of a fence greatly decreases the shear and roof uplift loads on a house which are reduced by a factor of 2 to 6 times. The fences were found to reduce the shear forces much more than the uplift forces. In mid-range of the sheltered space, the fence with 30.3% porosity were found to be much more effective than those of other porosities. The fences were found to provide shelter over a long distance, up to approximately 29H, where H is the height of the fences, while the range of sheltered space over which the total forces were most reduced was between 2H and 8H. The addition of a deflector atop of the fences provided increased effectiveness of sheltering.

CHAPTER 1. INTRODUCTION AND BACKGROUND

Shelterbelts, also called windbreaks, are used to protect structures, plants, soil and people from the damaging effects of wind. The ability of the shelterbelt to provide the maximum shelter leeward of the shelterbelt is dependent on the physical parameters of the shelterbelt.

1.1 Objective and Motivation

The objective of my research was to study different parameters of shelterbelts through a numerical model and a wind tunnel model that would influence their ability to mitigate the wind-induced damage to low-rise buildings in high winds. While various tree configurations were selected for the numerical model, various screens representing trees and/or fences were tested in the wind tunnel. The assumption of this study was that a porous shelter that is at least as tall as the structure it protects would provide mitigation of wind loads within distances equivalent to five shelter-heights.

This work was motivated by the need to reduced wind induced loads on structures without modifying the structures themselves. A common way to achieve this is through the implementation of barriers such a shelterbelts. However, there is a desire to optimize the shelterbelt's effectiveness, which is what these studies undertake.

1.2 Literature Review

A numerical model can be more effectively used to systematically study the effect of parameters of a shelterbelt on the amount of shelter provided depending on different configurations compared to field studies where there is so much variability in trees and plants that these cannot be used for this purpose. Wind tunnel studies can also be used to systematically do a

parametric study on the effectiveness of shelter designs by making quantitative measurement of wind-induced forces on buildings that are influenced by the presence of an upwind barrier. The current study uses a numerical model developed by Hao Wang that calculates the flow field around and through a shelterbelt in the atmospheric boundary layer. This numerical model can be also used to predict the flow through porous barriers or fences in an atmospheric boundary layer wind tunnel as used here where forces on buildings located behind the fences were measured.

A numerical model study by Wang and Takle (1997) concluded that there is minimal effect on the sheltered distance for wind speed with the different configurations tested. However prior to Wang and Takle, Woodruff and Zingg (1953) tested shelterbelt configurations in a wind tunnel and found there is dependency of the sheltered distance on shelter shape and width. Other prior investigators suggested that the effect of the shape on the shelter efficiency is important also (Caborn, 1957, 1965; Jensen, 1974; Gandemer, 1979). As far back as 1934, Finney found experimentally that the sheltered distance is directly proportional to height of the shelter, and, theoretically, could be found using a coefficient multiplier that can be empirically determined based on porosity of the shelter. Heisler and Dewalle (1988) also found this type of directly proportional relationship. The space between the rows of the shelterbelt not only affects the overall cross-sectional shape, it also creates momentum sinks between the lines in the shelterbelt. Another way to think of spacing is the tightness of the rows of trees within a certain distance, which is accomplished by having more or fewer trees in the same width. The width affects the resistance presented to the wind flow passing through the barrier because a thinner line of trees provides fewer total obstacles (leaves, branches, limbs, etc.) than a wider line of trees. The largest determining parameter of shelter efficiency is its porosity (Hagen and Skidmore, 1971; Wilson, 1987). Heisler and Dewalle (1988) suggested that there could be a minimum porosity beyond which trees generate more turbulence and hence the sheltered distance is reduced. While the study by Wang and Takle (1997) used uniform porosity shelters, Woodruff and Zingg (1953) used many different trees and shrubs to have a varied density throughout their shelterbelt. Woodruff and Zingg (1953) discussed

the advantages and disadvantages of different number of rows of trees in a shelterbelt ranging from land usage to self-preservation of the trees within the shelterbelt itself. Considering just wind speed reduction, they found that more rows achieve better sheltered distance. However they found no significant difference between 5, 7, and 10 row shelterbelt design. Thus, if land use is an issue they suggested using the 5 row design. Zhang et al. (1995) reported that many studies have found that the sheltered distance is completely independent of initial wind speed while others found a small reduction in near surface sheltered area with increasing wind speed.

Previous experimental and field work has been done with shelterbelts to determine the changes to the flow field caused by the presence of a shelterbelt. Some of this work has been done by Boldes et al. (2001), Dierickx et al. (2001), Cornelis and Gabriels (2005), and Frank and Ruck (2005) in which they studied the numbers of rows of screens and porosities to determine the combination(s) that gives the maximum benefit. However, no work has been done to directly measure the effect of a shelterbelt on reduction of wind-induced loads on structures. Frank and Ruck (2005) discuss some of these effects by assuming the relation of the force as proportional to the square of the wind speed. While this is a valid assumption, the actual force is an integration of the effects of variability in wind speeds across the face of the structure and flow around it. Therefore, directly measured forces on structures are more truly indicative of the protection given to a structure.

As with the numerical studies, the previous experimental studies have also concluded that the porosity of shelters has the largest influence on the wind field (van Eimern et al., 1964; Hagen, 1971). Porosities between 20% and 50% have been found to be the most effective (N*ö*kkentved 1938; N*ä*geli, 1946; Jensen, 1954; Blenk and Trienes, 1956; Tani, 1958; Schultz and Kelly, 1960; Marshall, 1967; Skidmore and Hagen, 1970a, b; Raine and Stevenson, 1977; Tillie, 1992). Cornelis and Gabriels (2005) found a smaller sub-range of 20% to 35% to be the most effective. Also, these studies concluded that shelter is directly proportional to its height (Frank and Ruck, 2005). Multiple rows in a shelter were also found to be favorable (Boldes, et al., 2001; Cornelis and Gabriels, 2005; Frank and Ruck, 2005).

1.3 Wang and Takle Shelterbelt Model

The numerical model used is described in Wang and Takle (1995). It was originally developed to study the aerodynamics of shelterbelts and their dependence on shelterbelt porosity. The model uses simplified two-dimensional atmospheric equations of motion and continuity equation. The second-order turbulent closure scheme κ-E-l is used following Yamada (1982). The model domain is quasi three dimensional [z is vertical and x is horizontal and perpendicular to the shelterbelt and y is along its length] in which the wind flow is along the x direction and although the shelterbelt is infinitely long in the y-direction the model allows fully three-dimensional simulation of flow (Wang et al. 2001). The incident wind was set to approach the shelter orthogonal to the axis of the shelterbelt line. Convergence is determined by the difference of mean kinetic energy between time steps at each grid point. When this difference is less than the set value of the convergence criteria that criteria value is assigned to that grid point; however, if the difference is more than the set value that grid point is assigned a value of 1 and then the values of all grid points are summed. Finally, the total number of grid points is multiplied by the convergence criteria value and divided by the summed grid-point value, and it is considered steady state when this ratio is greater than or equal to one. Alterations and improvements were made later to the original model. Most notably, temperature dependence was added. Despite some effects that buoyancy would have on high wind speeds, these simulations were run with stable nighttime conditions in order to avoid any buoyancy effects. Another change that was made was that the differencing scheme was changed from forward differencing to central differencing. At the boundaries of the numerical domain a modified central differencing was used where the inside grid point next to the one on the boundary and the corresponding grid point just inside the opposite boundary are averaged. Also, over the course of model usage and development, the original concept of reaching an unobstructed steady-state flow before the obstacle was removed and not used for the first parametric studies. This concept was reintroduced in the model for the tree parameterization study.

1.4 AABL Wind and Gust Tunnel

The Aerodynamic/Atmospheric Boundary Layer (AABL) Wind and Gust Tunnel was used for the experimental wind tunnel tests. The wind tunnel is designed for uniform flow and atmospheric boundary layer flow tests. For this work, an atmospheric boundary layer was used to simulate a coastal wind profile.

1.5 Organization of These Studies

The studies herein focus on two ways of examining the parametric effects of shelterbelt parameters. Chapter 2 is a report of parametric numerical studies of simple models of shelterbelts. In this study there were seven shelterbelt parameters studied: shape, height, spacing/line tightness, density/density distribution, line width, number of lines, and wind speed. Chapter 3 focuses on parameterizing realistic trees for use in the numerical model and their results. These trees were organized into sixteen arrangements for comparative analysis. Chapter 4 presents experimental work conducted in the wind tunnel. Here fence models made of screen were parametrically tested to determine the effectiveness of reducing wind-induced forces on structures. The fence parameters tested in the wind tunnel were the porosity of the fences, the spacing between the fences and the house models, the height of the fences and the effect of a deflector attached to the top of the fences. Chapter 5 is summary of each study and their conclusions as well as a recommendation of future work.

CHAPTER 2. PARAMETRIC NUMERICAL STUDIES

2.1 Introduction

The initial parametric numerical studies evaluated general cross-sectional shapes of shelterbelts, porosities, heights, spacing of lines, tightness of lines, width of lines and wind speed dependence. These initial studies were high wind-speed extensions of previous studies of other researchers (Finney, 1934; Woodruff and Zingg, 1952, 1953; Hagen and Skidmore, 1971; Cao et al., 1981; Heisler and Dewalle, 1988; Wilson, 1987; Wang and Takle, 1997). The results of these studies were mostly in agreement with the older studies. It was found that there is a direct correlation between height and sheltered distance, as was also determined by Finney (1934) and Heisler and Dewalle (1988). Much of the previous modeling work for natural shelterbelts has been done with uniform blocks of porosity in numerical models or with uniform porous screens in wind tunnels. That work was done under the assumption that the horizontal distribution of the porosity was of little consequence to the flow field behind the shelterbelt; therefore an aggregate value was sufficient (Wang and Takle, 1995). The initial numerical studies found that using these porosity blocks, the cross sectional shape of the shelterbelt had little effect on the sheltered distance, which was actually contrary to other studies done at lower wind speeds (Caborn 1957, 1965; Jensen, 1974; Gandemer, 1979). The initial studies also varied the porosity distribution throughout the shelterbelt by having each line's porosity vary.

There were two parametric studies conducted as preliminary work in this research. The first study explored and extended previous studies that used this model on shelterbelt shape. It also included the height, spacing and porosity parameters. The second study extended the first study by reexamining spacing and height while also studying line width, density distribution,

number of lines and wind speed dependence.

In order to perform a parametric study to determine the relative effect created by each parameter, all other variables are kept constant. In addition to the tested parameters other parameters that were kept constant for each study were the drag coefficient, incident wind direction, temperatures throughout the model domain so as to have no buoyancy effects, relative humidity, cloud cover, roughness length, model domain and grid spacing, time and date, latitude and longitude location, and time step.

2.2 Shape

The results from Wang and Takle (1997) showed that non-streamlined shapes had a slightly better wind-speed sheltered distance. Therefore in the first study only the non-streamlined shapes were modeled. The shapes modeled were based on three triangular shapes and a block. These shapes were entered into the model as step functions, having the shapes as shown in Figure 2.1.

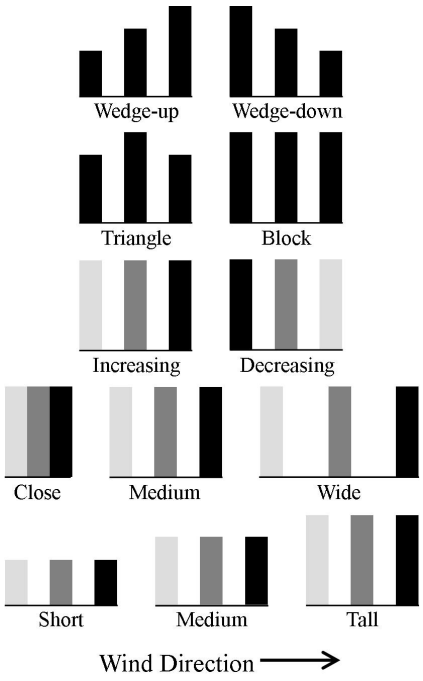

Figure 2.1 Configuration variables modeled

The cross-sectional shape of each line in the shelter is modeled as a rectangular volume with uniformly dispersed porosity. While this is not an exact representation of natural shelterbelts, the volume of the rectangle is assumed to be representative of the volume taken up by trees and bushes with the porosity averaged over the volume.

2.3 Height

The height of the trees in the each line was also a variable that was modeled. In the first study there were three configurations used. Each shorter level in the shelterbelt was 3 m shorter than the previous. The configurations were called short, medium, and tall. Short was defined as the tallest trees being 8 m. Medium was defined as the tallest trees being 10 m. Tall was defined as the tallest trees being 12 m. In the second study five different heights were tested. They were short, at 1 m; medium-short, at 4 m; medium, at 7 m; medium-tall, at 10 m; and tall, at 13 m.

This range covers the average height of many commonly used trees, such as pine and oak trees. Many trees used are taller than these, but this range is enough to see the trend produced by the height variation.

2.4 Spacing/Line Tightness

Another variable in the design of a shelterbelt is the spacing between the rows of trees. The three spacing configurations used were labeled close, medium, and wide. Close was defined as no space between the rows of trees. Medium was defined as 3 m between the rows of trees; and far was defined as 6 m between the rows of trees. Depending on the use of the shelterbelt, the distances may be larger or smaller than would be actually used. Yet the concept of closer or further tree spacing is easily represented with these values in this model.

In the second study, five different spacing widths were tested. They were close, with 0 m between the rows; medium-close, with 2.25 m between; medium, with 4.5 m between; medium-far, with 9 m between; and far, with 13.5 m between. Tightness, the number of trees within a certain total shelterbelt width, was also tested. To do this, the space required for a 7 row

shelter with 6 m wide rows and 4.5 m wide spaces (a total of 69 m) was used, and the number of lines in that space was increased from one to seven; to accomplish this the between row spacing was varied in order to use the entire 69 m, while the row width remained constant.

2.5 Density/Density Distribution

The density configurations used were increasing density and decreasing density going from the windward side of the shelterbelt to the leeward side. The densities chosen were based on measurements taken from an actual shelterbelt that was deconstructed in Nebraska. Three different representative densities were chosen to represent the low, medium and high density values. Since the data from the Nebraska shelterbelt were given in leaf area density (LAD), instead of using conventional porosity to define the density, the LAD was directly input rather than calculated from the porosity. However, the formula that is used in the model to relate porosity to LAD is

$$LAD = \left[\frac{1}{2}\left(\frac{3.0}{2 * porosity}\right) - 1.0\right]^2 \left[\frac{1}{width * C_D}\right] \tag{2.1}$$

which is based on Hoerner's (1965) empirical formula and the work of Wilson (1985) for porosity where width is the width of the shelterbelt and CD is the drag coefficient of the shelterbelt (0.23 in this model as determined by Falk). The three values of LAD used were 1.0 for the least dense, 1.5 for the medium density and 2.0 for the most dense, which correspond to 69% porosity, 62% porosity and 56% porosity respectively. While this does not completely cover the whole range from the Nebraska shelterbelt, it is representative of the middle of the range.

In the second study, to test the effect of different density configurations three properties of the configuration were tested. The first property, similar to the first study, was the ordering of the densities throughout the shelterbelt. The two tested were increasing density windward to leeward respectively and decreasing. Secondly, two density ranges were chosen to test. They were a large range of 80% porous to 20% porous leeward to windward respectively and a small range of 70% porous to 50% porous leeward to windward respectively. The ranges were divided evenly based on the number of tree lines in the shelterbelt. For example, in a three-line shelterbelt with the large spread of porosity, the windward line had 80% porosity; the next

line had 50%; and the leeward line had 20%. Thirdly, seven different uniform densities were tested to strictly test the effect of different values of density. In this study, the porosity values were input and then calculated within the model using Equation 2.1.

2.6 Line Width

The second study examined line widths. As Equation 2.1 shows, LAD is inversely proportional to line width. For example, the same porosity in a thinner line presents more resistance than in a wider line because the vegetation is closer together, reducing the open spaces between them. The four line widths that were chosen to test were 1.5 m, 3 m, 6 m, and 9 m.

2.7 Number of Lines

The number of lines also affects the resistance presented to the flow because the more lines there are the more obstacles the wind has to travel through. The second study tested four sets of lines: 1 line, 3 lines, 5 lines and 7 lines.

2.8 Wind Speed

While the initial incident wind speed is not a parameter of the shelterbelt itself it is a model parameter that changes the resulting wind speed reduction. The first study used only 100 m s^{-1} initial winds in order to capture the high wind range. Because that is an extremely high wind speed, one that most structures and vegetation cannot be expected to withstand for a significant period of time, the second study tested a range of wind speeds that included more reasonable values. The six wind speeds that were tested were 5 m s^{-1}, 10 m s^{-1}, 25 m s^{-1}, 50 m s^{-1}, 75 m s^{-1} and 100 m s^{-1}.

2.9 Results

Unfortunately, after all the model runs for the first study were completed it was discovered that the model boundary conditions were not correct for high velocity flows. The inflow and

outflow boundaries were too close to the area of interest so that the flow was not completely developed before it reached the shelter. Therefore the incident wind was not at its maximum value when it reached the shelter line. However, trends can still be inferred from the results. This was corrected for the second study.

The generally accepted definition for sheltered distance is the downstream distance where the wind is reduced by at least 20%, or in these plots where the wind-speed recovery is less than 80% (van Eimern et al. 1964, Heisler and Dewalle 1988). In the following plots negative wind-speed recovery often occurs in the lee of the shelterbelts. This is interpreted as oppositely directed flow, or recirculation flow. The following plots also show an acceleration of the flow in the windward approach region. This is an artifact of the model having too short of a model top boundary condition related to the height of the shelters.

2.9.1 Shapes

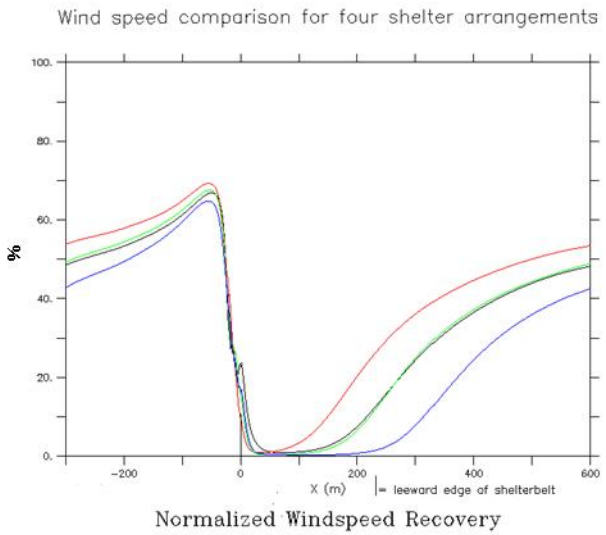

Figure 2.2 Wind speed comparison for four shelter shape arrangements

For shelterbelts of tall height, increasing density, and wide spacing, at 2 m above the surface (black: wedge-up, red: wedge-down, green: triangle, blue: block)

The wind speed recoveries plotted in Figure 2.2 show that the difference in the sheltered distance by the most effective shape configuration, block, is about double that of the least

effective, wedge down, when all other variables (increasing density, wide spacing and tall height) are kept equal. The middle range has the triangle shape nearly equally as effective as wedge up. Figure 2.3 is similar to Figure 2.2 except the opposite density configuration (decreasing) is used. Here the least effective shape was wedge-up, while block remained the most effective.

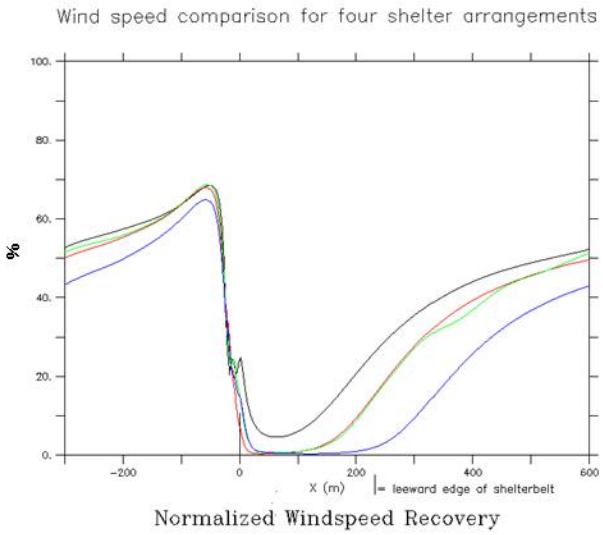

Figure 2.3 Wind speed comparison for four shelter shape arrangements

For shelterbelts of tall height, decreasing density, and wide spacing, at 2 m above the surface (black: wedge-up, red: wedge-down, green: triangle, blue: block)

Note that the least effective shape, wedge-up, for this density configuration does not achieve a 0% wind recovery at any point in the lee; that is, it does not completely stop the wind. Figure 2.4 is similar to Figure 2.2 except the close spacing configuration is used. Once again, the most effective shape is block and its sheltered distance is about double the distance of the least effective shape, wedge-down. Figure 2.5 is similar to Figure 2.2 except the short height configuration is used. This figure shows that the magnitude of the sheltered distances are significantly reduced compared to the tall case. Also, none of the configurations achieve a 0% wind speed recovery at any point in the lee. Although there is no complete wind speed reduction with the short trees, the most effective shape, block, has about a five times longer sheltered distance than the least effective shape, wedge-down. The most and least effective shapes are consistent with the tall case while the two mid-range effective shapes deviated in

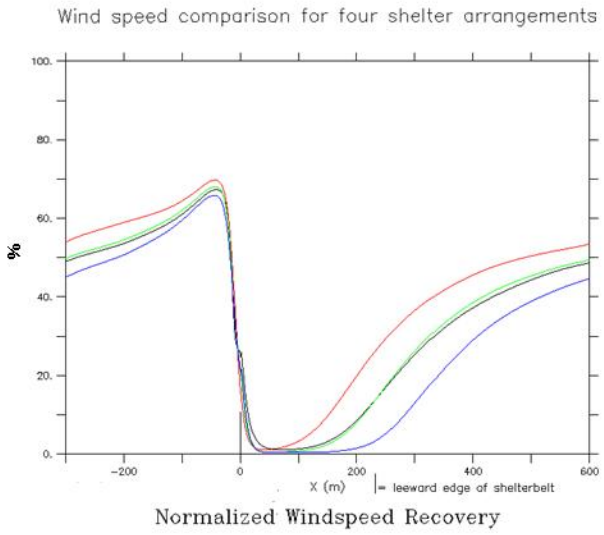

Figure 2.4 Wind speed comparison for four shelter shape arrangements

For shelterbelts of tall height, increasing density, and close spacing, at 2 m above the surface (black: wedge up, red: wedge-down, green: triangle, blue: block)

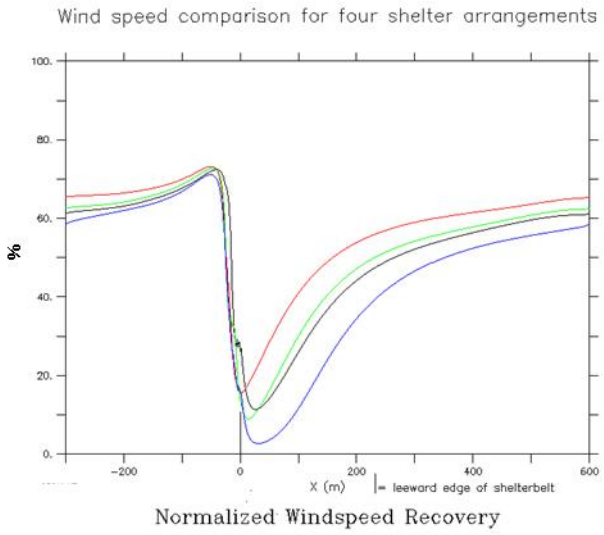

Figure 2.5 Wind speed comparison for four shelter shape arrangements

For shelterbelts of short height, increasing density, and wide spacing, at 2 m above the surface (black: wedge-up, red: wedge-down, green: triangle, blue: block)

their levels of effectiveness with wedge-up having a longer sheltered distance than triangle; however, triangle initially has a greater wind-speed reduction. For all arrangements, including the ones not presented here, the block shape configuration always gives an equal if not longer sheltered distance. The wedge-down shape configuration always gives the shortest sheltered distance except for the decreasing density configuration with the short height configuration where wedge-up is the least effective. Other selected plots can be found in the second appendix, Figures A.1 through A.5.

2.9.2 Height

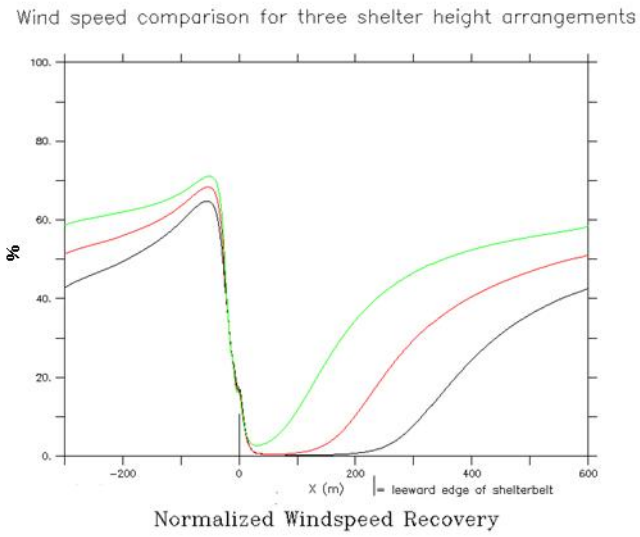

Figure 2.6 Wind speed comparison for three shelter height arrangements

For shelterbelts of block shape, increasing density, and wide spacing, at 2 m above the surface (black: tall, red: medium, green: short)

It has been found that the sheltered distance is proportional to the shelter height (Heisler and Dewalle, 1988). As shown in Figure 2.6, the first study found similar results. This figure uses the optimal setups for the other configuration variables, block, increasing density, and wide spacing, and shows the difference the height of the shelter has on the sheltered distance. Here the short shelterbelt has a sheltered distance of nearly half that of the tall shelterbelt and it is only one-third shorter. Figure 2.7 shows that even the least effective shape, wedge-down,

all other variables equal, gives the same result of taller being better. This positive correlation

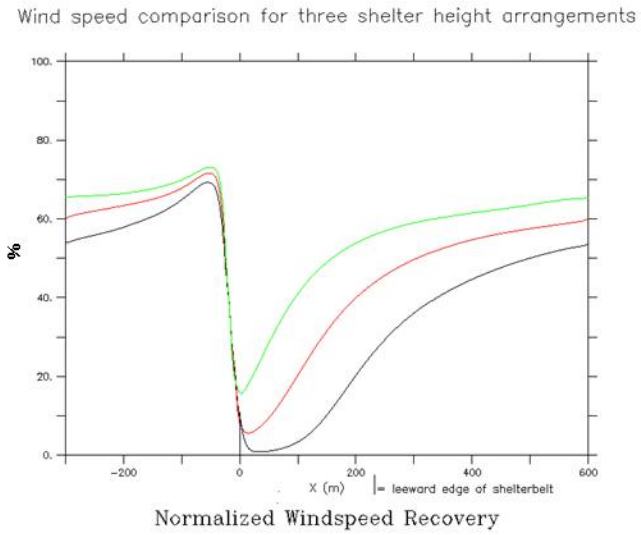

Figure 2.7 Wind speed comparison for three shelter height arrangements

For shelterbelts of wedge-down shape, increasing density, and wide spacing, at 2 m above the surface (black: tall, red: medium, green: short)

between increase in sheltered distance and increased height is true for all shape, density and spacing configurations modeled. Plots for selected other configurations can be found in the appendix in Figures A.6 through A.13.

The second study found similar results. Figure 2.8 shows that the short configuration, the black line across the top, has no wind speed reduction, or 100% wind speed recovery. Then increasing heights give an increasingly wider swath of low wind speed recovery. Figure 2.9, shows the difference between the medium-tall shelter and the shorter shelters in the lee of the shelters. The negative difference between the medium-tall configuration and the shorter configurations show that the taller configuration is better at reducing winds speeds than the shorter configurations.

2.9.3 Spacing/Line Tightness

Once again in the first study using the optimal shape configuration, block with tall height and increasing density, Figure 2.10 shows that having the rows of the shelterbelt spaced farther

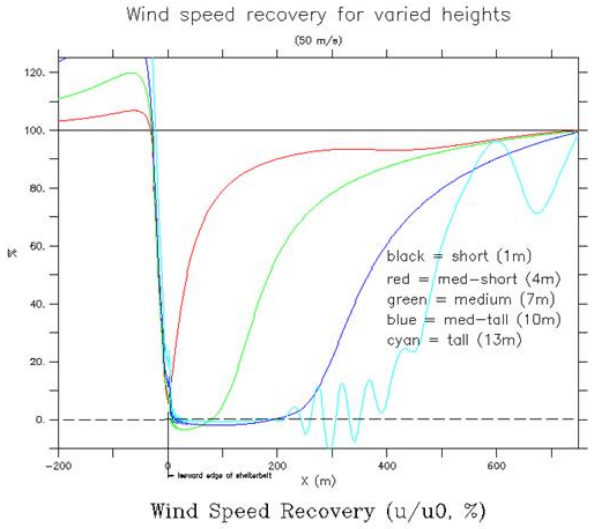

Figure 2.8 Wind speed comparison for five shelter height arrangements

For shelterbelts of block shape, large-spread increasing porosity, medium spacing, medium-wide line width, 3 lines, and medium wind speed, at 2 m above the surface

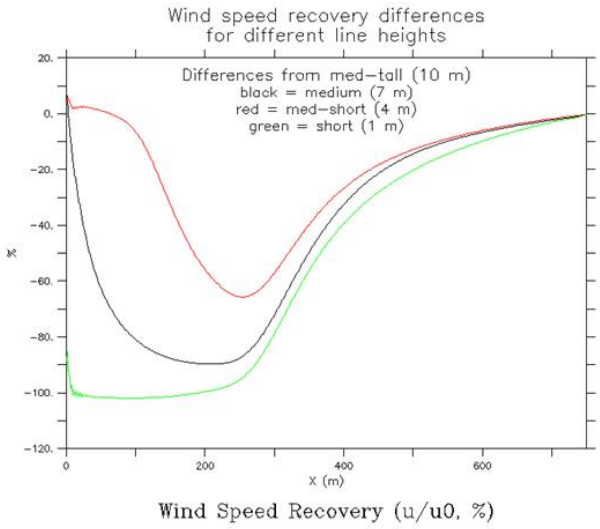

Figure 2.9 Wind speed differences for four shelter height arrangements

For shelterbelts of block shape, large-spread increasing porosity, medium spacing, medium-wide line width, 3 lines, and medium wind speed at 2 m above the surface

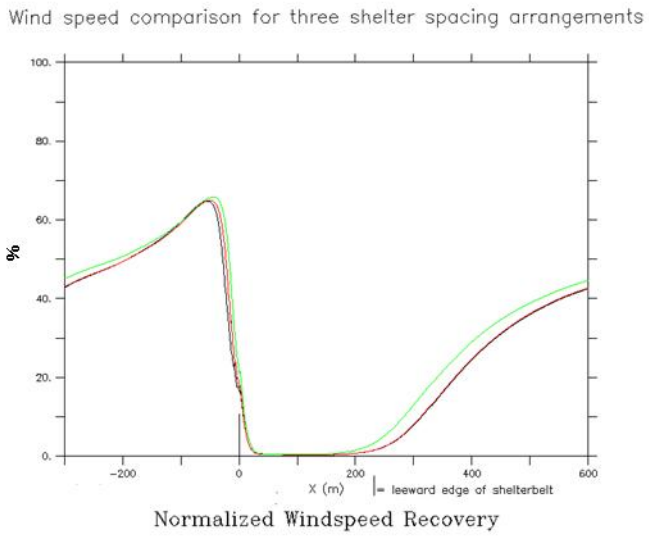

Figure 2.10 Wind speed comparison for three shelter spacing arrangements

For shelterbelts of block shape, tall height, and increasing density, at 2 m above the surface (black: wide, red: medium, green: close)

apart gives a larger sheltered distance near the surface. However, the increased improvement with increased distance is slight, approximately less than 25 m; there is hardly any difference between the wide and medium spacings. Thus, if the use of land is an issue it would be equally suitable to use the medium spacing. Figure 2.11 shows that for the least optimal shape, wedge-down, with everything else the same, tall height and increasing density, that the medium spacing is marginally favored. With the exception of only a few cases in the data set, the farther spacing configurations give an equal or greater sheltered distance near the surface. Plots for selected other configurations can be found in the appendix in Figures A.14 through A.20.

From the second study, Figure 2.12 suggests that less space between the lines provides better shelter, which is opposite of what was found in the first study. However, those findings showed that there is very little difference between the sheltered distances provided by any of the spacing intervals, which is consistent with the current findings. Figure 2.13 shows that there is less than 10% difference between any interval and the far-spaced option. Figures 2.14a and b show a momentum budget for the close spaced and the far spaced configurations respectively.

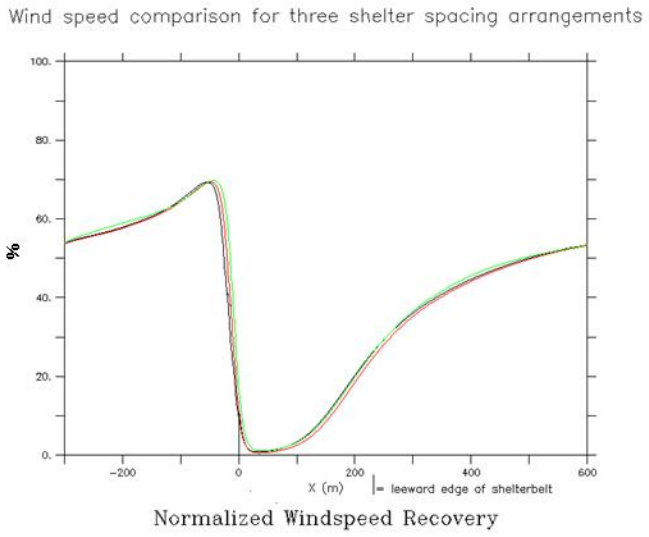

Figure 2.11 Wind speed comparison for three shelter spacing arrangements

For shelterbelts of wedge-down shape (tall height, and increasing density) at 2 m above the surface (black: wide, red: medium, green: close)

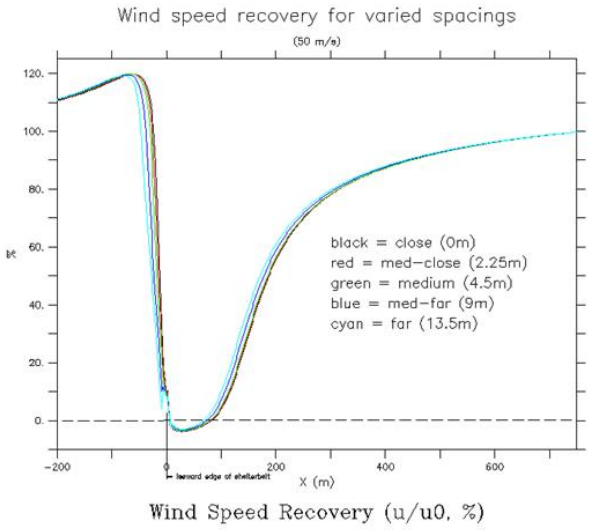

Figure 2.12 Wind speed comparison for five shelter spacing arrangements

For shelterbelts of block shape, medium-tall height, large-spread increasing porosity, medium-wide line width, 3 lines, and medium wind speed, at 2 m above the surface

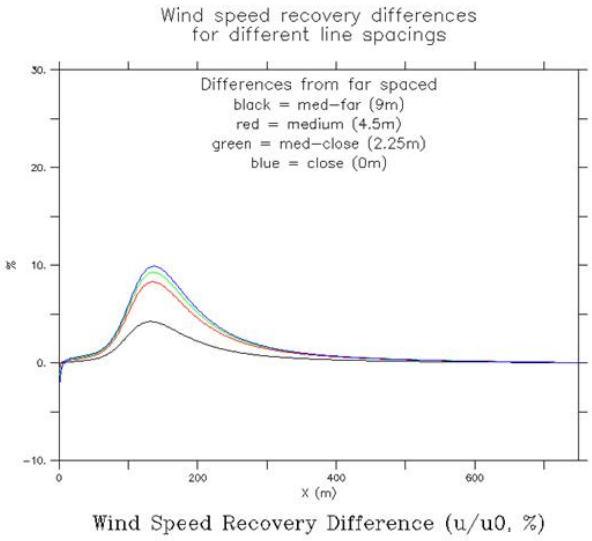

Figure 2.13 Wind speed differences for five shelter spacing arrangements

For shelterbelts of block shape, medium-tall height, large-spread increasing porosity, medium-wide line width, 3 lines, and medium wind speed, at 2 m above the surface

There is not a significant difference in the horizontal advection between the two configurations. The close configuration has a more concentrated drag force with larger spikes than the far spaced. The close configuration also has a more continuous positive vertical advection, which takes momentum away from the horizontal direction. The combination of higher drag forces near the exit of the barrier and more vertical advection can explain why there is slightly more sheltered distance for the close spaced rather than the far spaced configuration.

When considering the line tightness Figure 2.15 shows that for multiple shelter lines there is only a small difference between the sheltered distances despite the number of lines and the space between them. The figure shows that the two-line configuration, the configuration with the largest space between the shelter lines, provides slightly more sheltered distance than the other multi-line configurations. This is the opposite conclusion from Figure 2.13; however it is consistent with first study. Yet, it also shows that for more than two lines, more lines with less space is marginally better, which is consistent with the spacing tests. Figures 2.14c and d show a momentum budget for the tightly-spaced and the loosely-spaced configurations respectively. Similar to the closely-spaced configuration in Figure 2.14a, there is a spike in the drag force at

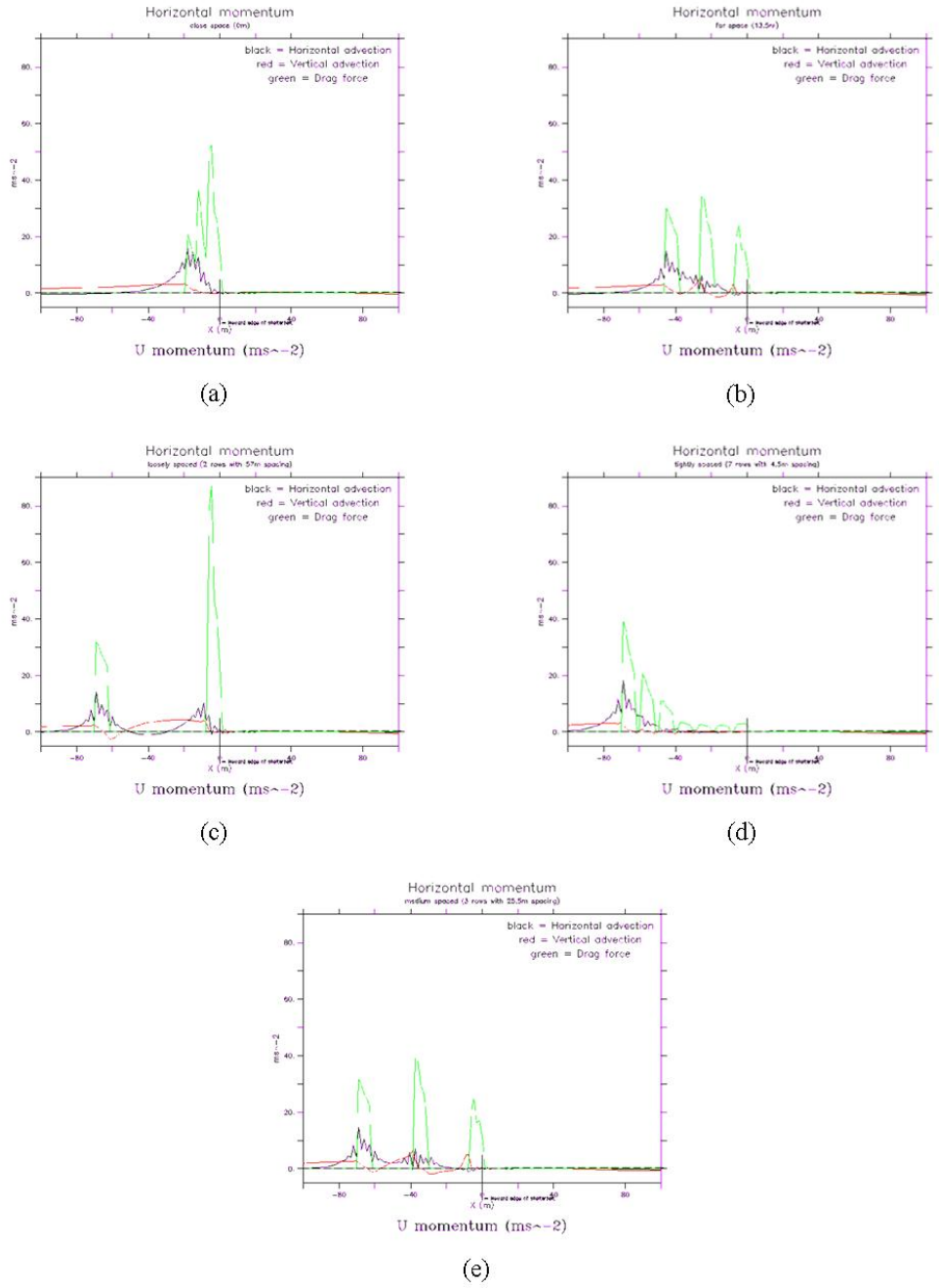

Figure 2.14 Momentum Budgets for five shelter spacing arrangements

For shelterbelts of block shape, medium-tall height, large-spread increasing porosity, medium-wide line width, 3 lines, and medium wind speed at 2 m above the surface

(a) close spaced, (b) far spaced, (c) loosely spaced, (d) tightly spaced, (e) medium spaced

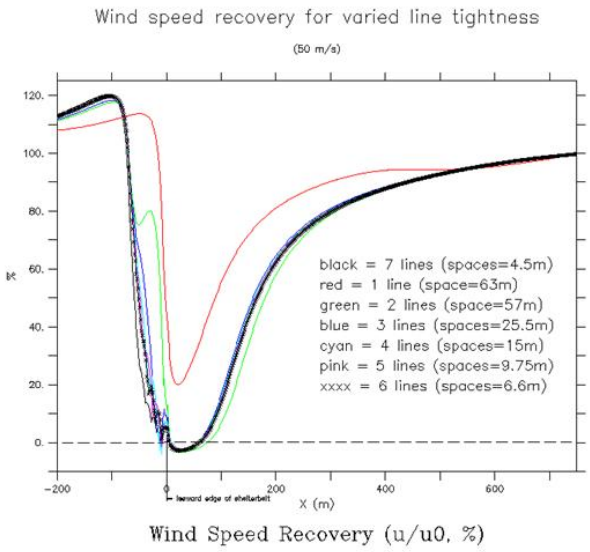

Figure 2.15 Wind speed comparison for seven shelter tightness arrangements

For shelterbelts of block shape, medium-tall height, large-spread increasing porosity, medium-wide line width, and medium wind speed, at 2 m above the surface

the exit of the loose barrier while the tightly-spaced configuration has decreasing drag forces across the barrier. The medium-spaced configuration, which is slightly less effective than the tightly-spaced configuration, has the momentum budget shown in Figure 2.14e. The total drag force of this configuration may be higher than the tightly-spaced, and it has more vertical advection throughout as well as more horizontal advection. The more horizontal advection of momentum aids the flow in passing through the shelterbelt more effectively, thus reducing the sheltered distance compared to the more tightly spaced configuration. This suggests there is an optimal set of shelter lines and spacing resulting in a maximum sheltered distance.

2.9.4 Density/Density Distribution

From the first study, using the optimal shape configuration (block) Figure 2.16 shows that for this shape there is minimal difference in the sheltered distance between the two density configurations using wide spacing and tall height. However, Figure 2.17 shows that for a less optimal shape configuration, wedge-up with wide spacing and tall height as well, the increasing density configuration produces a slightly longer sheltered distance over the decreasing config-

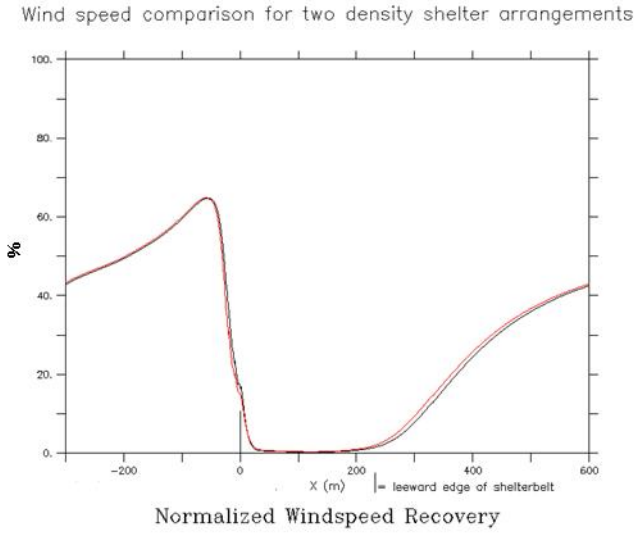

Figure 2.16 Wind speed comparison for two shelter density arrangements

For shelterbelts of block shape, tall height, and wide spacing, at 2 m above the surface (black: increasing density, red: decreasing density)

uration. For three configurations, wedge-up, triangle and block, the increasing density configuration gives at least the same sheltered distance as the decreasing if not better. However the wedge-down configuration always has a better sheltered distance with the decreasing density configuration as is shown in Figure 2.18. Plots for selected other configurations can be found in the appendix in Figures A.21 through A.29.

From the second study, Figure 2.19 shows that the large spread of porosity outperforms the small spread by having a longer range of influence in the lee. Figure 2.20 shows the difference between the two arrangements. Beyond the extremely near lee region both of the spread configurations have the increasing configuration with better results than the decreasing configuration. The difference between the large and small spreads for both arrangements is shown in Figure 2.21.

Both of the arrangements have a negative difference until the very far lee region, indicating the large spread gives better results. Figure 2.22 compares both porosity spreads and a uniformly dense shelter where all the lines have the same density. The porosity value for the uniformly dense shelter was chosen to be 50%. The figure shows that the uniform shelter

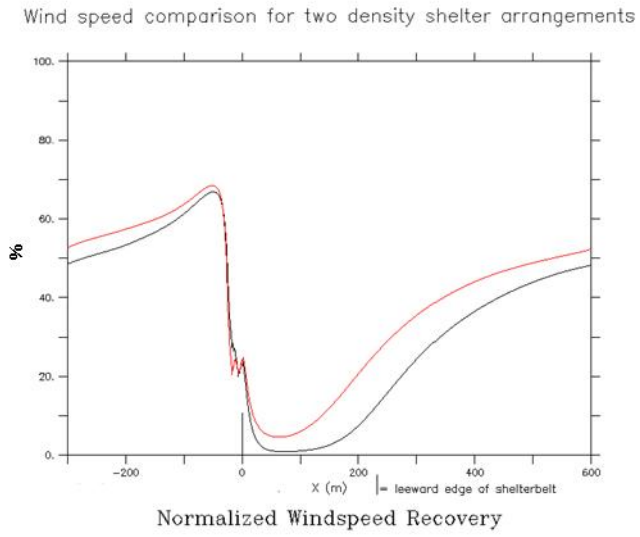

Figure 2.17 Wind speed comparison for two shelter density arrangements

For shelterbelts of wedge-up shape, tall height, and wide spacing, at 2 m above the surface (black: increasing density, red: decreasing density)

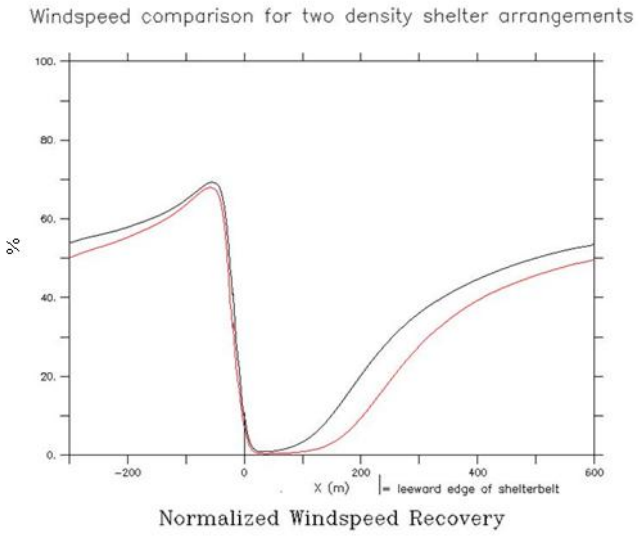

Figure 2.18 Wind speed comparison for two shelter density arrangements

For shelterbelts of wedge-down shape, tall height, and wide spacing, at 2 m above the surface (black: increasing density, red: decreasing density)

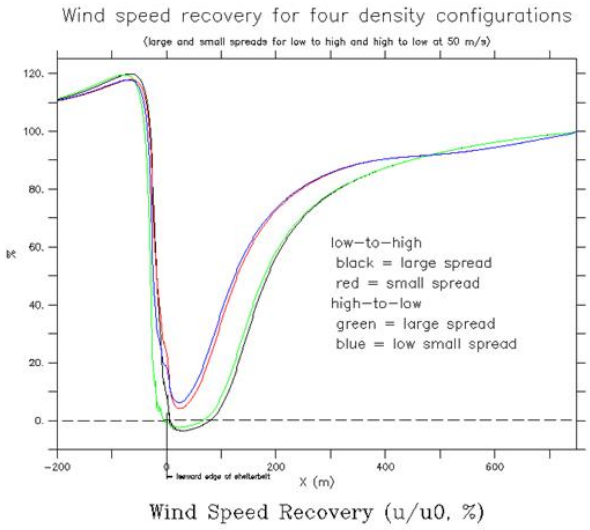

Figure 2.19 Wind speed comparison for four shelter density arrangements

For shelterbelts of block shape, medium-tall height, medium spacing, medium-wide line width, 3 lines, and medium wind speed, at 2 m above the surface

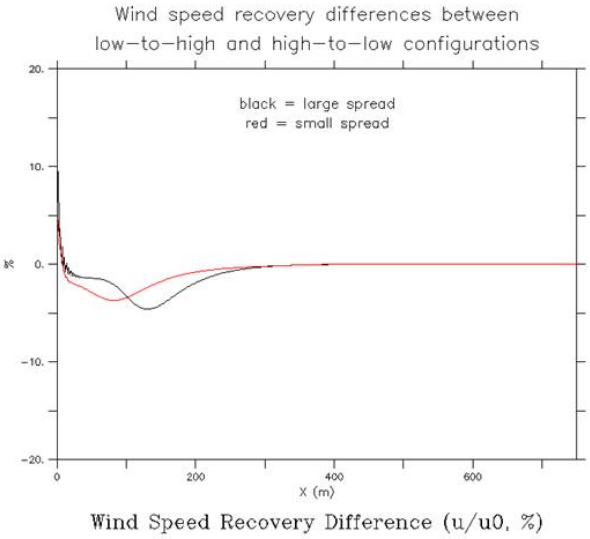

Figure 2.20 Wind speed differences for two shelter density arrangements

For shelterbelts of block shape, medium-tall height, medium spacing, medium-wide line width, 3 lines, and medium wind speed at 2 m above the surface

(from Figure 2.17 black: black minus green, red: red minus blue)

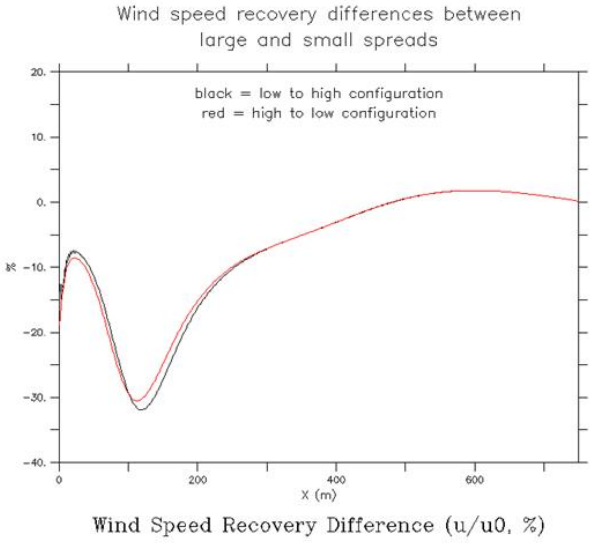

Figure 2.21 Wind speed differences for two shelter density arrangements

For shelterbelts of block shape, medium-tall height, medium spacing, medium-wide line width, 3 lines, and medium wind speed, at 2 m above the surface
(from Figure 2.18 black: black minus green, red: red minus blue)

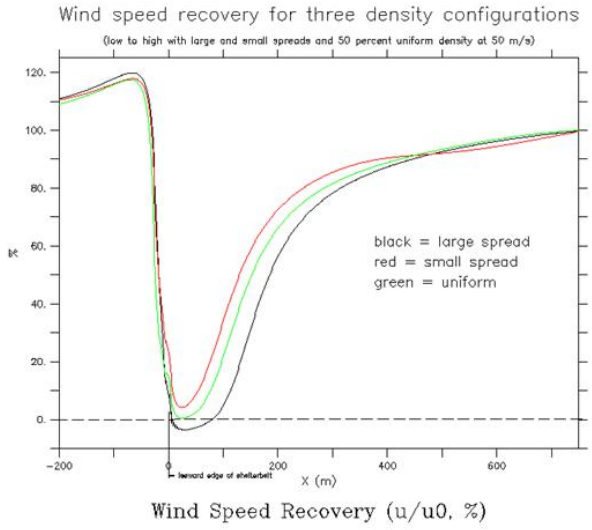

Figure 2.22 Wind speed comparison for three shelter density arrangements

For shelterbelts of block shape, medium-tall height, medium spacing, increasing porosity, medium-wide line width, 3 lines, and medium wind speed, at 2 m above the surface

outperforms the small range shelter, while the large range shelter is still the best. The whole range of uniform shelters is plotted in Figure 2.23. It clearly shows that increasing density

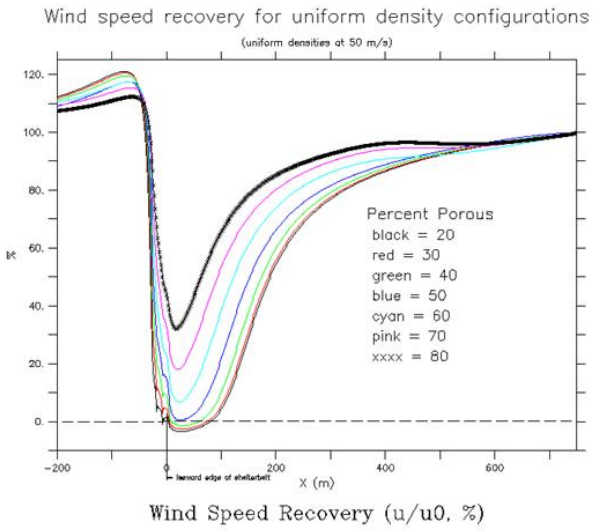

Figure 2.23 Wind speed comparison for seven uniform shelter density arrangements

For shelterbelts of block shape, medium-tall height, medium spacing, uniform porosity, medium-wide line width, 3 lines, and medium wind speed, at 2 m above the surface

gives increasing sheltered distance. However, as the density increases the improvement in the sheltered distance becomes less. At the very dense end of the spectrum there is very little difference between the 20% and 30% porous shelterbelts. Figure 2.24 emphasizes the decreasing difference in the amount of shelter provided for porous shelters by comparing all the shelters to the least porous (20%) shelter. The maximum difference between the 20% and 80% porous shelters is near 60% different, whereas the difference between the 20% and 30% porous shelters is nearly zero.

2.9.5 Line Width

As discussed above, increasing line width with the same porosity decreases the total resistance provided to the wind flow. Figure 2.25 shows that increasing line width slightly decreases the protected distance behind the shelterbelt. However, there is not much difference

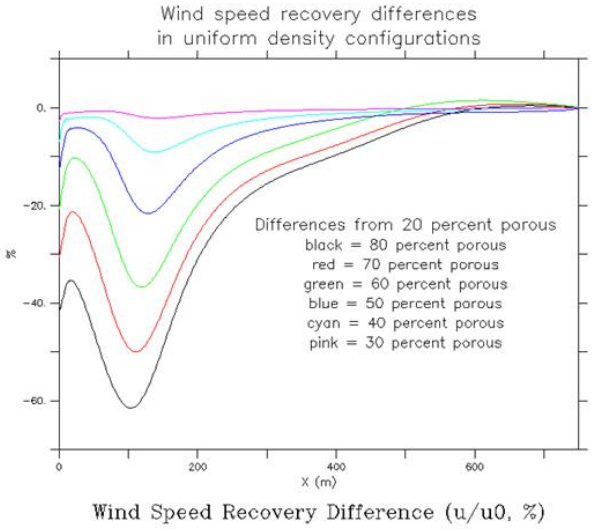

Figure 2.24 Wind speed differences for seven uniform shelter density arrangements

For shelterbelts of block shape, medium-tall height, medium spacing, uniform porosity, medium-wide line width, 3 lines, and medium wind speed, at 2 m above the surface

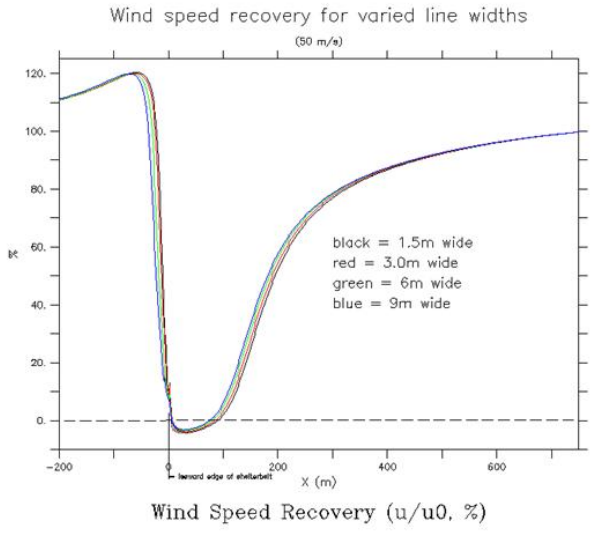

Figure 2.25 Wind speed comparison for four shelter line width arrangements

For shelterbelts of block shape, medium-tall height, medium spacing, large-spread increasing porosity, 3 lines, and medium wind speed, at 2 m above the surface

between the different widths. Figure 2.26 shows that there is less than 10% difference between any of the widths and the worst width of 9 m.

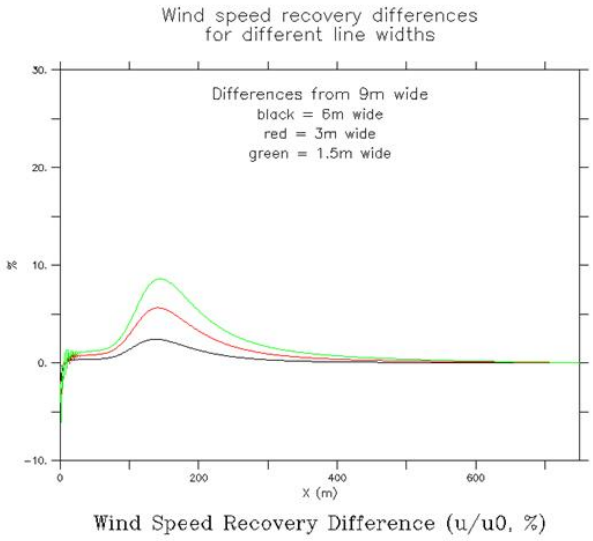

Figure 2.26 Wind speed differences for four shelter line width arrangements

For shelterbelts of block shape, medium-tall height, medium spacing, large-spread increasing porosity, 3 lines, and medium wind speed, at 2 m above the surface

2.9.6 Number of Lines

Figure 2.27 shows that having more than one line is best. However, it also shows that increasing numbers of multiple lines actually decreases the sheltered distance. This is inconsistent with the tightness results in Figure 2.15. Figure 2.28 shows that compared to the seven-line configuration (the worst multi-line configuration) that the three-line configuration is the most positively different, or improved, and that the one-line configuration is significantly negatively different (i.e. much worse).

2.9.7 Wind Speed

The initial wind speed determines the momentum the flow has going into the shelterbelt. Figure 2.29 shows that increasing the wind speed reduces the recirculation zone in the lee of the shelterbelt. It also shows that for higher wind speeds, roughly between 25 m s^{-1} and

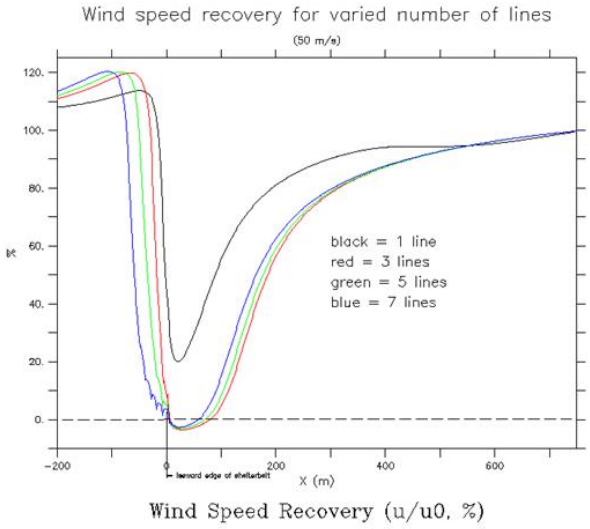

Figure 2.27 Wind speed comparison for four different numbers of lines shelter arrangements

For shelterbelts of block shape, medium-tall height, medium spacing, medium-with line, large-spread increasing porosity, and medium wind speed, at 2 m above the surface

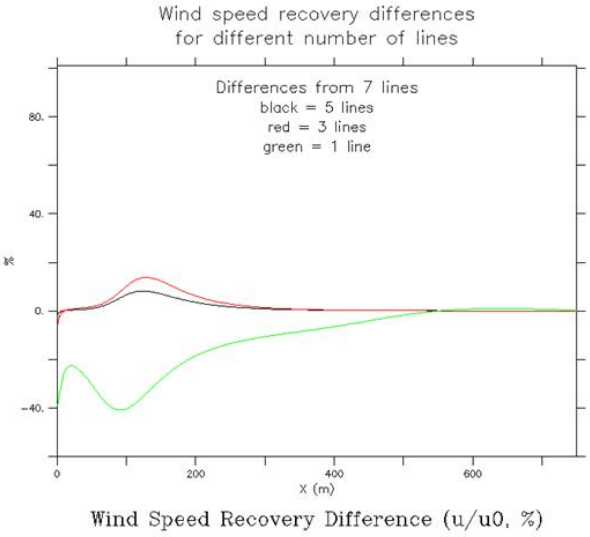

Figure 2.28 Wind speed differences for four different numbers of lines shelter arrangements

For shelterbelts of block shape, medium-tall height, medium spacing, medium-width line, large-spread increasing porosity, and medium wind speed, at 2 m above the surface

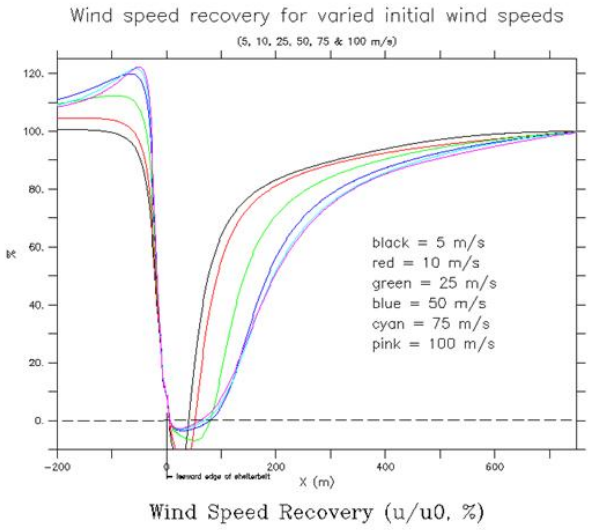

Figure 2.29 Wind speed comparison for six different initial wind speeds

For shelterbelts of block shape, medium-tall height, medium spacing, medium-with line, large-spread increasing porosity, and 3 lines, at 2 m above the surface

50 m s^{-1}, there is not a significant difference in the sheltered distance for increasing wind speeds. Figure 2.30 confirms that at high wind speeds there is little difference; both 50 and 75 m s^{-1} have nearly 0% difference from 100 m s^{-1}, the 25 m s^{-1} only has a difference of near 20%, while 5 and 10 m s^{-1} have over 40% differences.

2.9.8 Turbulent Kinetic Energy

The first study also examined the effect of the arrangements on the turbulent kinetic energy (TKE), which is a measure of the momentum extraction from the mean flow. The TKE can be interpreted as a measure of the deviation of the flow from the mean; thus the large values are related to peak flow values. Therefore, the location of the maximum values of TKE is another important shelter efficiency factor. If the increased values of TKE are kept above the height of buildings the peak forces will be reduced. The optimal configuration for TKE is the same as for wind speed recovery, tall block, increasing density, wide spacing. The figures plot the normalized TKE, $(TKE/TKE_0(H))$. Figure 2.31 shows that this configuration maintains the lee TKE values higher above the surface than the other shapes. Other figures in the

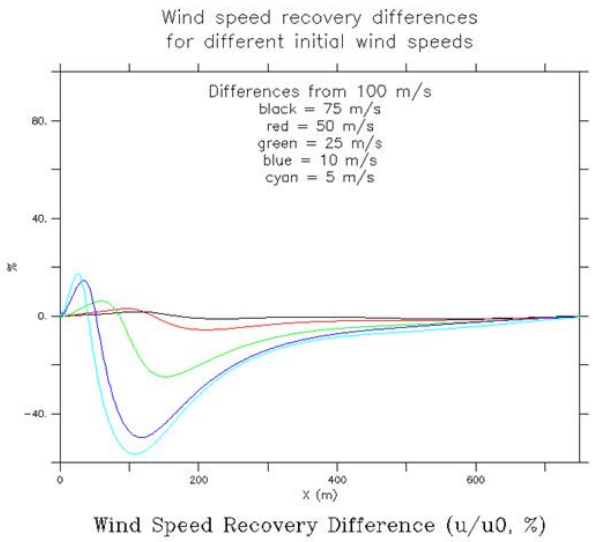

Figure 2.30 Wind speed differences for six different initial wind speeds

For shelterbelts of block shape, medium-tall height, medium spacing, medium-with line, large-spread increasing porosity, and 3 lines, at 2 m above the surface

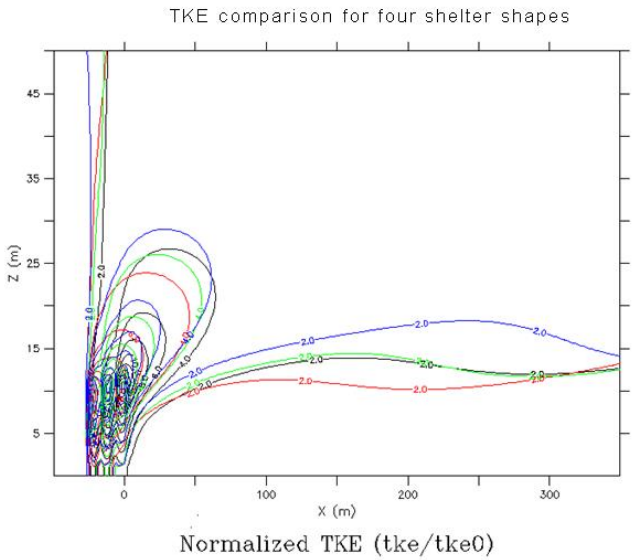

Figure 2.31 TKE comparison for four shelter shape arrangements

For shelterbelts of tall height, increasing density, and wide spacing, at 2 m above the surface (black: wedge up, red: wedge down, green: triangle, blue: block)

appendix (A.30 through A.47) show that the block is better than the other shapes, and that tall height, wide spacing, and increasing density are generally better than their alternates. Figure 2.32 shows that for the least effective shape, wedge-down, with wide spacing and tall height, the decreasing density is more effective at keeping the TKE above the surface.

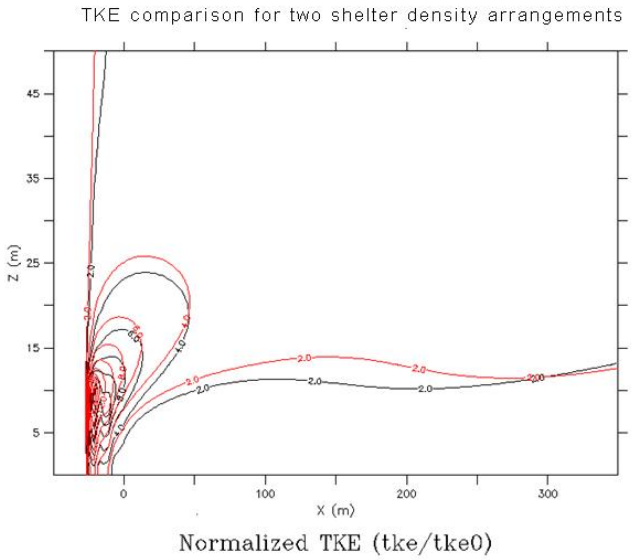

Figure 2.32 TKE comparison for two shelter density arrangements

For shelterbelts of wedge-down shape, tall height, wide spacing, at 2 m above the surface (black: decreasing density, red: increasing density)

A budget for the TKE shows how the different components are affected by the shelter. Equation 2.2 shows the TKE budget equation from Stull (1997) is

$$\underbrace{\frac{\partial \bar{e}}{\partial t}}_{I} + \underbrace{\bar{U}_j \frac{\partial \bar{e}}{\partial x_j}}_{II} = \underbrace{\delta_{i3} \frac{g}{\bar{\theta}_v} \left(\overline{u_j' \theta_v'}\right)}_{III} - \underbrace{\overline{u_i' u_j'} \frac{\partial \bar{U}_i}{\partial x_j}}_{IV} - \underbrace{\frac{\partial \left(\overline{u_j' e}\right)}{\partial x_j}}_{V} - \underbrace{\frac{1}{\bar{\rho}} \frac{\partial \left(\overline{u_i' p^i}\right)}{\partial x_i}}_{VI} - \underbrace{\epsilon}_{VII} \tag{2.2}$$

where (I) is the storage term, (II) is the advection term, (III) is the buoyant production/loss term, (IV) is the mechanical and shear production/loss term, (V) is the turbulent transport term, (VI) is the pressure redistribution term and (VII) is the dissipation. Terms (I), (V), and (VI) do not create or destroy TKE so they are not shown in the plot of the TKE budget. Figure 2.33 shows the TKE budget for the optimal configuration, tall block, increasing density and tall height. The dominant factors are the dissipation, mechanical generation, and horizontal advection. All terms drop off in the lee of the shelterbelt, however mechanical

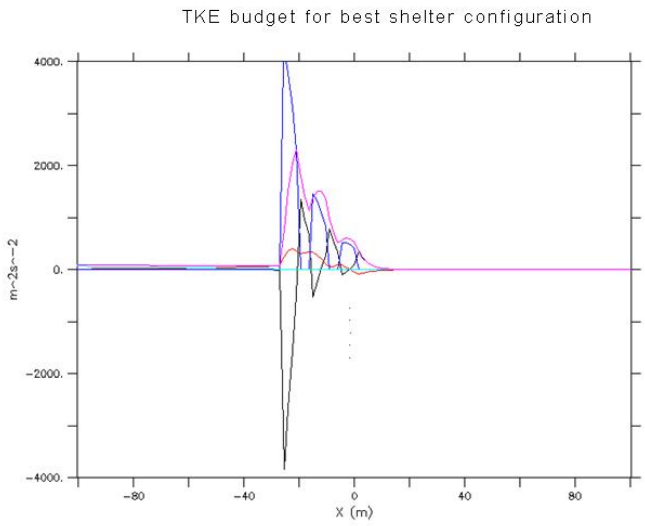

Figure 2.33 TKE budget for the best shelter arrangement

For shelterbelts of block shape, tall height, increasing density, wide spacing, at 2 m above the surface (black: horizontal advection, red: vertical advection, green: buoyant production/loss, blue: mechanical generation, cyan: shear generation, pink: dissipation)

generation, dissipation, and horizontal advection still dominate. After just a few meters the mechanical generation goes to zero leaving just the dissipation and horizontal advection. These two terms are nearly equal, meaning that the dissipation is canceling out the horizontal advection, which indicates that the zone of 0% wind speed recovery is due to a lack of production. As a reminder, Figure 2.34 is a wind speed reduction comparison of the optimal and worst configurations. Figure 2.35 shows the TKE budget for the least optimal configuration, short wedge-down, increasing density, and close spacing. Once again the dominant factors are the dissipation, mechanical generation, and horizontal advection; however shear production plays a larger role. Unlike in the optimal configuration, dissipation is larger than horizontal advection in the lee, however, shear production is also significantly present in the lee. This presence of two significant production terms in the lee supports the assertion that the wind speed recovery never gets down to 0% for this configuration.

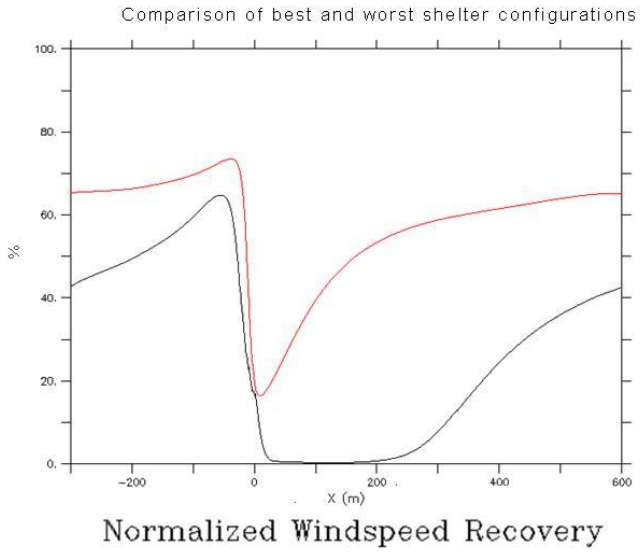

Figure 2.34 Wind speed comparison for the best and worst arrangements

For shelterbelts of block shape, tall height, wide spacing, and increasing density vs. wedge-down shape, short height, close spacing, and increasing density, at 2 m above the surface
(black: best (block), red: worst(wedge-down))

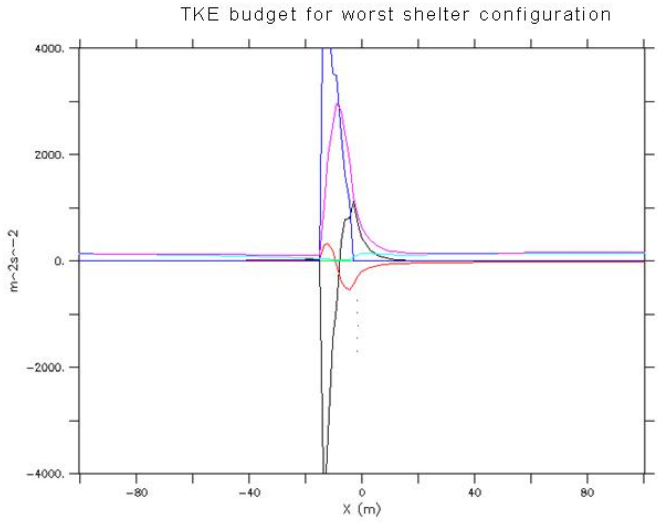

Figure 2.35 TKE budget for the worst shelter arrangement

For shelterbelts of wedge-down shape, short height, increasing density, and close spacing, at 2 m above the surface
(black: horizontal advection, red: vertical advection, green: buoyant production/loss, blue: mechanical generation, cyan: shear generation, pink: dissipation)

2.10 Conclusions

Most effective and least effective configurations shelterbelt configurations were determined using a numerical model to study the effects of shelterbelt shape, density, spacing and height configurations on sheltered distance near the surface based on wind speed sheltered distance. The model results showed that the configurations that gave the most shelter near the surface are tall blocks with a increasing configurations and widely spaced or medium distance apart. The medium distance configuration has an additional benefit that it uses less land that might make it more appealing for agricultural settings. Conversely the results showed that a wedge-down shaped, short shelterbelt with a increasing density configuration at any spacing gives the shortest sheltered distance near the surface. The optimal configuration, a block with increasing density and tall height, is effective over a longer region than the less effective shapes. For the near lee (approximately 0H-13H) the same general conclusions can be drawn for TKE as for wind speed recovery.

Contrary to previous conclusions that shelterbelt shape has minimal effect on sheltered distance for normal wind speeds, the first study found that, at high wind speeds, the shelter shape does appear to affect the shelter efficiency. Figures 2.2 through 2.5 and Figure 2.31 show a clear difference in the shelter provided by each of the four shapes tested. Of the four, the block performs the best.

The height tests are consistent with past findings (Finney, 1934; Heisler and Dewalle, 1988), that is, sheltered distance increases as height increases. Comparing Figures 2.2 and 2.5 shows that the taller arrangements have much longer sheltered distances. Figures 2.6 and 2.7 also show that the sheltered distance increases with the height of the shelter despite the shelter shape. The flat-line for the 1-m shelter in Figure 2.8 suggests that a 1-m shelter has no effect at the 2-m level of the plot. Figure 2.9 shows that the short height has a 100% difference from the tall height. A threshold value at which there is less improvement for the increase in the parameter, i.e. a threshold of lesser returns, can be used to estimate a practical value to implement in a real situation. The height values in this test do not appear to present a threshold of lesser returns. However, the shelters of medium height and taller do reduce the

winds 100% (0% recovery) for some distance, whereas the shorter shelters do not. Therefore, an upper threshold on height may not be able to be determined here, but a lower threshold of moderately tall trees can be inferred.

The first study found that there is little difference in the sheltered distance with increased spacing. Figures 2.10 and 2.11 show that anything beyond close spacing is an improvement. The general conclusion from the data set was that any arrangement with space because the lines is adequate. The results from the spacing comparisons versus the tightness comparisons in the second study lead to opposite conclusions. The spacing tests suggest that less spacing results in a longer sheltered distance. However, the tightness test suggests that having only two lines with more spacing results in a longer sheltered distance; while when there are more than two increasing lines with decreasing spacing the sheltered distance is improved. The overlapping conclusion between the spacing and the tightness results suggest that less space with more lines is going to give the best result. However there is not much improvement between wide spaces and no spaces. Therefore the spacing plays a minimal role in the shelter efficiency.

From the first study Figures 2.16, 2.17 and 2.18 show that for the block, the two density arrangements have little difference. However, the density arrangements for the other shapes do produce more significant differences. The general conclusion from the data set is that the increasing density arrangement is best, except for the wedge down shape. The density tests in the second study, using only the block shape, show that the denser shelter produces a better sheltered distance. Denser shelter lines provide more elements to extract momentum from the flow. Therefore, it makes sense that dense shelters result in flows that take longer to recover. The trend that can be deduced from these results is that higher density is better. However, at higher densities there is little gained by the increased density in terms of wind speed recovery distance indicating a threshold of diminishing returns for density around 50-60% porous.

Similar to the spacing, tightness and number of lines, line width does not appear to be a major factor in increasing or decreasing the sheltered distance. Thinner lines are slightly more effective than wider lines when the porosity is constant. Because land usage and/or availability

can be an issue in areas where shelterbelts are needed, thinner lines reduce total space for the shelter, which is good.

The comparison of the number of lines in Figure 2.25 also emphasizes that multiple lines are best, but there is only a slight improvement with many lines over few. The major consistency through both the tightness and the line spacing comparisons is that multiple lines are far better than a single line.

Initial wind speed is not a design parameter of the shelters themselves. Therefore, it cannot be used to determine the best sheltered distance. Examining the initial wind speed does help to know what to expect for different situations. Ideally, all of the parameters should be tested to see how they perform under various wind speeds to determine the best shelter for different environments. However, comparing the results from one configuration for different wind speeds does reveal that roughly 50 m s^{-1} is the threshold of diminishing returns. However it is likely that, for a natural shelterbelt, 50 m s^{-1} is at or above the threshold of wind throw for many plants; for these conditions an artificial shelterbelt would be an attractive option.

Knowing the trends produced by different values of shelterbelt parameters provides guidance for designing real shelters. Using a computer model is the most efficient way to study these different parameters. These studies found that height and density have the largest effect on shelter provided. The other shelter parameters tested (spacing, number of lines, and line width) showed very little variation throughout the range of values test. When comparing the effectiveness of a shelter at different wind speeds, it was shown that in the model above 50 m s^{-1} there is not a significant difference in the shelter given. These tests suggest that height and porosity are the most important design factors for a shelterbelt because they have such a wide range of effectiveness determined by their respective values. To truly understand what set of parameters is most effective, it would be advantageous to test combinations of all the different parameters. This may be possible with the improvement of computing resources to complete so many tests. Other future work could also include a larger domain size to allow for taller trees.

CHAPTER 3. TREE PARAMETERIZATION STUDIES

3.1 Introduction

The initial numerical modeling work followed the convention of using the block of porosity to simulate trees while other parameters were varied. Work reported in this chapter focused on parameterizing trees with a porosity distribution that more closely represents real trees. These new tree parameterizations were studied to determine how different tree shapes and porosity distributions affect the flow field.

To more closely model the structure of real trees, information on parameter values was collected for many kinds of trees. These parameters were the tree shape, height and width as well as the drag coefficient. In most cases, average values were used to represent a type of tree. In other cases when there was no information about a parameter for a certain kind of tree values were assumed based on similarities and differences to other trees. The inexactness of this method was determined to be acceptable because it is understood that this is still an approximation.

3.2 Tree Types

The first step in designing trees for the numerical model was to choose tree types. The tree types were chosen in an attempt to have several distinctly different tree shapes and porosity distributions. The seven tree types chosen were based on broad classes of trees and then slightly more narrowed down to general tree types that grow in coastal areas. Coastal trees were chosen because of the potential effectiveness shelterbelts could have in those regions for hurricanes, sea breezes and even tsunamis (Takle et al., 2006). The seven types were deciduous, coniferous, casuarinas, mangroves, palms, hedges and willow trees. Because of the focus on

the coastal region the roughness length was set to be 0.0005 m, so that a coastal wind profile would be calculated.

3.2.1 Average Tree Measurement Values

In each tree type average values of height and span were tabulated for several different species of that type. Because deciduous and coniferous trees grow in many regions and can vary widely by region, species that were specified as being located in coastal regions by Harlow and Harrar (1969) and Dirr (1990) were chosen as the characteristic trees for those types. For the deciduous trees the American Elm, Live Oak, Red Maple and the River Birch were chosen to use for average values. For the coniferous trees the Loblolly Pine, Long Leaf Pine and the Short Leaf Pine were chosen to use for average values. For the casuarina River Sheoak, Beach Sheoak, and Australian Pine species were used. Black Mangrove, Blind-Your-Eye Mangrove, and Red Mangrove were used for the mangroves. Palmyra Palm, Coconut Palm, Cabbage Palm and Chinese Fan Palm were used for the palms. A wide variety of hedges were averaged, including the Rose-of-Sharon, Boxwood, Variegated Ligustrum, Florida Yew, Japanese Laurel, and Carissa Holly. Willows were based on the Black Willow and the White Willow.

3.2.2 Height

Typical heights were found for the above trees using Harlow and Harrar (1969), Dirr (1990), *USDA Agricultural Handbook 654* (1990), *Tree Fact Sheets* (1993), Vozzo (2003) and Sydnor and Cowen (1994). These values were then averaged to obtain a value for the tree type. The height values for all tree types are complied in Table 3.1.

3.2.3 Span

Typical span values were found for the trees using Herman et al. (1996), *Tree Fact Sheets* (1993), and Vozzo (2003). Based on a suggestions from Dr. Janette Thompson of the Department of Natural Resource Ecology & Management at Iowa State University a smaller value than was tabulated was used for the span of the willow trees. The span values that were used

Tree Type	**Height** (m)	**Span** (m)	**High Porosity** (%)	**Medium Porosity** (%)	**Low Porosity** (%)
Deciduous	19	12	70	55	35
Coniferous	25	9	65		40
Casuarina	25	11	85		50
Mangrove	5	5	55		30
Palm	22	7	80		50
Hedge	3	3	50		30
Willow	20	7	85		50

Table 3.1 Average height and span values and porosity values used to design trees for model parameterization

for all tree types are complied in Table 3.1.

3.2.4 Porosity

Aerodynamic porosity would be the best description of the porosity of a tree because of its three-dimensionality; unfortunately the only way to easily measure the porosity of a tree is optical porosity (Loeffler et al., 1992). To determine the optical porosity, photographs of trees were studied in a similar, while less exact, manner to the process described in Loeffler et al. (1992). For simplification purposes the trees only have two or three different regions of porosity assigned to them to describe the entire crown of the tree. However, to account for the three-dimensional shape of the tree, the values of porosity are weighted based on how much of the horizontal cross-sectional area each porosity value occupies, while also accounting for the vacant space between trees in the line. The trees were assumed to be uniform in the x- and y-directions. The lines were assumed to be spaced so that the farthest extent of their crowns were touching. Similarly, while in reality trunks have zero porosity, because the model is two-dimensional the vacant space around the trunk was accounted for by weighting the trunk porosity by how much of the horizontal cross section it occupied. The silhouette of a cross-section of the center of each tree can be seen in Figure 3.1. The mangrove trees do not have a trunk because their complex root system acts as the main support for the tree, therefore the bottom of the tree is given a porosity value rather than a trunk.

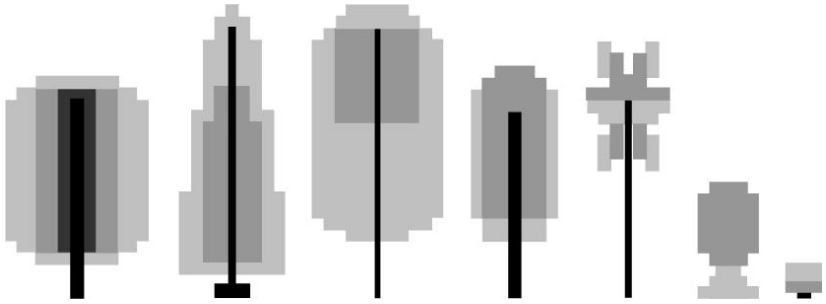

Figure 3.1 Silhouettes of parameterized trees

Left to right: Deciduous, Conifeous, Casuarina, Willow, Palm, Mangrove and Hedge
Dark colors represent more dense areas

3.3 Drag Coefficient

Because the model is a fluid flow model, it accounts for the drag coefficient, c_D, of the obstacles placed in the domain. Once again for simplification the trees were split into two parts as far as the drag coefficient is concerned: the trunk and the crown.

3.3.1 Trunk

Since drag coefficients are functions of wind speed three values of the coefficient were chosen for each tree for three ranges of wind speeds. The drag coefficient values for the trunk are based on the idea of a tree trunk being a rough cylinder. There are three different values for the drag coefficient of the tree trunks based on wind speed; zero to 1 m s^{-1}, 2 to 5 m s^{-1}, and greater than 5 m s^{-1}. The values were estimated based on a plot from Simiu and Scanlan (1996) where the Reynolds number is calculated using Equation 3.1

$$Re = \frac{UD}{\nu} \tag{3.1}$$

where U is the wind speed, D is the characteristic dimension, and ν is the kinematic viscosity of air. For simplification a single value of 0.67 m was used for the characteristic dimension of the trunk of the trees, so that the trunk drag coefficient is the same for all trees except the mangrove. A value of $1x10^5 m^2 s^{-1}$ was use for ν. For the mangrove the drag coefficient was chosen to be twice the value for a standard single-trunk tree. The trunk drag coefficient values that were used are compiled in Table 3.2.

Tree Type	Trunks			Crowns		
	0-1 ms^{-1}	**2-5 ms^{-1}**	**>5 ms^{-1}**	**0-1 ms^{-1}**	**2-5 ms^{-1}**	**>5 ms^{-1}**
Deciduous	1.20	0.30	0.45	0.35	0.29	0.17
Coniferous	1.20	0.30	0.45	1.10	1.00	0.46
Casuarina	1.20	0.30	0.45	0.73	0.67	0.31
Mangrove	2.40	0.60	0.90	0.90	0.48	0.42
Palm	1.20	0.30	0.45	0.53	0.44	0.26
Hedge	1.20	0.30	0.45	0.73	0.65	0.32
Willow	1.20	0.30	0.45	0.83	0.75	0.35

Table 3.2 Drag coefficient values for tree trunks and crowns based on wind speed values

3.3.2 Crown

The drag coefficient values for the crowns of the deciduous and coniferous trees were estimated from graphs of wind speed versus drag coefficient measurement plots in Vogel (1989) and Rudnicki et al. (2004), respectively. The mangrove tree drag coefficient values were estimated from graphs in Mazda et al. (1997) of Reynolds number versus drag coefficient measurement plots. The values for the other three tree types were then based on the similarities/differences to the values of the first three types. For example, the casuarinas is somewhat similar to a conifer in the size of the vegetation, but with less volume, so the casuarinas values are assumed to be 67% of the conifer values. The palm tree was considered to be broad leaved like deciduous trees, but with bigger leaves, so the palm values are assumed to be 150% of the deciduous values. The willow tree is similar to a conifer in that is has smaller leaves with more movement, like the needles of the conifers, but they are less stiff than the conifers, so the willow values were assumed to be 75% of the conifer values. The hedge values were an average of the deciduous and conifer values because of the variety of vegetation types that make up hedges. The crown drag coefficient values that were used are compiled in Table 3.2.

3.4 Shelterbelt Coding

The values of the tree parameters were then used to create the "design trees". The drawings shown in Figure 3.1 were formulated and then the shapes of the trees were programmed into

the model. Because the model is only two dimensional, the three dimensionality of the trees had to be accounted for as stated above in order to not have the effect of a solid wall of trees.

To make the tree parameterization more universally usable, the tree shapes were programmed as a function of the height and span of the design trees so that any size tree can be modeled. Therefore the user can input the tree type, height, span, porosities and the spacing between the trees and the tree configuration is calculated automatically.

Another parameter that affects how this parameterization of the shelterbelt is calculated in the model is the grid spacing in both the x- and the z-directions. It was found that if the grid spacing is larger than a parameterized part of a tree, that part of the tree will not be accounted for by the model. Therefore 0.1666667 m grids were used in the horizontal direction and 0.10 m grids were used in the vertical direction. It was also found that if the horizontal and vertical grid spacings are not similar in size the model will not work properly. Because of the large size of the domain around the shelterbelt the grid was stretched in the region beyond the boundaries of the shelterbelt from 0.1666667 m within the shelterbelt to 1.5 m beyond the shelterbelt in the horizontal direction and from 0.10 m to 1.0 m in the vertical direction by a 1.1 stretching factor. This helped with reducing the total number of grid points to be calculated in order to reduce the run time of the model.

3.5 Methods

The possible combinations of the different parameters leads to many potential configurations. In order to limit the number of tests to be run a set of arrangements was designed to test a sampling of the parameters.

3.5.1 Height sets

Several different arrangements of trees based on their height were designed for testing. Six sets of trees were designed for both tall-to-short and short-to-tall arrangements for two or three lines of trees including one arrangement each of all tall and all short trees. “Tall” and “short” were determined based on relative size. The tall-to-short arrangements had the taller trees on

the windward side of the shelterbelt, assumed to be the sea side. Conversely the short-to-tall arrangements had the shorter trees on the windward side of the shelterbelt. To have a system of consistency, the size of the space between lines of trees was the average of the spans of the flanking tree lines. These two series of arrangements are listed in Table 3.3.

Line 1 (windward)	**Line 2**	**Line 3** (leeward)
Palm	Mangrove	
Palm	Mangrove	Mangrove
Casuarina	Palm	Mangrove
Coniferous	Deciduous	
Coniferous	Hedge	
Willow	Coniferous	Casuarina
Mangrove	Palm	
Mangrove	Casuarina	
Palm	Casuarina	
Deciduous	Coniferous	
Deciduous	Willow	
Mangrove	Mangrove	Hedge

Table 3.3 Sets of height tree arrangements tested.

3.5.2 Space sets

Four arrangements were also designed based on two coastal scenarios: beaches and waterfront property that is slightly back away from the beach. Two arrangements were designed for the beaches and two were designed for the waterfront property. These scenarios focused mainly on spacing; for example, a shelter with trees at the water's edge and also behind the beach, or a shelter with trees at the property line and also next to the house. These arrangements are listed in Table 3.4.

3.6 Results

The shelterbelt model is designed to determine a steady state of the model based on the convergence criteria as described Chapter 1. However, many of the tree arrangements studied here shed eddies in their wake and produced recirculation zones in the far lee. Therefore, while

Line 1 (windward)	**Space** (m)	**Line 2**	**Space** (m)	**Line 3** (leeward)
		Beach		
Casuarina	50	Palm		
Palm	20	Mangrove	0	Mangrove
		Waterfront Property		
Coniferous	10	Deciduous	6	Hedge
Hedge	6	Deciduous	10	Coniferous

Table 3.4 Sets of spacing tree arrangements tested.

the mean field was unchanging these recirculation zones caused the model to never reach a steady state. To determine when a model run was in a constant state of creating recirculation eddies the mean wind speed reduction, turbulent kinetic energy and pressure perturbation fields were studied in a time lapse. Once there was no change in the background fields from one time step to another for two or more time steps the model state was considered to have reached the quasi-steady state. Of the time steps where the background fields were unchanged the time step with the largest values in the fluctuating eddies were chosen to use for evaluation because those would represent the worst-case scenarios.

The results of the model runs for the normalized values of wind speed, turbulent kinetic energy and mean kinetic energy were analyzed and compared. This normalization was done by dividing the value of the variable at the location by the value at the same height at the upstream boundary of the domain. The runs were plotted at five heights, two within the experiential layer near the surface where people and low-rise structures generally interact with the wind (1 m and 3 m) one at the typical wind measurement height (10 m) one at the height of the tallest tree top in the arrangement, and one above the shelter (30 m).

3.6.1 Wind speed reduction

One measure of shelter efficiency is how much the wind speed is reduced compared to the upstream values, and how long it stays reduced under a certain threshold. The common threshold is at least 20% wind speed reduction, or as little as 80% wind speed recovery (van Eimern et al. 1964, Heisler and Dewalle 1988). Wind speed recovery is a normalized value

that represents the percentage the local wind speed is of the upstream wind speed value at the same height. Since most buildings that would benefit from a shelterbelt are low-rise buildings, the following analysis will focus mainly on the flow patterns at and below 10 m.

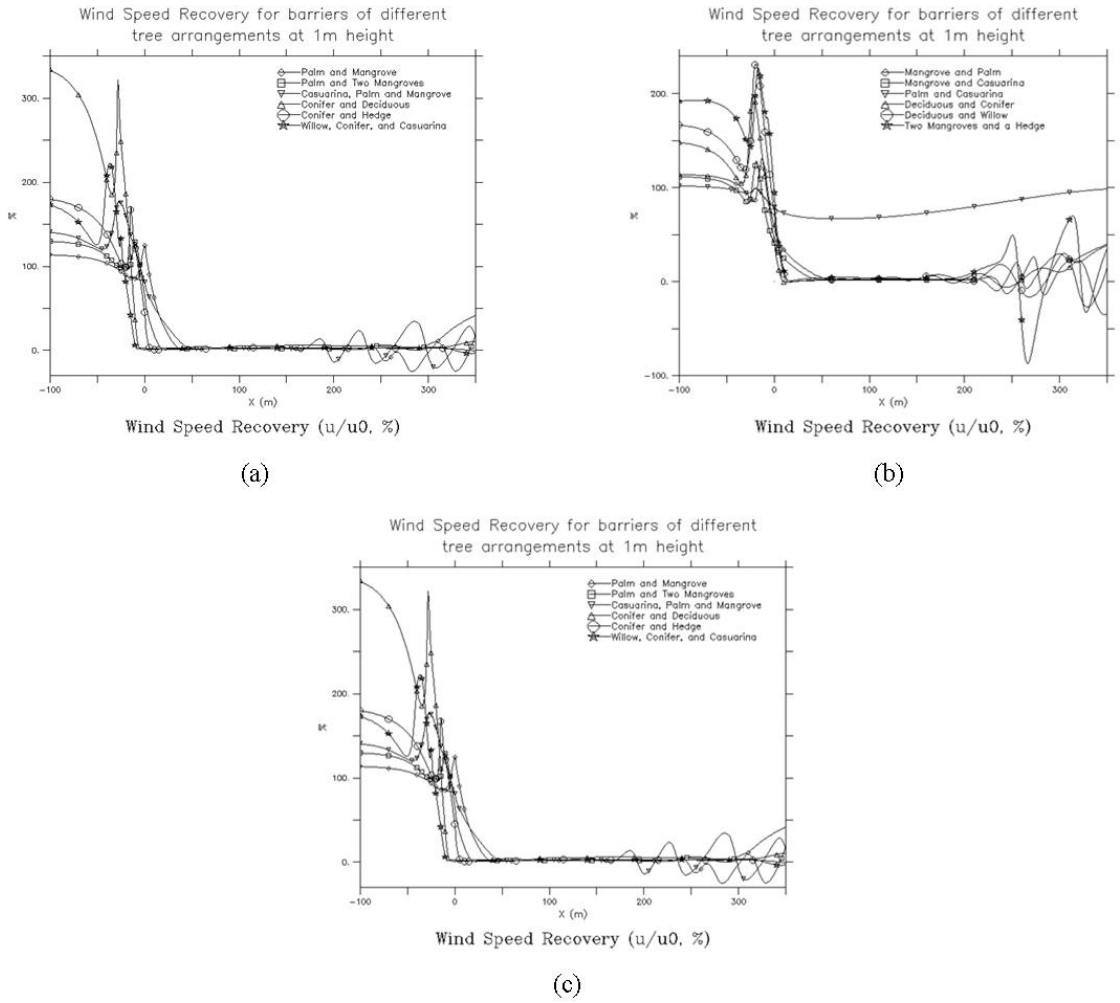

Figure 3.2 Horizontal wind speed recovery at 1 m height for all sixteen arrangements

Arrangements that had low trees were found to be the most effective at reducing the wind to zero near the surface. Figures 3.2a, b, and c show that the arrangements that only had casuarinas and palms did not reduce the wind completely (0% wind speed recovery) while all other arrangements did at 1 m. The other arrangements that did not have low trees (Conifer and Deciduous, Willow, Conifer and Casuarina, Deciduous and Conifer, and Deciduous and

Willow) all had the advantage of more dense trees and/or a Conifer, which is more dense and also has low foliage, in the arrangement. Figures 3.3a, b, and c show the same patterns at 3 m height. Combining trees does not lead to a linear combination of the protection that each

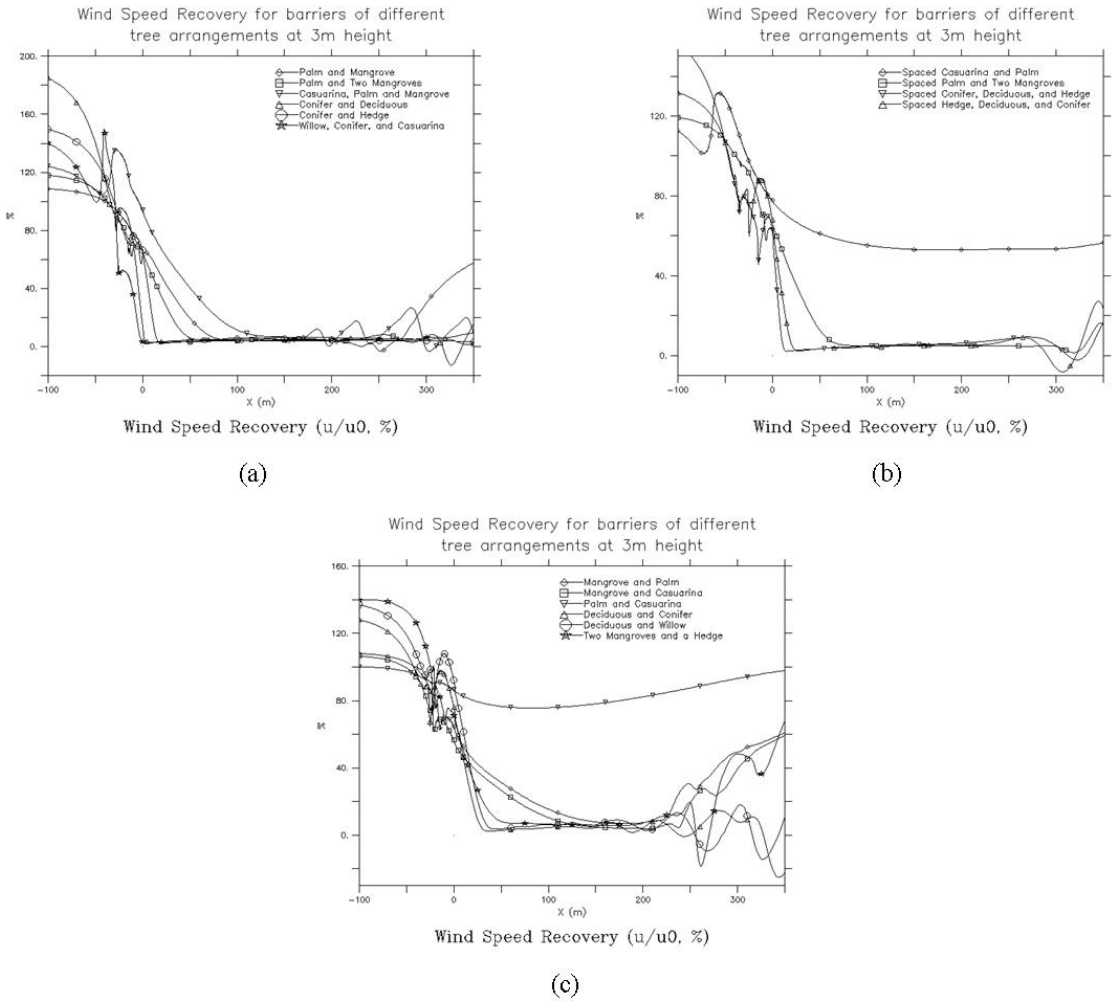

Figure 3.3 Horizontal wind speed recovery at 3 m height for all sixteen arrangements

individual tree provides. The arrangements of the palms and mangroves in Figures 3.4a, 3.5b, and 3.6a are a significant improvement over the single palm line in Figure 3.7a and the single mangrove line in Figure 3.7b. The amount of the protection is increased over the palm and the length of the protection is increased over the mangrove. When comparing the Palm and Mangrove arrangement with the Casuarina, Palm and Mangrove arrangement in Figures 3.2a,

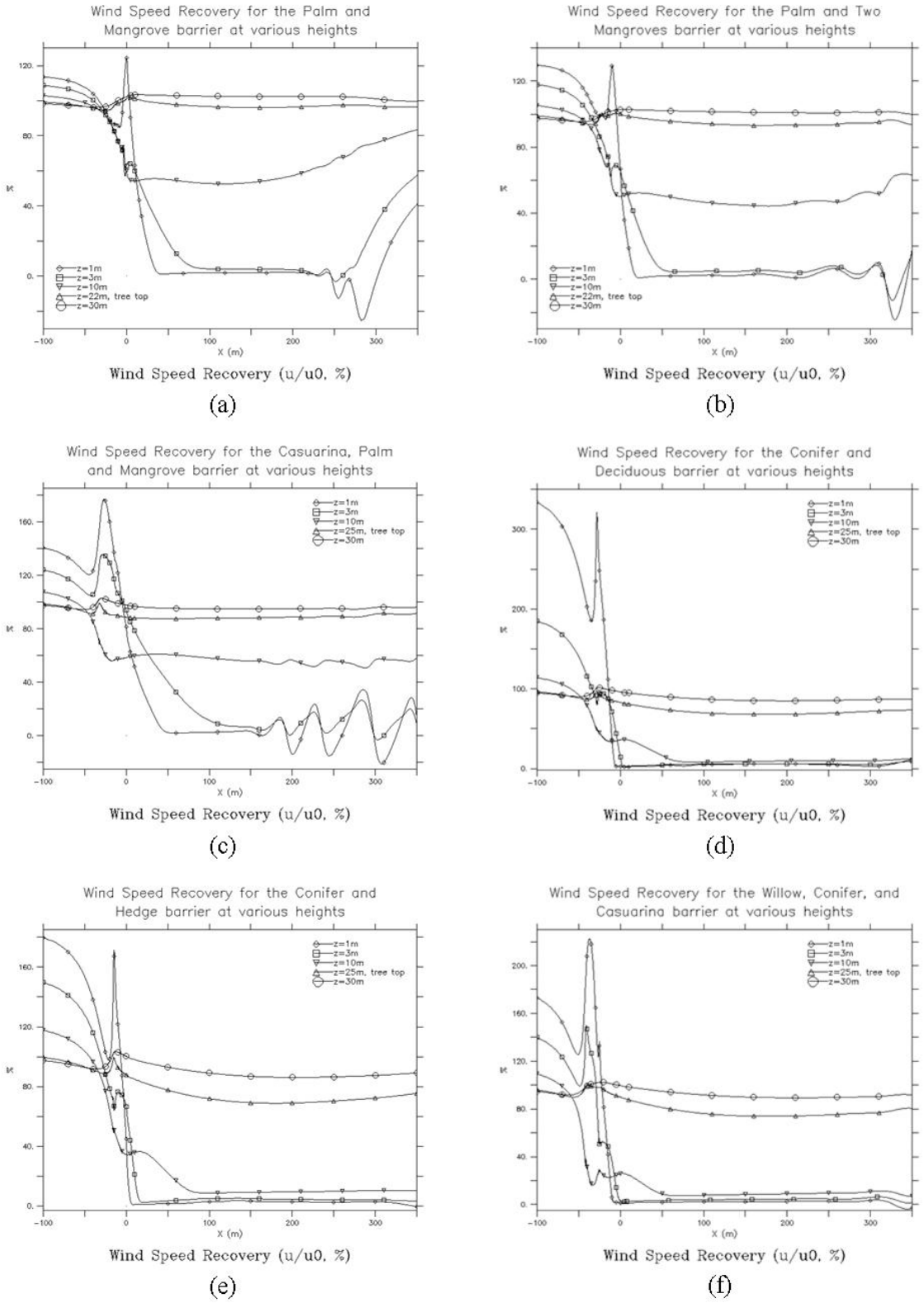

Figure 3.4 Horizontal wind speed recovery at five heights

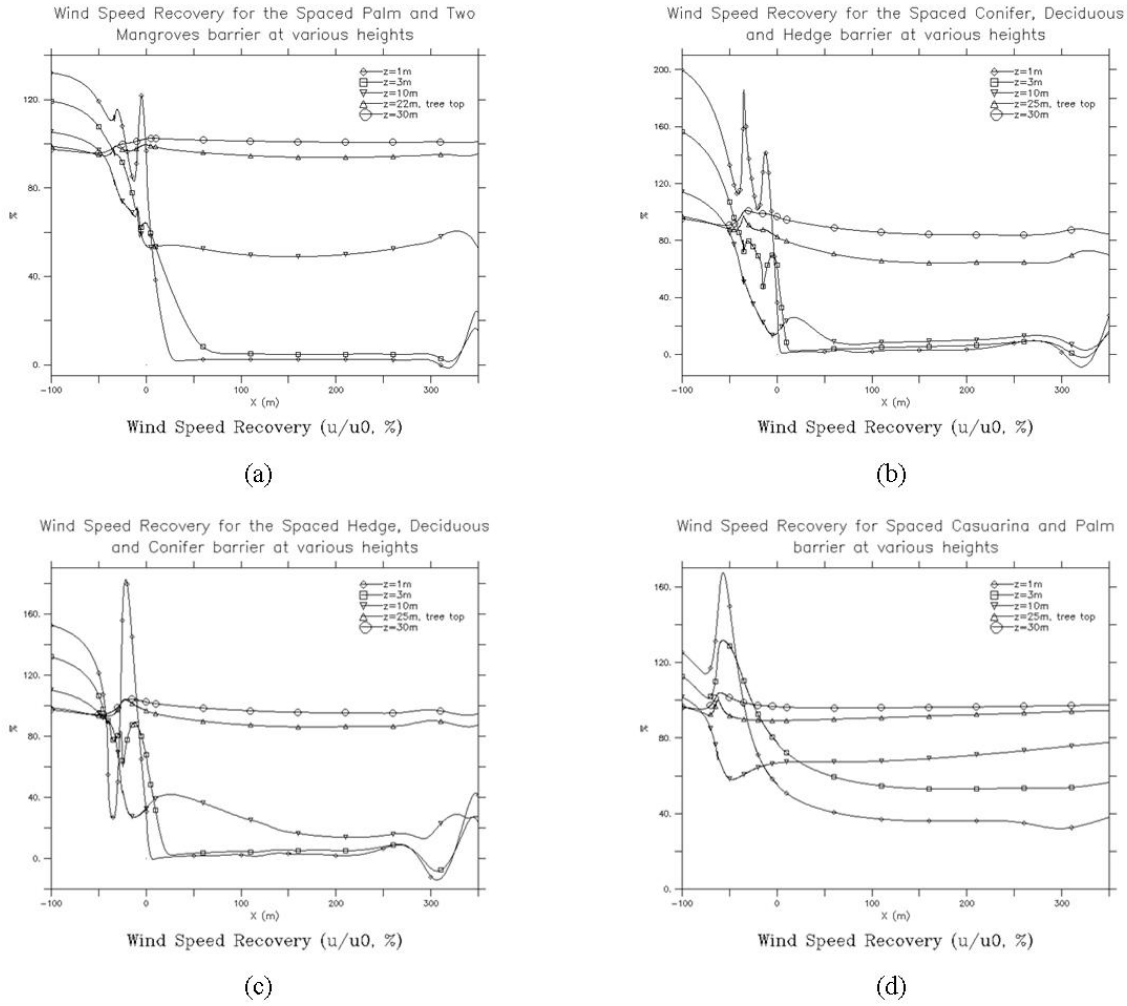

Figure 3.5 Horizontal wind speed recovery at five heights

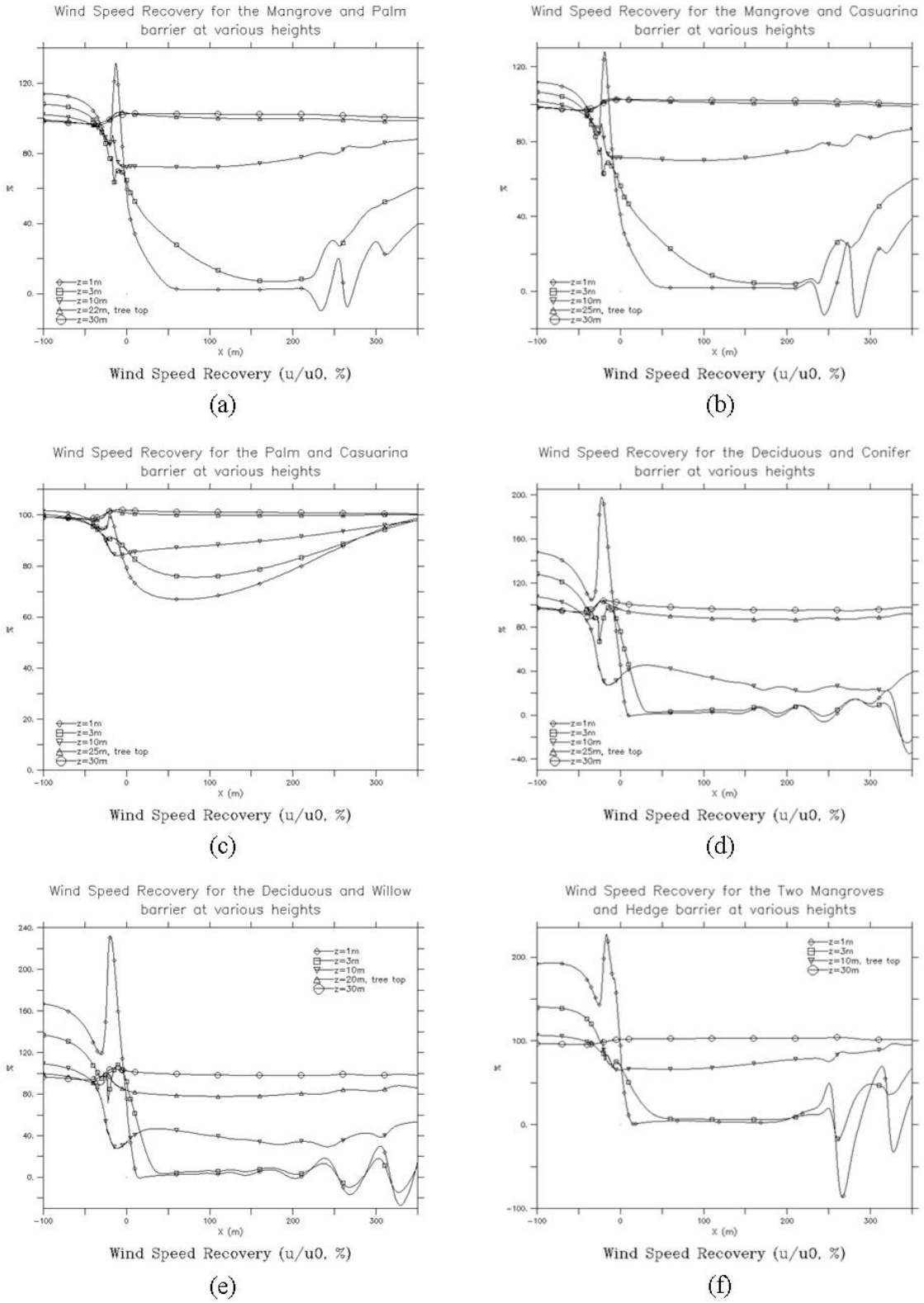

Figure 3.6 Horizontal wind speed recovery at five heights

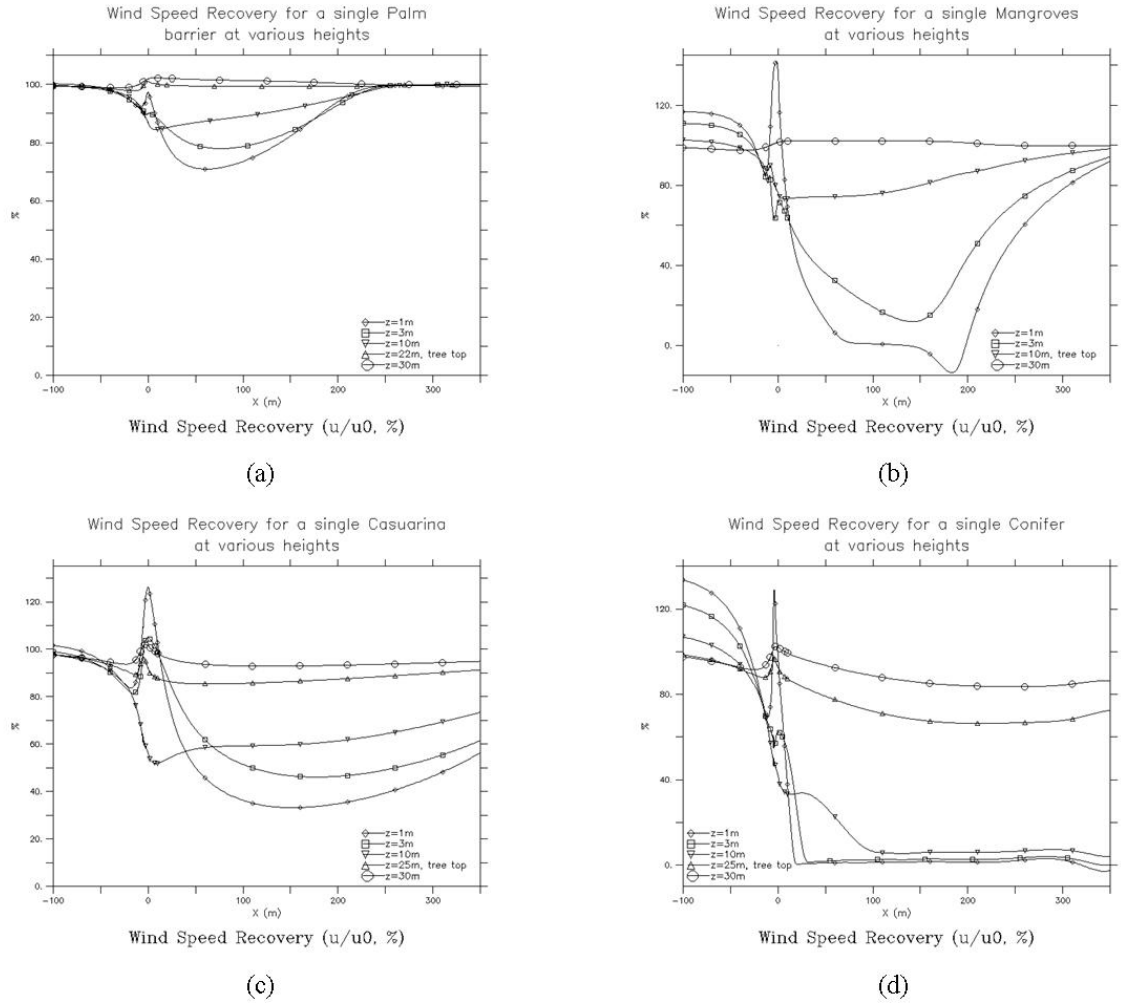

Figure 3.7 Horizontal wind speed recovery at five heights in the lee of the single tree shelterbelts

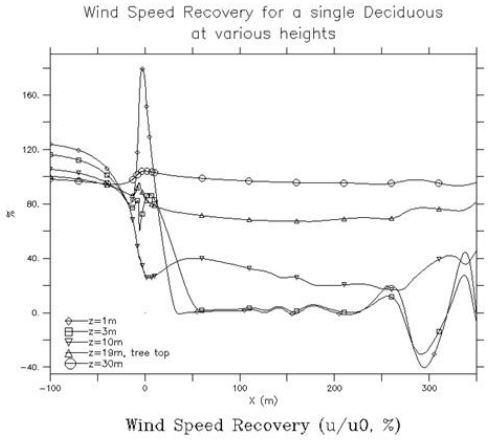

(d)

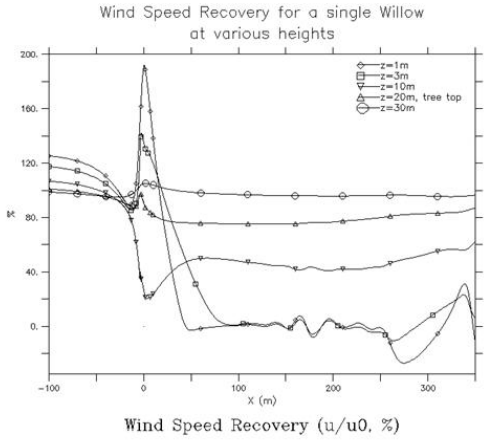

(f)

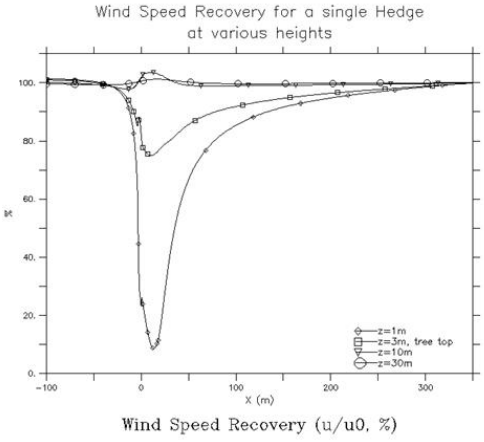

(g)

Figure 3.7 (Continued)

Horizontal wind speed recovery at five heights in the lee of the single tree shelterbelts

3.3a, and 3.8a it is shown that the addition of the casuarina deteriorates the effectiveness; it increases the distance to complete reduction near the surface and decreases the amount of protection at 10 m. The Deciduous and Willow arrangement in Figure 3.8c compared to the single deciduous and single willow in Figure 3.9c shows that the two-tree arrangement has less protection than the single line of deciduous but better protection than the single line of willows.

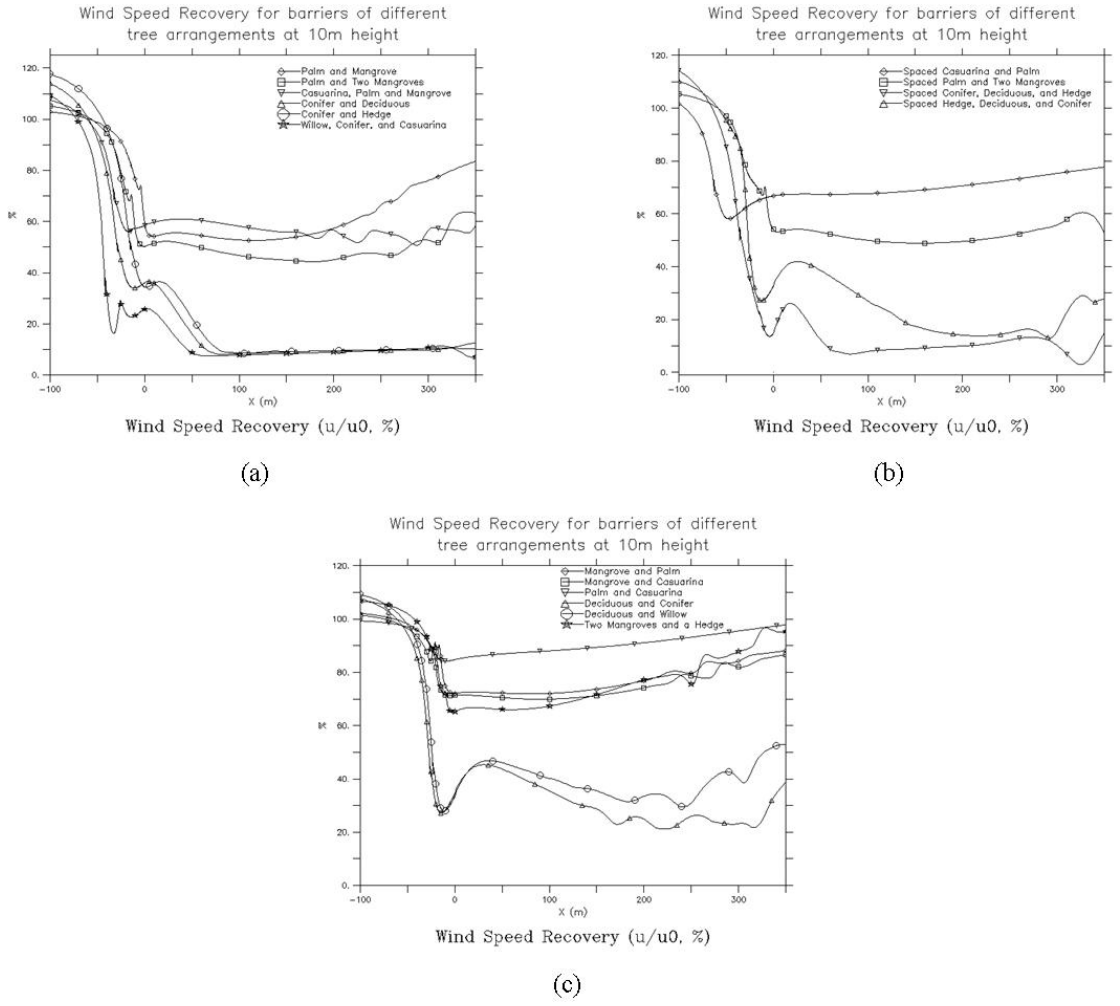

Figure 3.8 Horizontal wind speed recovery at 10 m height for all sixteen arrangements

The Conifer and Hedge arrangement in Figures 3.2a, 3.3a, and 3.8a compared with the single conifer line and the single hedge line in Figure 3.9, the addition of the hedge, which itself does not achieve complete reduction, improves the near lee reduction of the conifer alone. When

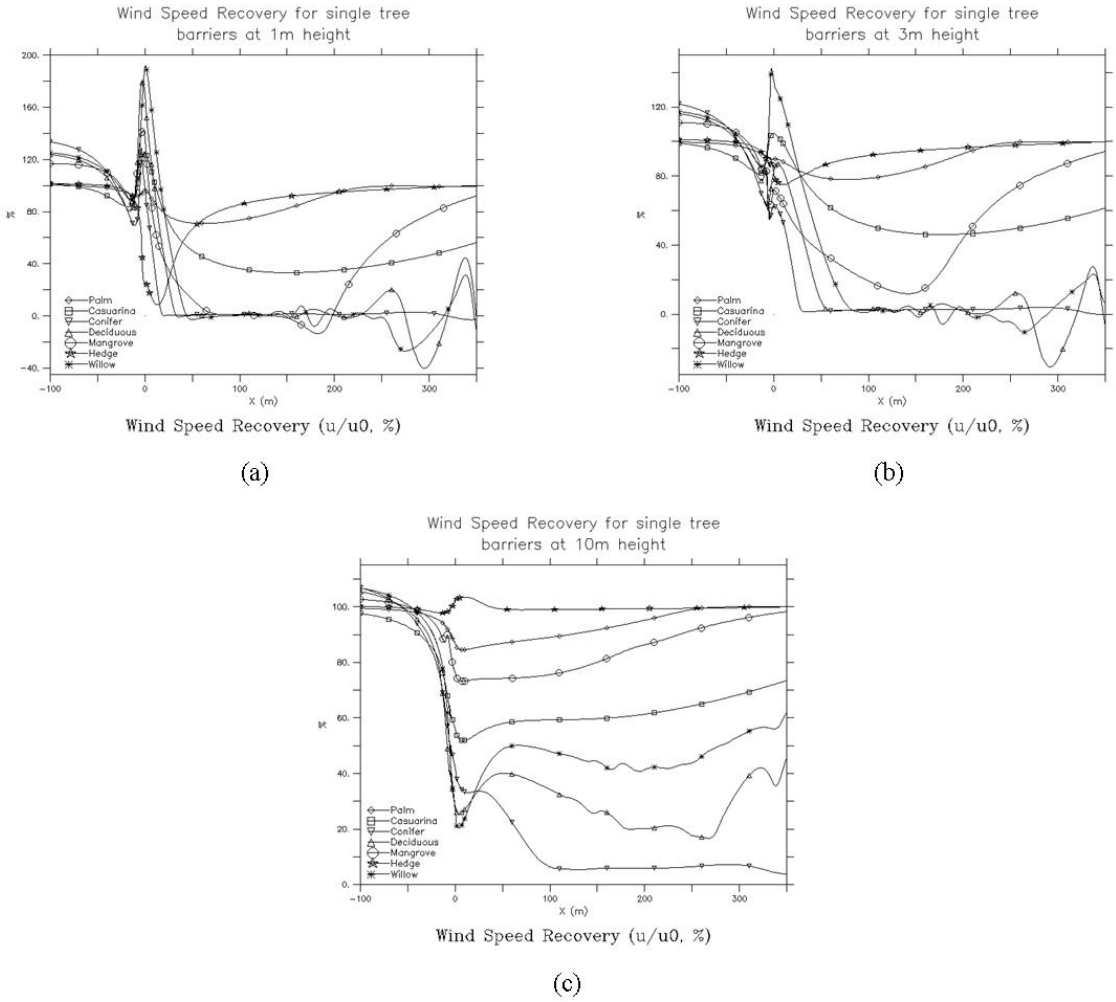

Figure 3.9 Horizontal wind speed recovery at 1 m, 3 m and 10 m heights for all seven individual trees

comparing the Casuarina and Palm arrangement in Figure 3.5a with the individual trees in Figures 3.7c and a, the amount of protection over all is most noticeably improved over the single line of casuarinas in the near lee; however, the addition of the palm still did not bring complete reduction. When comparing the two arrangements of the conifer, deciduous and hedge in Figures 3.5c and d, having the conifer to the windward side gives more reduction in the near lee at 10 m than to the leeward side. It could also be that having the short hedge to the leeward side gives better protection. Similarly, when comparing the Palm and Mangrove arrangement in Figure 3.4a to the Mangrove and Palm arrangement in Figure 3.6a, having the short mangrove to the leeward side gives better protection.

At 10 m there is a noticeable difference between the arrangements that have dense and/or low trees and those that do not, especially in abruptness of reduction, as seen in Figures 3.8a, b, and c. Examining the arrangements of a conifer paired with other trees as in Figures 3.4d, e, and f, 3.5c and d, and 3.6d and comparing it with the single line of conifers in Figure 3.7d it is obvious that the conifer is the dominant factor. The most significant improvement over the single line of conifers is that the rate to complete reduction is improved with the multiples trees. With the exception of the Spaced Hedge, Deciduous and Conifer arrangement, the three-tree arrangements have further improved near lee protection at 10 m than the two tree arrangements. The arrangements that have mangroves as their densest element or with no low trees do not at 10 m, if ever, achieve high amounts of reduction; note that none have 100% reduction. From examination of these plots it is apparent that the arrangements with the taller and denser trees on the windward side give the best amount of protection at 10 m. Similarly, when examining the two arrangements of the conifer, deciduous and hedge in Figures 3.2b, 3.3b, and 3.8b, the arrangement that has the conifer to the windward side has reduction that is larger and more abrupt.

When comparing the Palm and Casuarina arrangement in Figures 3.2c and 3.3c with the Spaced Casuarina and Palm arrangement in Figures 3.2b and 3.3b it is shown that the arrangement with more spacing and with the casuarina to the windward side is better in terms of the amount of protection as well as the length of the protected zone. Comparison of the Palm

and Mangrove arrangement with the Palm and Two Mangroves arrangement in Figures 3.2a and 3.3a shows that the addition of the second mangrove improves the length of protection. This can also be seen in Figures 3.4a and b. When comparing the Palm and Two Mangroves arrangement in Figure 3.4b with the Spaced Palm and Two Mangroves arrangement in Figure 3.5b, the added space between the palm and the mangroves does not provide any noticeable improvement in the amount of protection or the protected distance. The spaced arrangement does however have less recirculation in the far lee. Also, the Deciduous and Conifer arrangement in Figure 3.8c shows that the two tree arrangement gives less protection than either of the single trees as shown in Figure 3.9c. The length of protection is also reduced compared to the single line of conifers. When comparing the Casuarina and Palm arrangement in Figure 3.5a with the individual trees in Figures 3.7c and a, the length of protection is improved with the addition of the palm.

The plots in Figures 3.2 and 3.3a, b, and c also show that the arrangements without the low trees also have both quicker wind speed recovery and less wind speed reduction. The surface plots at 1 m in Figure 3.2 and at 3 m in Figure 3.3 arrangements with multiple dense trees and/or conifers show a much quicker reduction than the arrangements without. However, these also show that having any low element makes the reduction more abrupt. For example, comparing the Conifer and Hedge arrangement in Figures 3.2a, 3.3a, and 3.8a with the single Conifer in Figure 3.9, the addition of the hedge brings the point of complete reduction closer to the leeward edge of the shelterbelt. Also, comparing the Palm and Mangrove arrangement with the Palm and Two Mangroves arrangement in Figures 3.2a and 3.3a, it shows that the addition of the second mangrove quickens the reduction. When comparing the Deciduous and Conifer arrangement in Figure 3.6d and the Conifer and Deciduous arrangement in Figure 3.4d having the conifer to the windward side gives quicker reduction near the surface, as well as more reduction at 10 m.

3.6.2 Kinetic Energy

The destructive power of wind comes from transferring its kinetic energy into forces against the obstacles it interacts with. The total kinetic energy can be split up into mean and fluctuating, or mean and turbulent components (Stull, 1988). This is achieved by using the idea that an instantaneous field A, can be split up such that

$$A = \bar{A} + a' \tag{3.2}$$

where $\bar{A}$ is the mean value and a' is the fluctuating value.

3.6.2.1 Mean Kinetic Energy

The mean kinetic energy (MKE) is closely related to the wind speed. It is calculated using Equation 3.3

$$MKE = \frac{1}{2}\left(\bar{u}^2 + \bar{w}^2\right) \tag{3.3}$$

where $\bar{u}$ is the horizontal component of the wind and $\bar{w}$ is the vertical component of the wind. In general the plots for the wind speed recovery look very similar to the MKE plots only with different scaling. Because the MKE is driven by both the horizontal and vertical wind components the more different the MKE is from the wind speed recovery is an indication of how much the vertical winds are affecting the flow. Also, the MKE is a function of the square of the velocities, whereas the wind speed reduction in directly proportional to the horizontal velocity. Therefore, large effects on the velocity will be magnified in the MKE. Most of the higher values compared to the wind speed recovery occur within the shelterbelt since the trees are what are causing the most vertical motion in the winds. Also, because the values are squared there are no longer negative numbers representing the recirculating flow; rather the small, fairly even recirculations are smoothed out and the larger recirculations are represented as sinusoidal waves above the 0% line.

A noticeable difference from the wind speed recovery is the amount of reduction, particularly at 10 m. For example, comparing the MKE for the Palm and Mangrove arrangement in Figure 3.10a with the wind speed recovery for that arrangement Figure 3.4a, in the lee

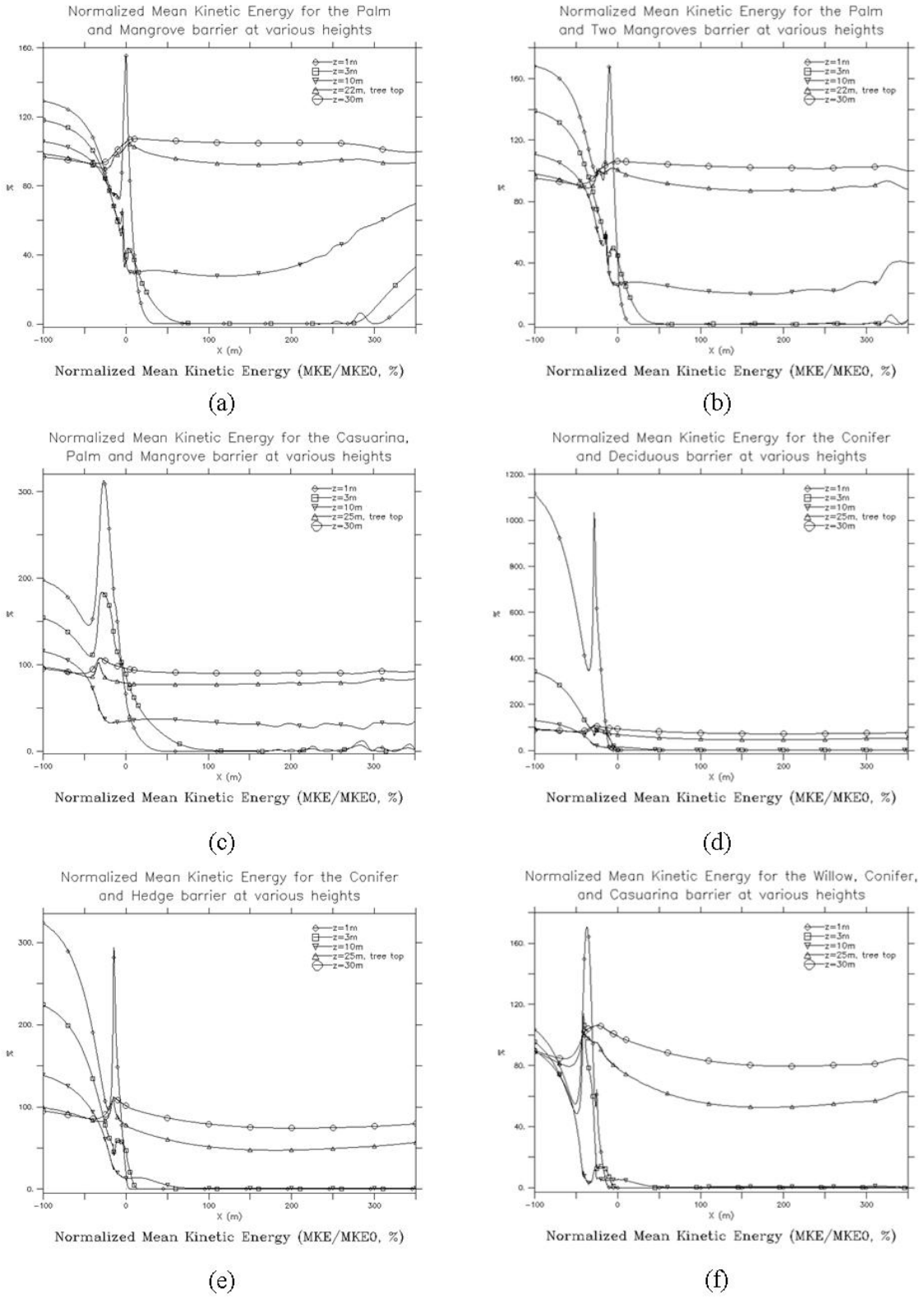

Figure 3.10 Normalized mean kinetic energy at five heights

the 10 m MKE is approximately 35% of the upstream value, while the wind speed recovery at 10 m is approximately 55% of the upstream value. Also, the lower heights have an initial near lee MKE value of approximately 35%, while the near lee wind speed recovery value is approximately 55%. This trend of up to 30% more reduction can be seen in comparing all the MKE plots in Figures 3.10, 3.11, and 3.12 with the wind speed recovery plots in Figures 3.4, 3.5, and 3.6. This same range of improvements is seen in all the arrangements, so the same observations from the wind speed recovery apply to the MKE plots as well.

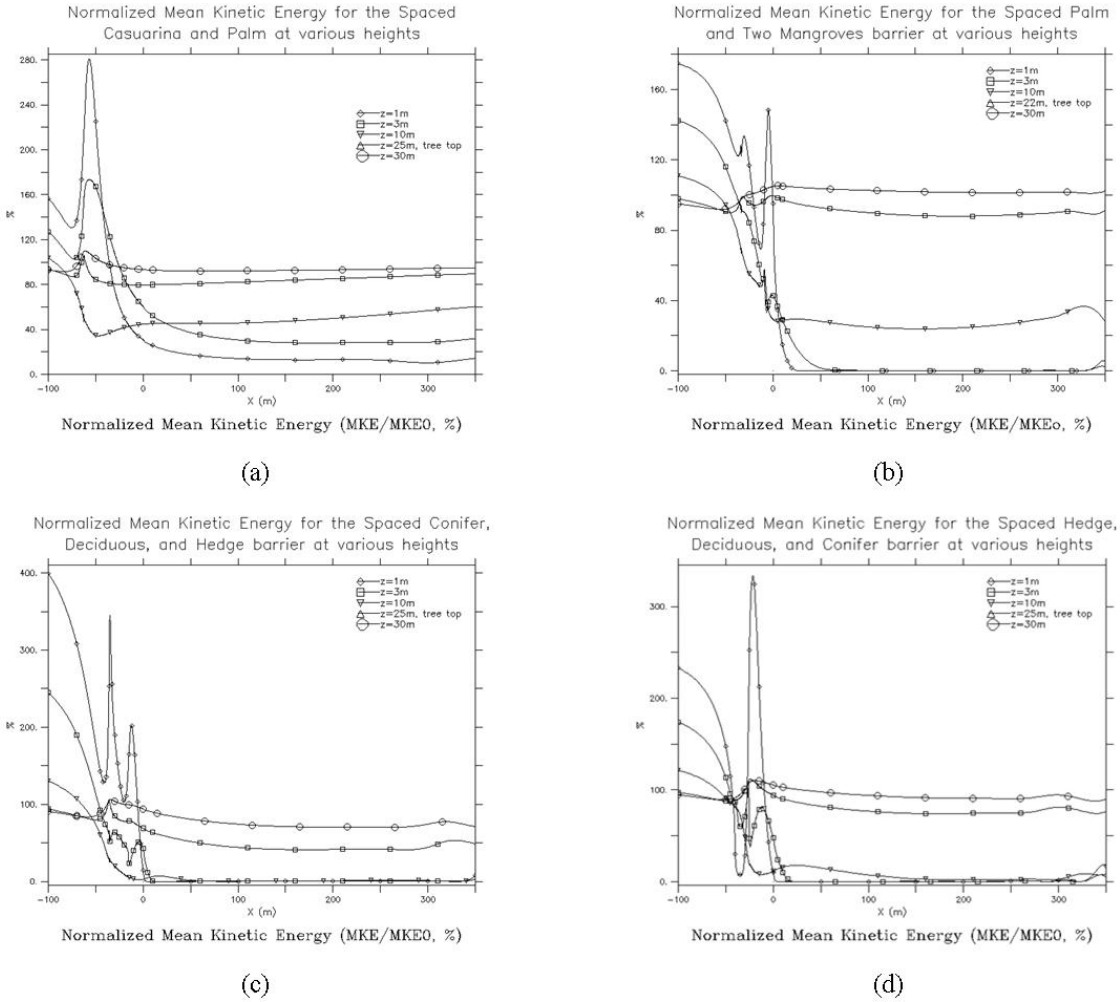

Figure 3.11 Normalized mean kinetic energy at five heights

The one arrangement that had decreased peak MKE values within the shelterbelt compared to the wind speed recovery was the Willow, Conifer and Casuarina arrangement in Figures 3.4f

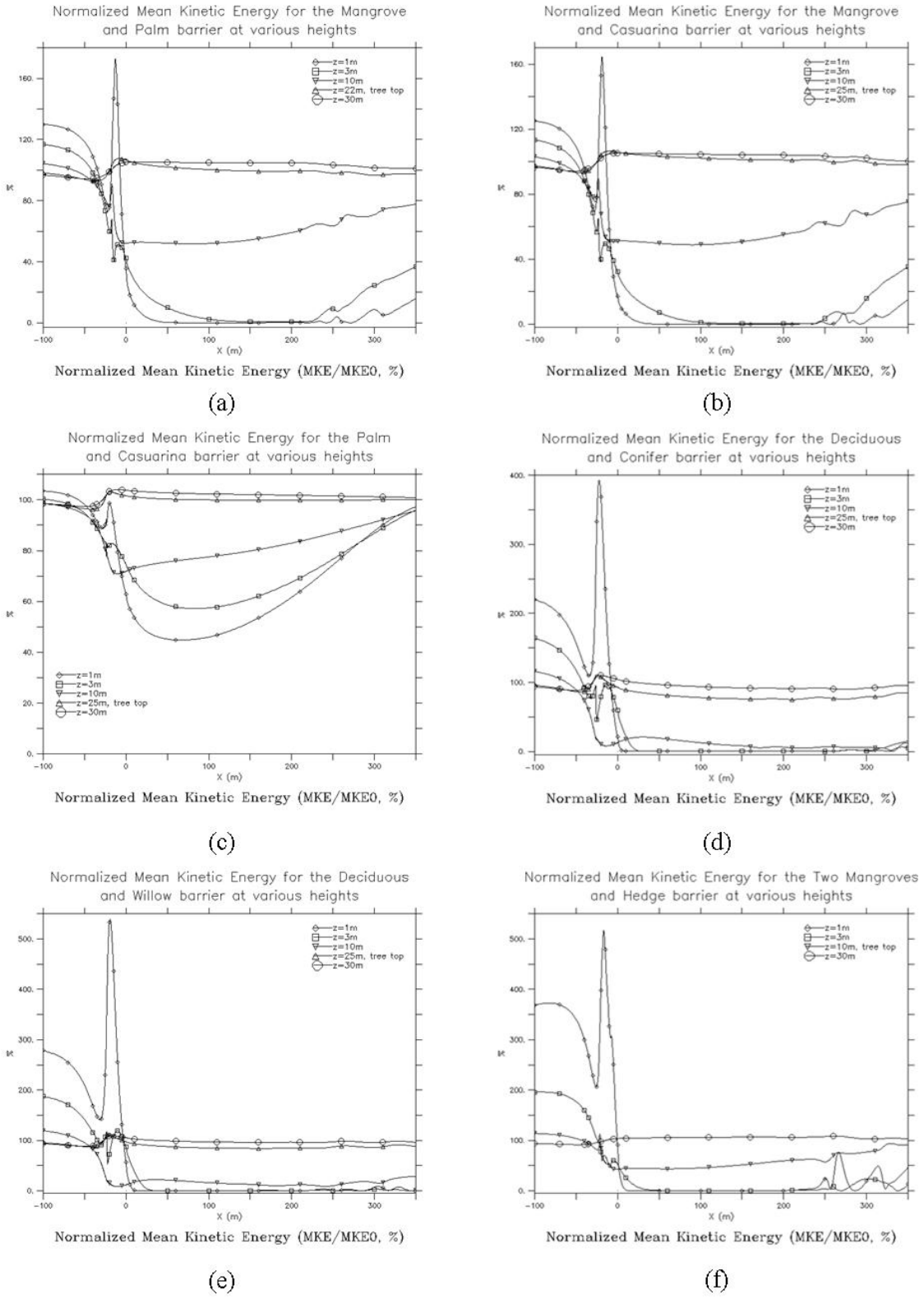

Figure 3.12 Normalized mean kinetic energy at five heights

and 3.10f which means that this arrangement has reduced vertical wind speeds within the shelterbelt. Conversely, the Conifer and Deciduous arrangement in Figures 3.4d and 3.10d has a large increase in MKE peak over the wind speed recovery peak, which means that there is a significant amount of vertical winds produced within this arrangement.

3.6.2.2 Turbulent Kinetic Energy

The peak values of the fluctuating part of the wind can be more damaging than the mean wind even though they occur for a shorter period of time if they are strong enough. The effect of these peak values of the wind can studied from the turbulent kinetic energy (TKE), which is calculated using Equation 3.4

$$TKE = \frac{1}{2}\left(u'^2 + w'^2\right) \tag{3.4}$$

where u' is the horizontal fluctuating part of the wind, and w' is the vertical fluctuating part of the wind. Therefore, another measure of protection is the location of the increased values of TKE; or where the normalized TKE is greater than 100%.

The most noticeable trend with the TKE is that any arrangement with short trees has significantly less TKE produced than arrangements without low foliage. Figures 3.13b and c and Figures 3.14b and c show that near the surface the arrangements of only casuarinas and palms do not give as much protection as the other arrangements that have low elements. In fact, these arrangements result in only a slight reduction in TKE compared to the other arrangements that completely eliminate the TKE. Figures 3.15a and 3.16c show that the Spaced Casuarina and Palm only gives approximately 50% reduction at best and the Palm and Casuarina only gives approximately 15% reduction at best. While having low elements is an overall improvement, arrangements that have shorter elements have more TKE production in the very near lee, as can be seen in Figures 3.13a and 3.14a. These plots show that the arrangements that have the mangroves and hedges have TKE production in the near lee while the arrangements that have the conifer as the low element have complete TKE reduction at the leeward edge of the shelterbelt. The addition of a second low element does reduce the TKE production as can be seen in the arrangement of the Palm and Two Mangroves where it has

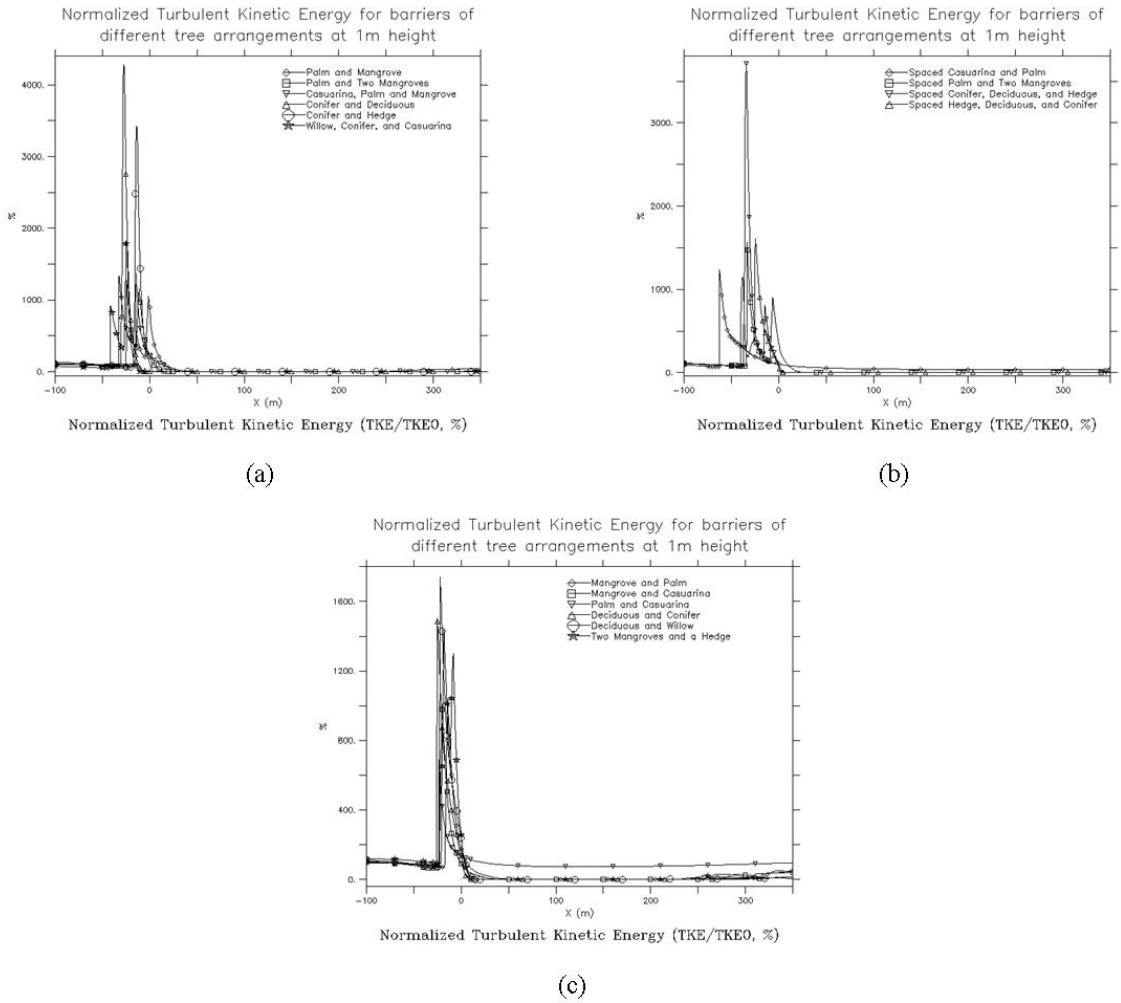

Figure 3.13 Normalized turbulent kinetic energy at 1 m height for all sixteen arrangements

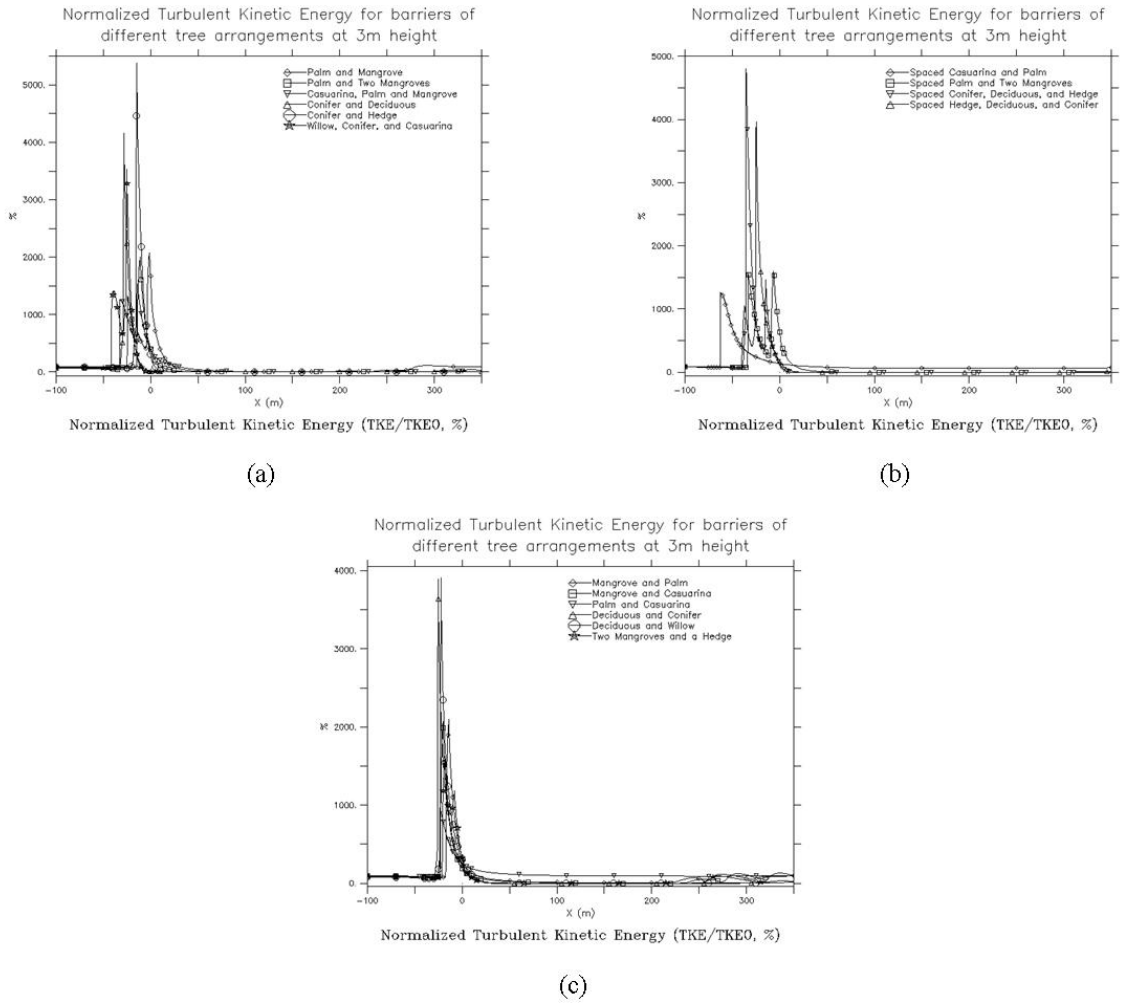

Figure 3.14 Normalized turbulent kinetic energy at 3 m height for all sixteen arrangements

less TKE produced than the arrangement with just the one mangrove, as seen in Figures 3.13a and 3.14a and Figures 3.17a and b.

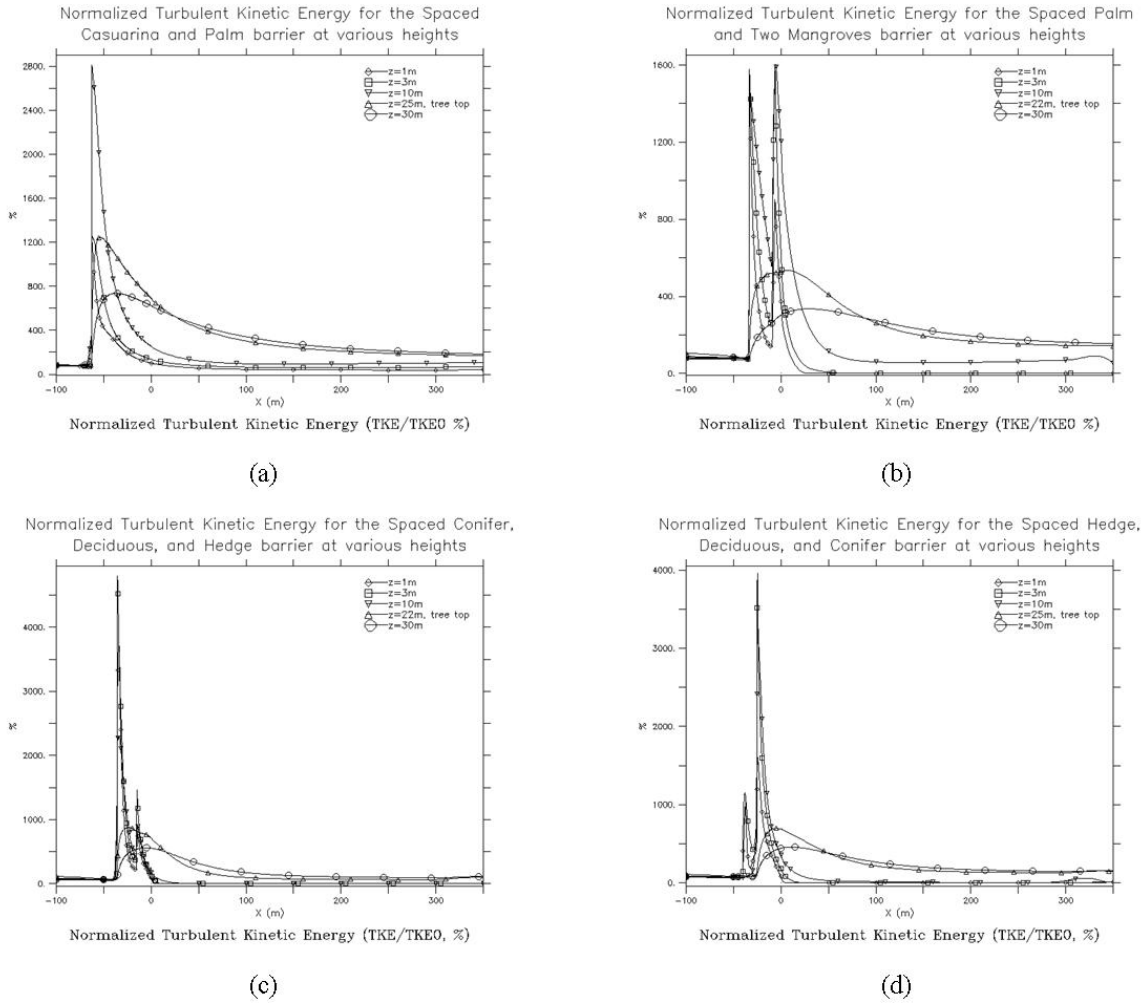

Figure 3.15 Normalized turbulent kinetic energy at five heights

Examining Figures 3.13, 3.14 and 3.18 shows that of the arrangements that do reach complete reduction, those with mangroves are the slowest to achieve this while arrangements with conifers are the quickest. For example in Figure 3.13b the Palm and Two Mangroves arrangement does not reach complete reduction until approximately 1.2H while the two arrangements of conifers, deciduous and hedges reach complete reduction at approximately 0.2H. Also, Figure 3.13a shows that the three arrangements that have conifers are completely reduced within approximately 0.4H while the other arrangements take up to approximately 2H to completely

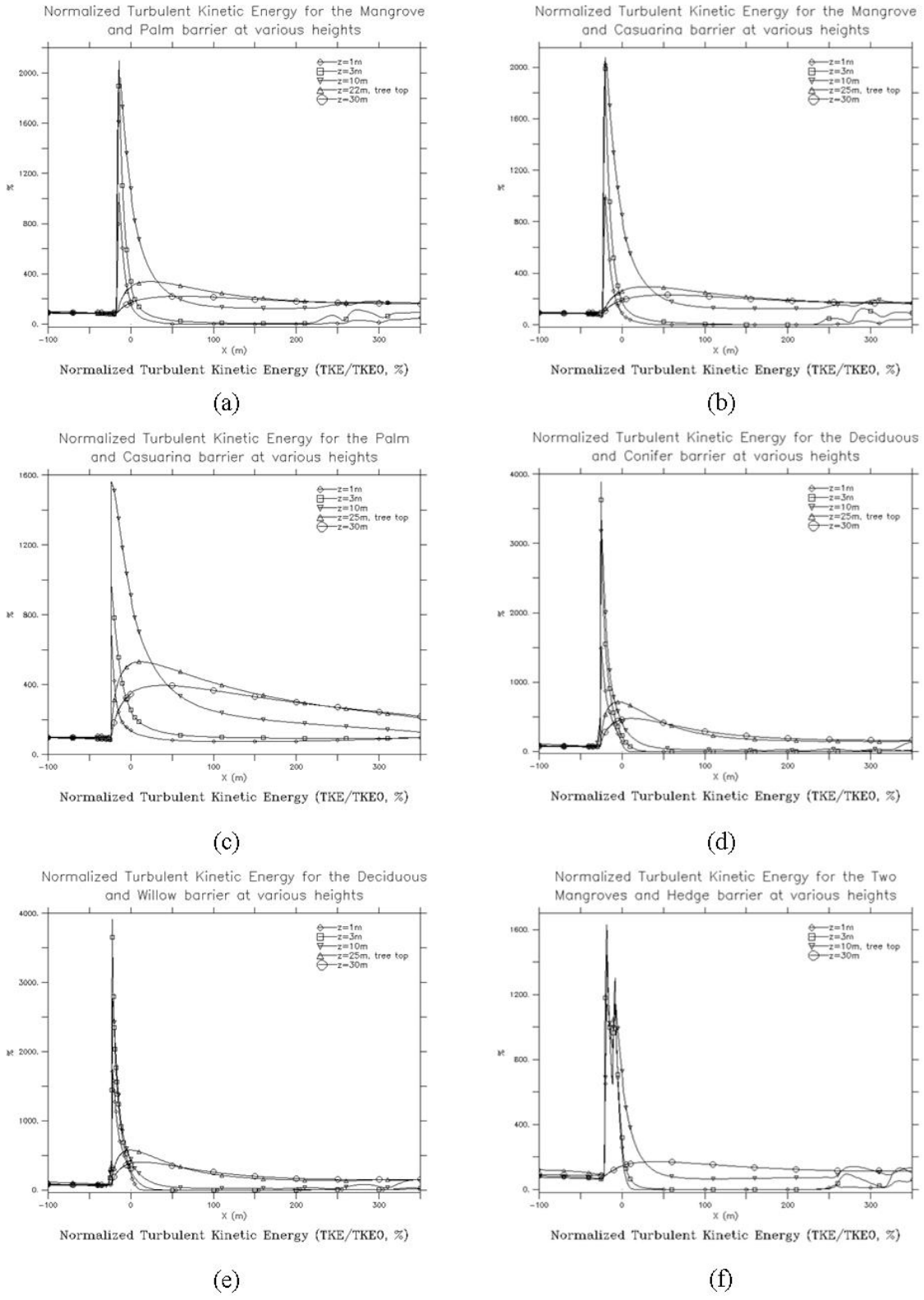

Figure 3.16 Normalized turbulent kinetic energy at five heights

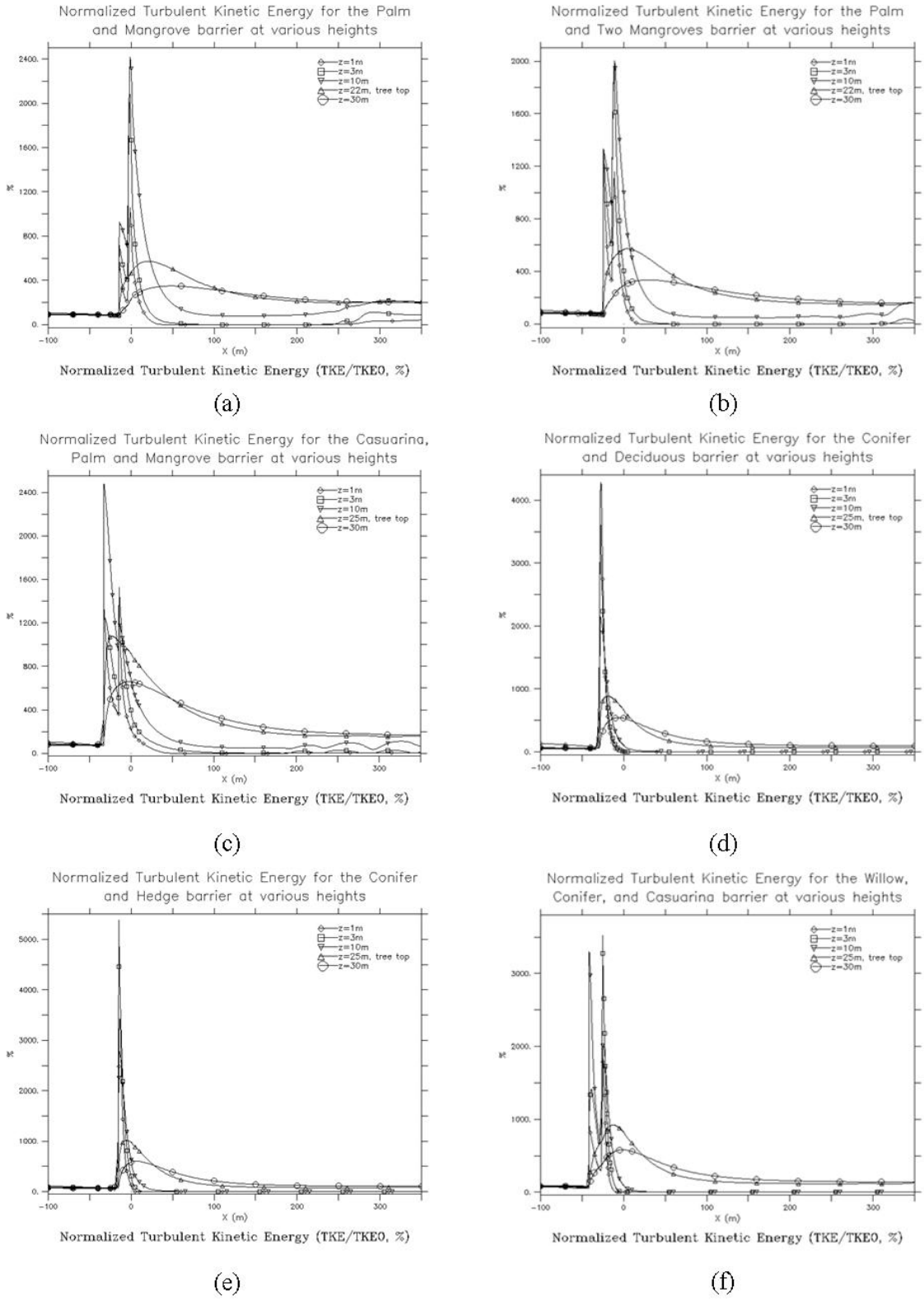

Figure 3.17 Normalized turbulent kinetic energy at five heights

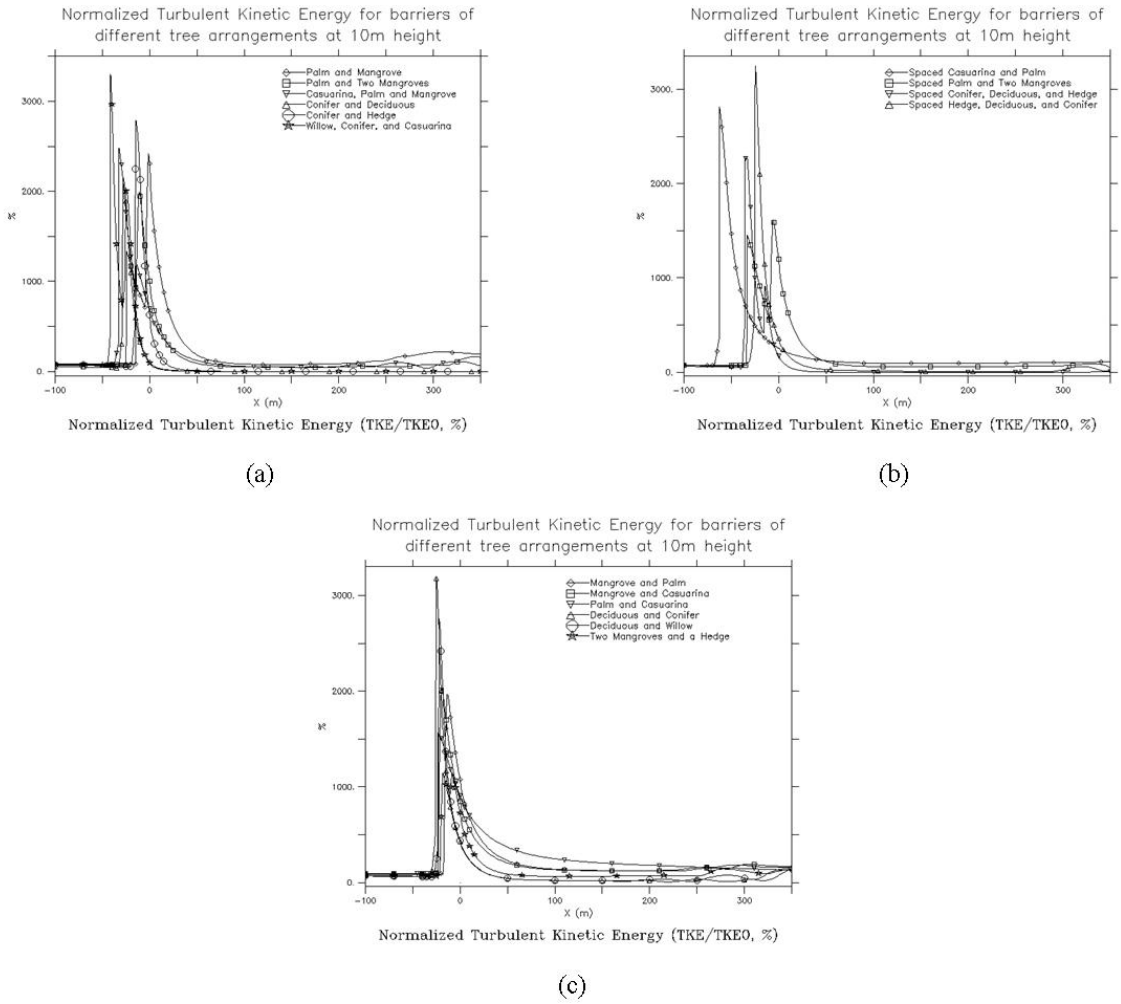

Figure 3.18 Normalized turbulent kinetic energy at 10 m height for all sixteen arrangements

reduce the TKE. When comparing the Palm and Mangrove arrangement in Figures 3.13a, 3.14a, and 3.18a to the Mangrove and Palm arrangement in Figures 3.13c, 3.14c, and 3.18c having the shorter mangrove to the leeward side has quicker reduction. This is also seen when comparing these arrangements in Figures 3.17a and 3.16a. Similarly, comparing the two conifer, deciduous, and hedge arrangements in Figures 3.14b and 3.18b shows that having the shorter hedge to the leeward side gives complete reduction quicker.

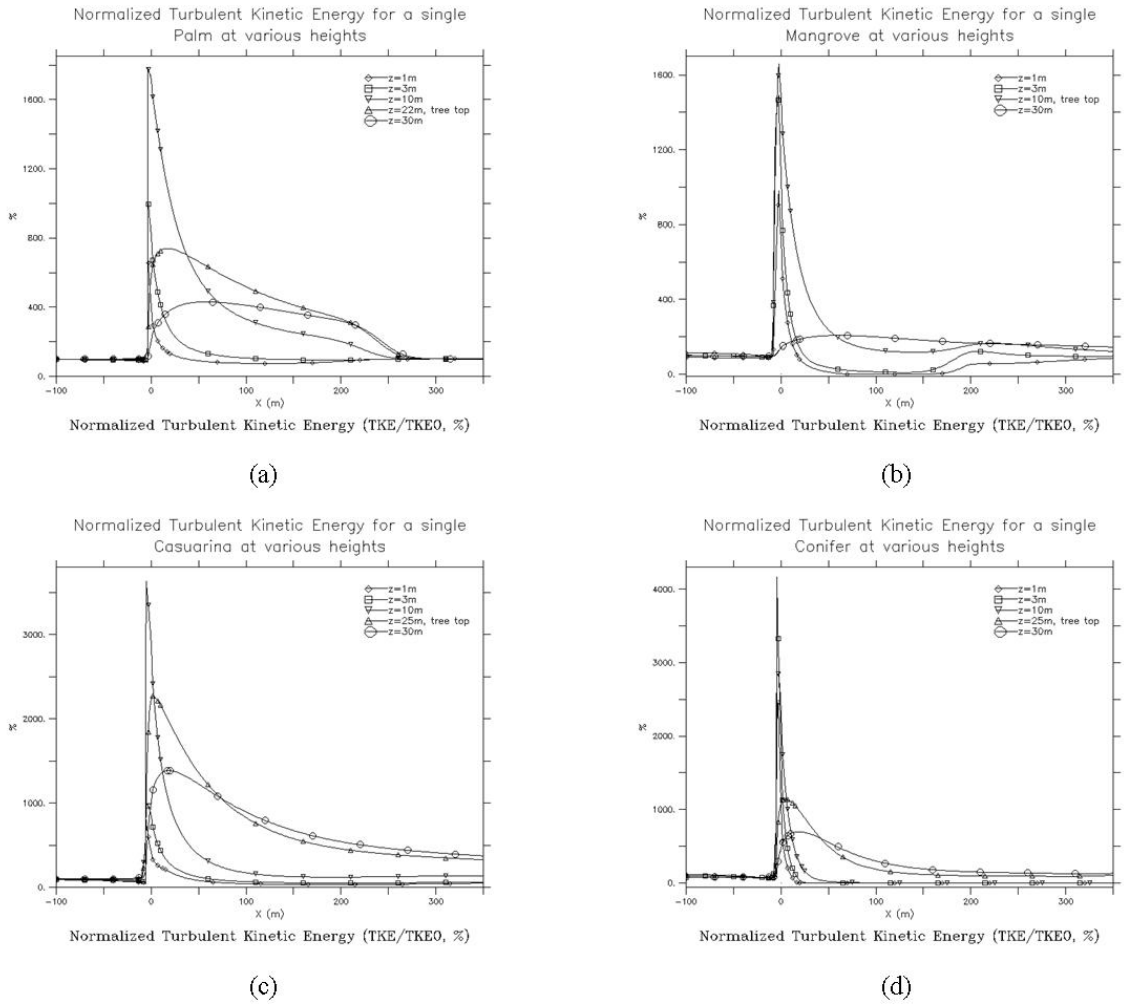

Figure 3.19 Normalized turbulent kinetic energy at five heights for the single tree shelterbelts

As with the wind speed reduction, the effect of the individual tree lines on the TKE does not add linearly. Having multiple tree lines is always an improvement over any single tree line.

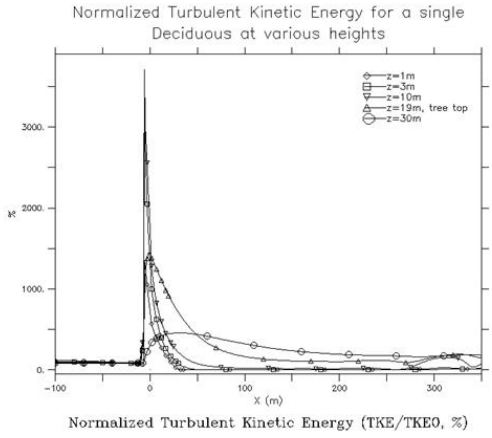

(e)

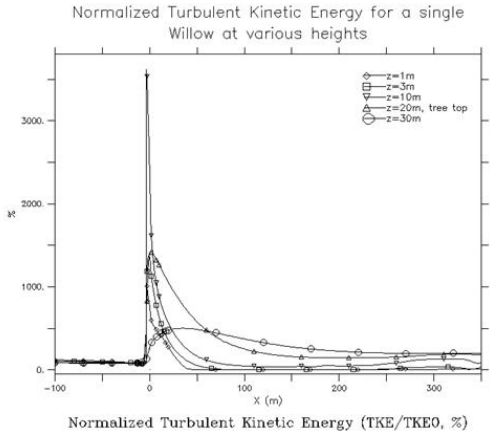

(f)

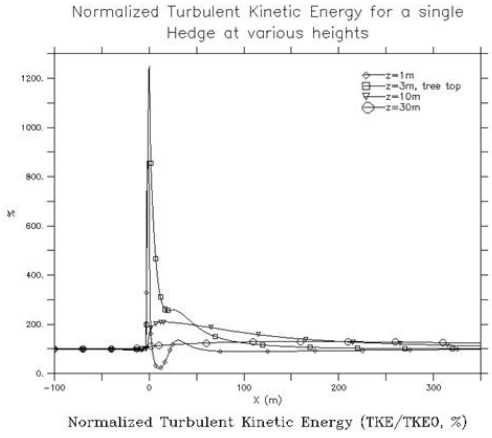

(g)

Figure 3.19 (Continued)

Normalized turbulent kinetic energy at five heights for the single tree shelterbelts

A single mangrove line does reach complete reduction of TKE, but only for a comparatively short while, as seen in Figure 3.19b; and the single palm line does not ever reach complete reduction as seen in Figure 3.19a. Comparing these with the Palm and Mangrove arrangement in Figure 3.17a and the Mangrove and Palm arrangement in Figure 3.16a shows that pairing the mangrove with the palm increases the length of complete reduction over either single tree line. Similarly, while a hedge line alone does not completely reduce the TKE, as shown in Figure 3.19g, when comparing the single conifer line in Figure 3.19d with the Conifer and Hedge arrangement in Figure 3.17e it can be seen that the addition of the hedge line quickens the time to complete reduction. Also, adding a mangrove line to a casuarina line, as in Figure 3.16e, compared to just a single casuarina line, as in Figure 3.19c, brings the reduction down all the way to 100%, however adding the mangrove line also adds recirculation to the flow reducing the long range effectiveness.

3.7 Conclusions

Arrangements that had low trees were found to be the most effective at completely eliminating the wind near the surface as well as reducing the TKE produced as shown in Figures 3.2, 3.3, 3.13 and 3.14. Arrangements without low trees, such as the Casuarina, Palm and Mangrove have increased wind speeds in the near lee suggesting that jetting below the trees' crowns is influencing the flow, where low trees would have reduced this jet. Also, having multiple low elements improves the length of protection for the wind speed as well as the TKE, as found when comparing the Palm and Mangrove arrangement with the Palm and Two Mangroves arrangement.

It was also found that having the taller trees to the windward side, or the shorter trees to the leeward side, is better for both abruptness and magnitude of wind speed reduction as well as the reduction of TKE production. Since the wind speed reduction and the TKE are the driving forces behind the MKE and the total kinetic energy respectively, these trends are applicable for determining that the mean and total forces on the buildings would be reduced most effectively with the taller trees being windward and the short trees being leeward.

It was also found that combining trees does not lead to a linear combination of the protection that each individual tree provides. In all cases, having more than one line of trees improved the amount of protection from the wind speeds and the protected distance, as well as reducing the amount of TKE produced. In terms of wind speed reduction it was found that the conifer is the dominant factor in arrangements where one is present. More generally it was found that arrangements with multiple dense trees had a protected zone that started closer to the leeward edge of the shelterbelt. It was also found that the added space between the lines of the palm and mangrove arrangement did not appreciably improve the amount of protection; however it did reduce the amount wind speed recovery in the far lee.

The magnitude of the leeward values of kinetic energy is an indicator of the amount of protection the shelterbelt provides because the lower the values indicates less energy present at those levels behind the shelterbelt, meaning less energy to be transmitted to the structures to damage them while higher values are diverted above the shelter, and, consequently the structures behind the shelter. When studying the MKE it was found that the MKE was reduced by up to approximately 30% more than just the mean horizontal wind, for all arrangements.

CHAPTER 4. EXPERIMENTAL STUDIES

4.1 Introduction

Lessons learned from the numerical modeling were combined with other researchers' results and then taken into the wind tunnel to experimentally test how the loads on buildings were changed due to the presence of the shelterbelts. Because accurately modeling of trees in a wind tunnel is extremely difficult, the convention of using porous screens was determined to be the best option. Seven screens, of five different porosities and three different heights, were used to test the effect of barrier height and porosity on wind loads exerted on a building placed downstream of the fence. These fences were tested at different distances in front of a one-story or a two-story building model on which force measurements were made. Tests were also conducted with a small deflector attached to the top of the screen in an attempt to give an angle to the flow to carry it over the building.

To determine the best combination of variables the first set of tests varied both the porosity of the screens and the spacing between the screen and the building models. A wide range of porosity values was chosen based on both actual tree values and previous studies' findings of optimal porosities. Because trees are relatively porous the higher porosity values represented the trees. The lower porosity values were based on the generally accepted range of most effective porosity, 20% to 50% (N*ö*kkentved 1938; N*ä*geli, 1946; Jensen, 1954; Blenk and Trienes, 1956; Tani, 1958; Schultz and Kelly, 1960; Marshall, 1967; Skidmore and Hagen, 1970a, b; Raine and Stevenson, 1977; Tillie, 1992).

When considering the range for the spacing between the screen and the building model, the separation bubble created by the screen was a major consideration. Also, research done by Dierickx et al. (2001) found that near the surface the highest reduction of wind speeds was

near 10H, where H represents the screen height; therefore this distance was included.

Because the relationship of the fence height to the protected distance downstream of the fence has been well established, as discussed in the numerical work, only a few heights were chosen to test. They were chosen to represent typical surroundings of low-rise buildings, specifically fences and trees.

Additionally, a deflector was added to the top of one screen to determine the effectiveness of using such a device to lift the flow higher over the low-rise buildings studied here.

4.2 Wind Tunnel and Measurement Setup

4.2.1 Coastal Boundary Layer

For these tests the flow was designed to simulate a coastal atmospheric boundary layer. This was achieved by using roughness elements in the fetch of the atmospheric boundary layer test section of the wind tunnel. The design of the roughness elements was done by Jones (2008). The roughness was chosen in order to match the standard boundary layer velocity profile for coastal settings. The roughness elements used were 28 rows of 0.5 in thick chain spaced 17 in apart starting 6 ft from the center of the model and extending back down the length of the fetch; three spires with a base to height ratio of 0.1107, that were 0.5625 ft wide at the base and 5.1 ft tall were installed at the beginning of the fetch that is 50 ft long. There was also a 12 in tall wall attached to the front side of the spires. The mean velocity profile that the roughness created is shown in Figure 4.1. A power law can be defined to describe the mean velocity profile as shown in Equation 4.1.

$$\frac{U(z)}{U(z_g)} = \left(\frac{z}{z_g}\right)^{\alpha} \tag{4.1}$$

where U is the mean wind speed at the level z or z_g and α is a constant, with z_g and α dependent on the terrain. z_g is the gradient height above which the velocity is taken as constant with height. The α for the coastal terrain in the wind tunnel was determined to be 0.13. Another measure of terrain profiles is the turbulence intensity; for the coastal terrain the turbulence intensity profile is shown in Figure 4.2. The boundary layer profile was matched

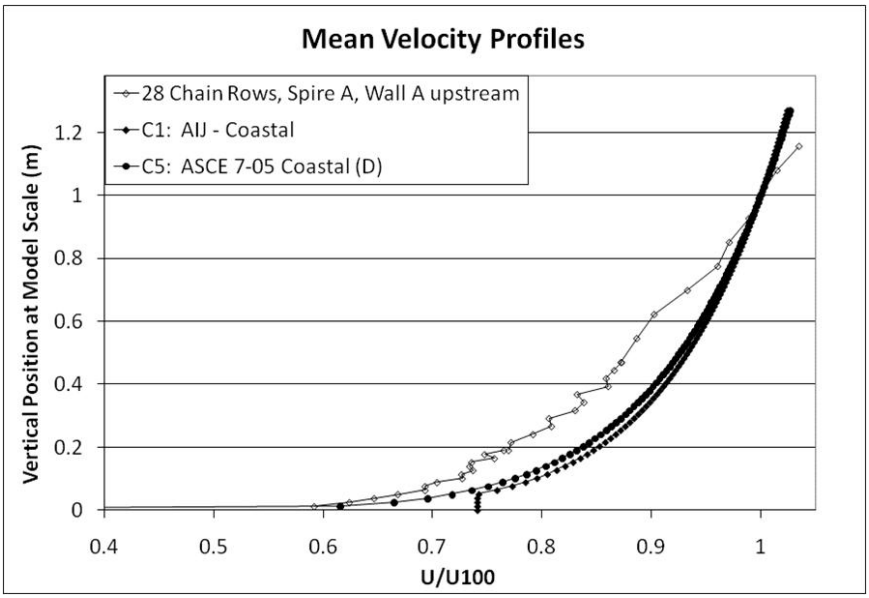

Figure 4.1 Coastal mean velocity profile created in AABL wind tunnel and the standard AIJ (1996) and ASCE 7-05 (2005) coastal wind profiles

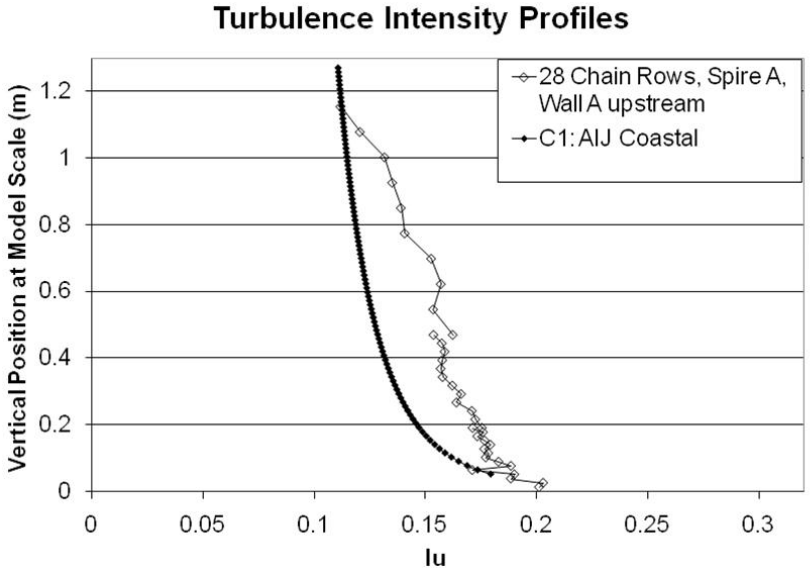

Figure 4.2 Coastal turbulence intensity profile created in AABL wind tunnel and the standard AIJ (1996) coastal turbulence intensity profile

based on a 1:100 length scale. The roughness elements can be seen in Figure 4.3.

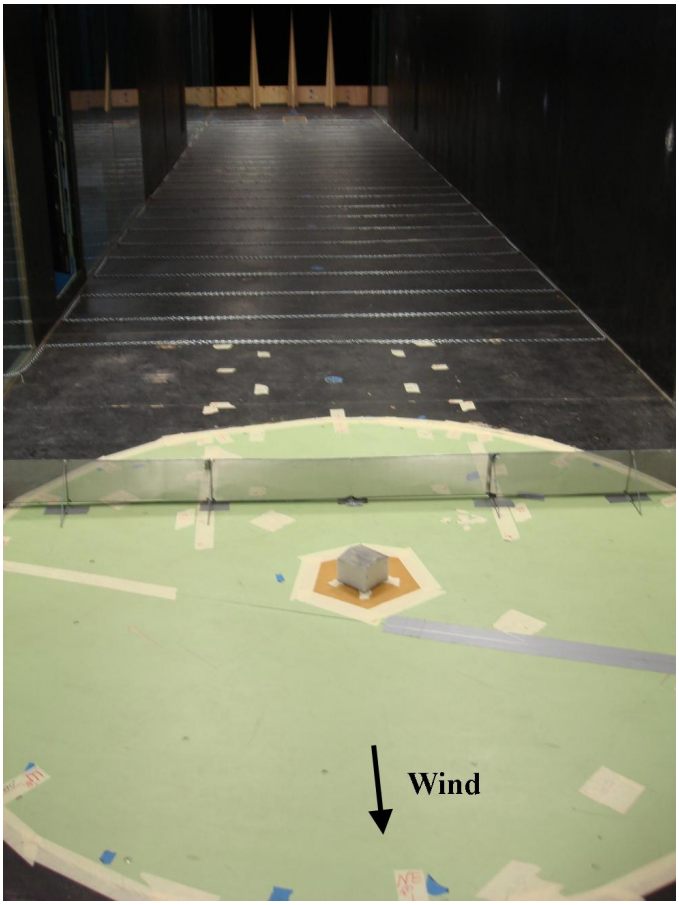

Figure 4.3 House model and fence orientation

4.2.2 Building and Fence Models

A one story and a two story building models of a typical gable roof home with a roof pitch angle of 13.7° were used. The full-scale dimensions of the houses were 9.14 m (l) by 9.14 m (b), 3.05 m (h) tall for the one story and 6.10 m (h) for two story. The models were hollow plastic structures that were sealed on the bottom.

For rigidity, the fences were made of screens affixed to a thin wire frame with supports as seen in Figure 4.4. The fences spanned across the entire width of the wind tunnel, as seen in Figure 4.5, so that there would be no edge effects. The screens were chosen based on their manufacturer specified porosity. Figure 4.6 shows pictures of the screens used.

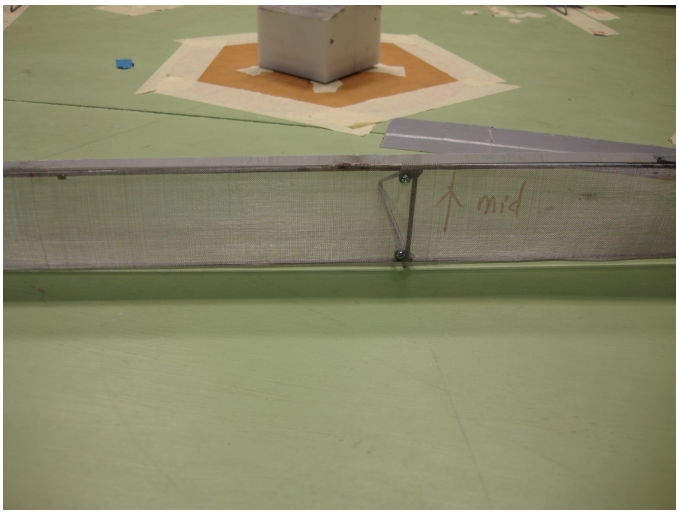

Figure 4.4 Screen and frame structure of the fence

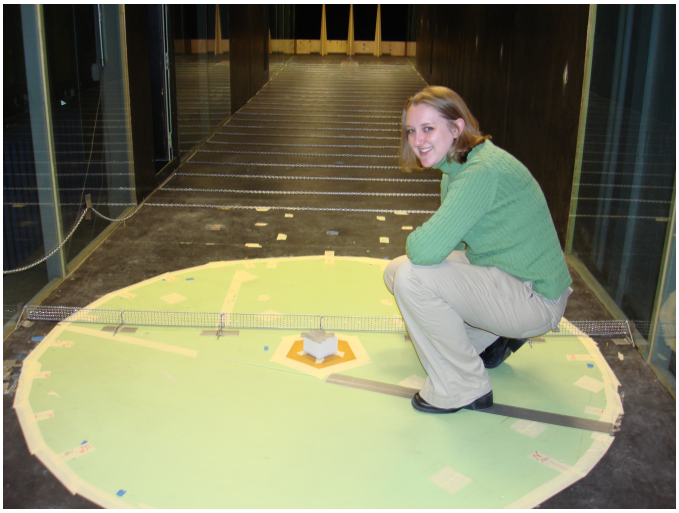

Figure 4.5 Experimental setup and author

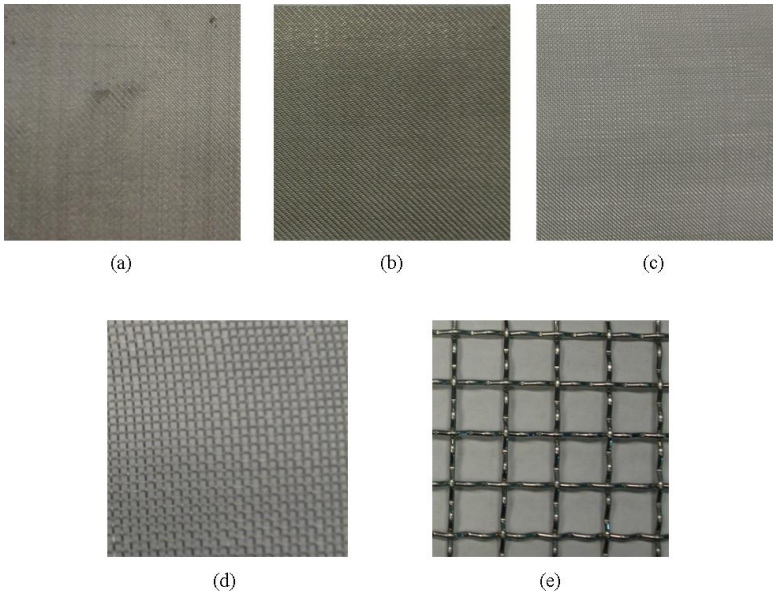

Figure 4.6 Screens used to make the fences

Porosities: (a) 11.7%, (b) 19.4%, (c) 30.3%, (d) 51.8%, and (e) 76.4%

4.2.3 Wind Speed Selection

Since high-intensity hurricanes will produce wind that could not be generated in the wind tunnel it was decided to conduct the tests at a much lower wind speed. To determine an adequate wind speed tests were done at several wind speeds first to see if there is any effect of the wind speed on the force coefficients that are a normalized form of forces with respect to dynamic pressure and projected area of the building model. Figure 4.7 shows that while the force coefficients do change marginally with wind speed, they do not increase significantly, nor do they jump, indicating no significant Reynolds number dependence. Therefore, the tests were done at a wind speed of 9.9 m s^{-1}.

4.2.4 Sampling and Averaging Times

The sampling rate of the force measurement was set at 500 Hz. To capture time series of sufficient length the tests were run for 180 seconds and averaged over the first ten seconds, then the first twenty seconds, etc., to determine the sampling time needed to capture the widest range of load values. It was determined that after 130 seconds of averaging the mean values

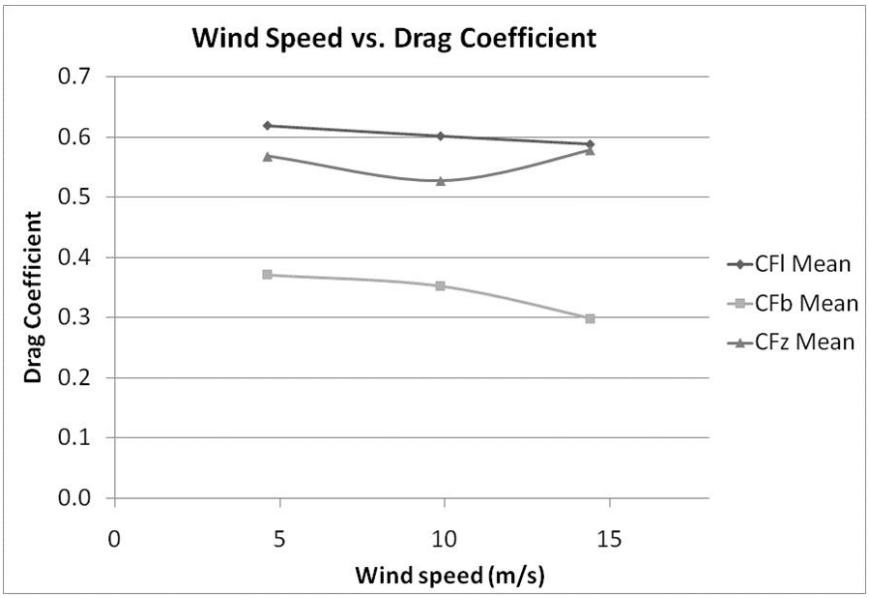

Figure 4.7 Force coefficients as a function of wind speed

showed little time dependence, as seen in Figure 4.8. For the study, each test was run three or more times for the chosen averaging time of 130 seconds, and then results of those tests were averaged to decrease the variability due to turbulence or other factors.

4.3 Fence Parameters

4.3.1 Porosity/Distance

Five porosity values were chosen for the fence: 11.7%, 19.4%, 30.3%, 51.8%, and 76.4%. The highest porosity, 76.4%, easily represents many kinds of trees. The second highest porosity, 51.8%, can represent very dense trees or a porous engineered barrier. The lowest three porosities represent artificial barriers that would have to be engineered as well. The porosity tests were conducted using the shortest fence, of height 6.10 cm.

4.3.2 Height

Three different fence heights were tested. The full-scale heights were chosen as 6.10 m, 13.7 m and 21.3 m. The length scale was 1:100, so the geometrically scaled fence heights were 6.10 cm, 13.7 cm, and 21.3 cm respectively. The smallest height possibly represents fences,

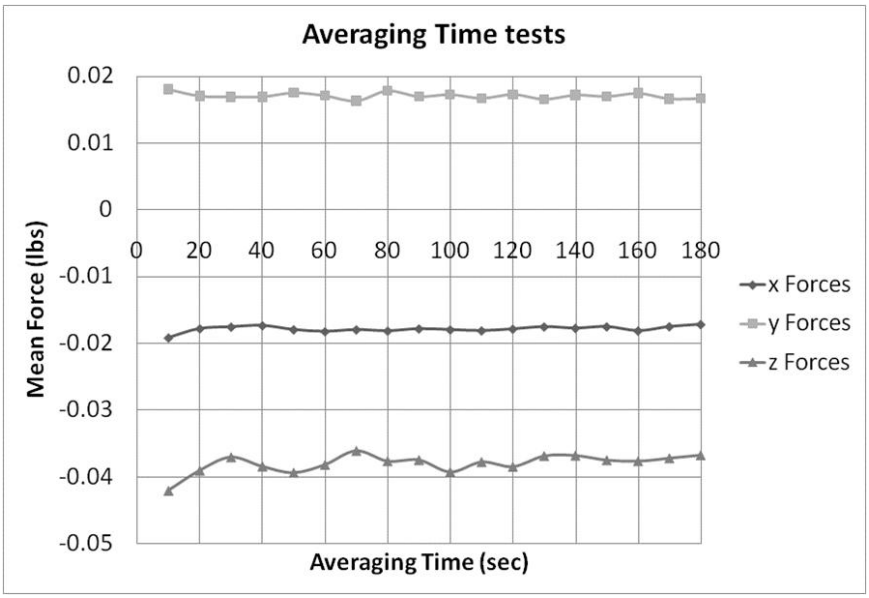

Figure 4.8 Forces as a function of averaging time

walls, or small trees. The taller heights likely represent natural shelters made of larger trees. In an effort to reduce the total number of tests the height tests were conducted using one of the screen porosities that performed the best, 30.3% porous.

4.3.3 Distance

The distance between the fence and the building it protects is a variable that also was studied. Dierickx et al. (2001) found that for a single porous fence the maximum wind speed reduction occurs between 10H and 15H distance from the fence, where H is the height of the fence. Therefore, the wind tunnel experiment was designed to test the fence at locations upstream of the building center within that range at 2H, 4H, 6H, 8H, 10H and 12H. These tests were done using the shortest fence, 6.10 cm, so as to maximize the range of distances in multiples of H.

4.3.4 Deflector

To study the effect of deflection of the flow over the low-rise building a small (solid) deflector was mounted on top of a fence, as can be seen in Figure 4.9. The full-scale length of this

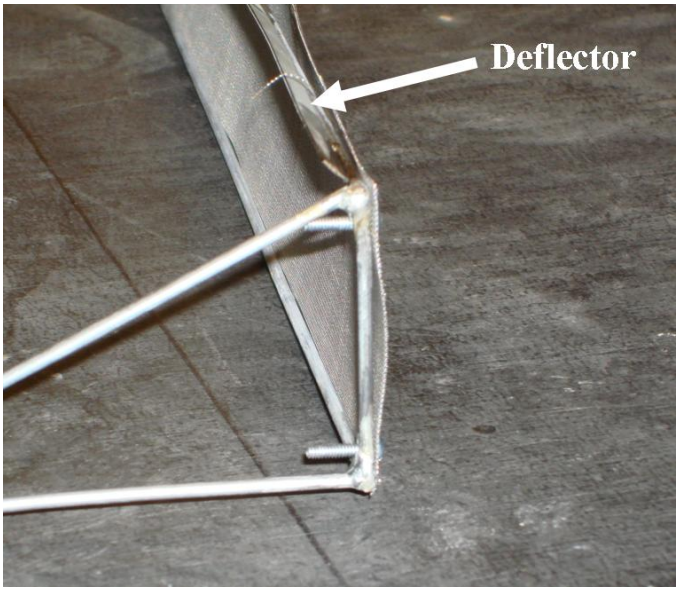

Figure 4.9 A fence with the deflector attached

deflector was 0.305 m, which is 5% of the height of the fence used. The angle of the deflector was chosen to be 45° for ease of construction of the fence model. For these tests, the shortest fence (6.10 cm) with 30.3% porosity (medium) was used.

The list of the force balance tests conducted are listed in Table 4.1.

4.4 Methods

The building orientation to the mean wind direction was chosen as 45° as shown in Figures 4.3 and 4.10 based on previous studies that have shown occurrence of larger forces on the building at that orientation. The forces along the major axis and minor axis of the building model, longitudinal (F_l) and side (F_b) respectively, can be calculated as

$$F_l = F_x sin45^\circ + F_y sin45^\circ, F_b = F_x cos45^\circ - F_y cos45^\circ \tag{4.2}$$

where F_x and F_y are forces measured in the x and y directions, respectively, using the JR3 force balance, shown in Figure 4.11. In this study, the two forces that will be compared for the buildings without and with the fence are the z direction force, F_z (uplift), also measured

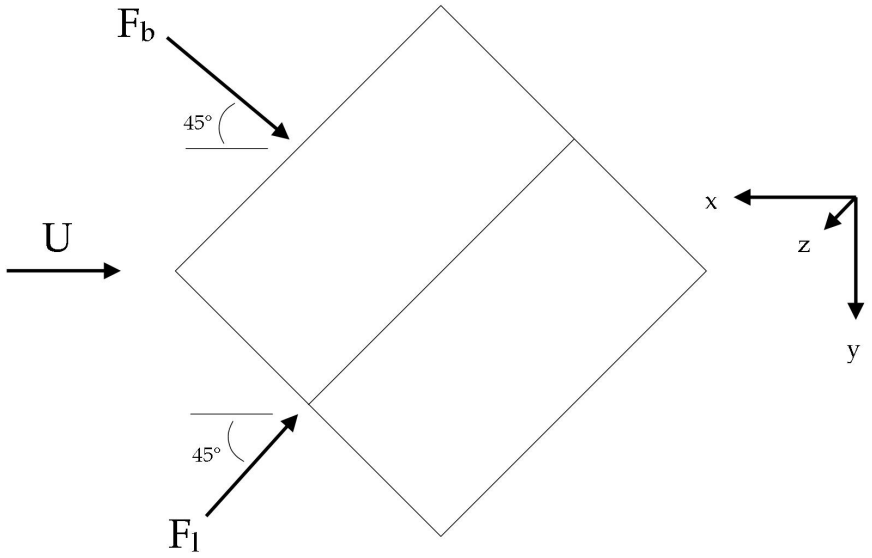

Figure 4.10 Plan view schematic of the orientation of the house models to the wind direction

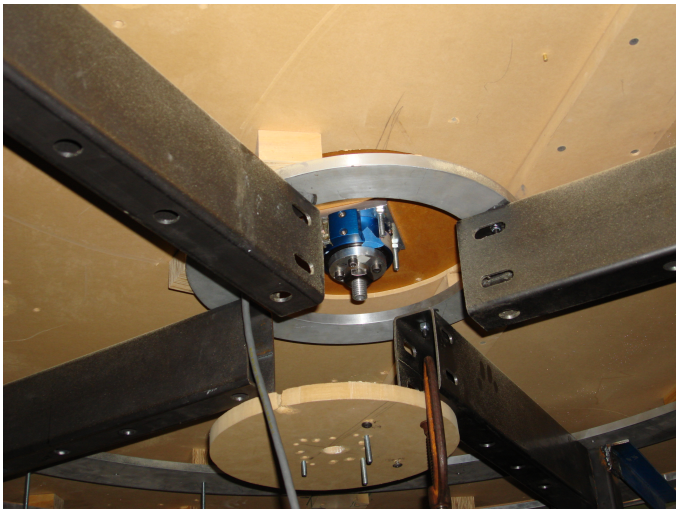

Figure 4.11 JR3 force balance mounted underneath the test section of the wind tunnel as fixed to the building model above the test section

Porosity & Spacing Tests
Single height, no deflector
Spacings: 2H, 4H, 6H, 8H, 10H, 12H
11.7% Porous
19.4% Porous
30.3% Porous
51.8% Porous
76.4% Porous
Height Tests, *H*
Single porosity, no deflector
Spacings: 2H, 4H, 6H, 8H, 10H, 12H
6.10 m
13.7 m
21.3 m
Deflector Tests
Single height, single porosity
Spacings: 2H, 4H, 6H, 8H, 10H, 12H

Table 4.1 Force balance wind tunnel tests conducted.

using the JR3, and F_s (shear force). The resultant shear force (F_s) is calculated by

$$F_s = \sqrt{F_l^2 + F_b^2} \tag{4.3}$$

Also, the total force on the building is calculated by

$$F = \sqrt{F_l^2 + F_b^2 + F_z^2} \tag{4.4}$$

A screen shot of the LabView program that was used to collect the data is shown in Figure 4.12.

For easy comparison, dimensionless force coefficients, C_s and C_z were used rather than measured forces. Normalized forms of Equations 4.3 and 4.5 can be used to calculate C_s and C_f from the three force coefficients defined by

$$C_{l,b,z} = \frac{2F_{l,b,z}}{\rho U^2 A} \tag{4.5}$$

where $F_{l,b}$ are the computed forces from force measurements using Equation 4.2, ρ is the air density, U is the wind speed at 10 m (33 ft) equivalent full-scale height, and A is the projected

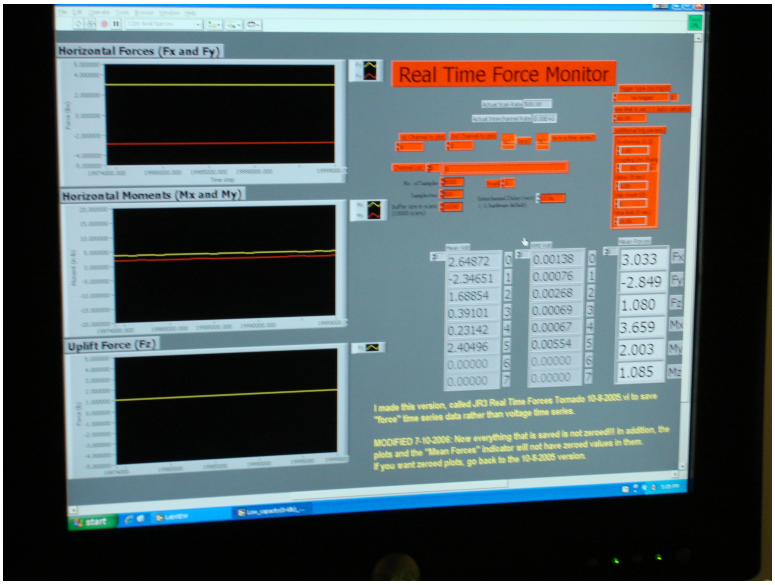

Figure 4.12 Screen shot of LabView program used to collect data

area of the building orthogonal to the force direction. The air density was calculated using Equation 4.6

$$\rho = \left(\frac{273.13}{T_K}\right)\left[\frac{B - 0.3783e}{760}\right] P \quad kgm^{-3} \tag{4.6}$$

where ρ is the air density, T_K is the air temperature in Kelvin of the air measured inside the wind tunnel test section, B is the barometric pressure in torr measured in the lab, e is the vapor pressure in torr, and P is the density of dry air at sea level (1.25 kg m^{-3}) (Kershner, 1977). The vapor pressure, in millibars, was calculated using the identity

$$e = \frac{RH\%}{100\% \times e_s} \tag{4.7}$$

where $RH\%$ is the relative humidity measured inside the wind tunnel test section, in percentage, and e_s is the saturation vapor pressure, calculated by

$$e_s = 6.112exp\left(\frac{17.67T_C}{T_C + 243.5}\right) mb \tag{4.8}$$

where T_C is the temperature in degrees Celsius inside the wind tunnel test section (Bolton, 1980).

The building force coefficients of the test runs with no fences were divided by the corresponding values from those with fence cases, and these quantities are referred to as the force

attenuation factors as defined in Equation 4.9.

$$f_{s,z} = \frac{C_{s,z}^{nofence}}{C_{s,z}^{fence}} \tag{4.9}$$

For each tested case, a force attenuation factor between zero and one means that the fence increased the forces on the model and a force attenuation factor of more than one means that the fence decreased the forces on the model. For aggregate comparisons the shear and uplift force attenuation factors were each averaged over both the one and two-story models.

4.5 Results

4.5.1 Porosity

Figure 4.13a shows the shear force attenuation factors for the building models with different porosity fences placed at six spacings. All five fences of different porosities result in reduction in the loads on the models. As is evident in this figure the most porous fences are the least effective in comparison to other less porous ones; but even these result in reduction of more than a factor of two. At the opposite end of the porosity spectrum, the lowest porosity fence is only best at very far distances. The range between 2H and 8H, where H is the height of the fence, is generally the most effective across all porosities. Over this range, the 30.3% porosity was determined to be the best.

Figure 4.13b shows the uplift force attenuation factor for the models. Comparison of Figures 4.13a and b reveals that the fences do not reduce the uplift nearly as much as the shear forces. However, the uplift is still reduced at least by a factor of nearly 2, and on an average by a factor of about 4. For the uplift force the least porous fence is the most effective. Similar to the shear forces, the most porous fence (76.4%) is marginally effective compared to the other fences. For the uplift, there is much less variation in the force attenuation factors with placement distance of the fence. This plots shows that perhaps around 2H-4H and 8H are the most optimal positions for the fence.

Figure 4.13c shows the average force attenuation factors for combined the shear and uplift forces. Because the magnitude of the improvements in the shear forces dominates the im-

(a)

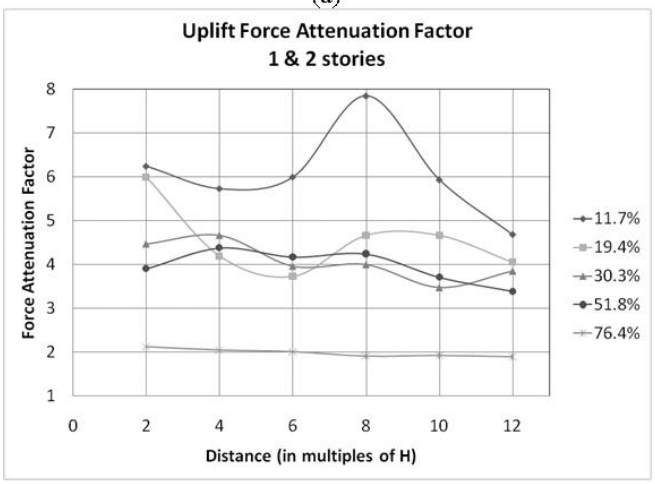

(b)

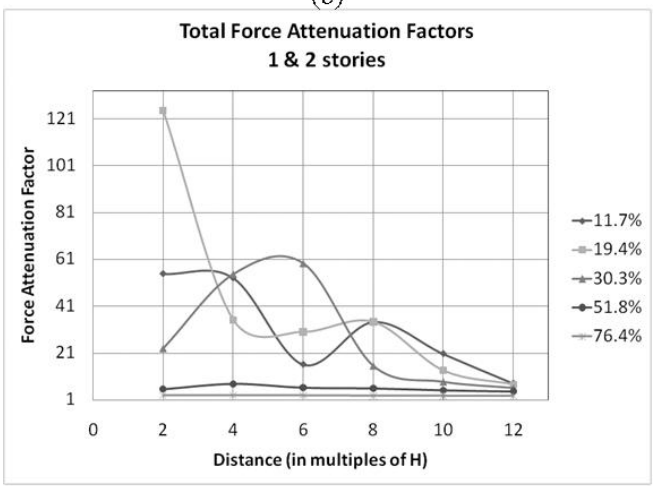

(c)

Figure 4.13 Force coefficients for different porosity fences

provement in the uplift force, and because the uplift force is comparatively linear across the distances, the total force plot trends very similar to the shear force plots.

4.5.2 Heights

As with the porosity results, all the three heights of fences considered resulted in reduction in the forces on the building models. Figure 4.14a shows that for the shear force all three fences have improvement in forces. The mid-height fence, 13.7 m, far exceeds the short and tall fences for maximum protection. In the normalized distance plot, Figure 4.15a shows the same decaying trend starting at 8H that was evident in the effect of fence porosity tests on shear force. The range of maximum effectiveness is between approximately 3H and 7H.

Figure 4.14b shows the uplift force attenuation factors for the fences of different heights. This plot shows again that all three fences reduce the uplift although with significantly less reduction compared to the shear forces. In the mid-distances, the mid-height fence performs the best like the shear force. Figure 4.15b shows that the mid-height fence performs best out to 6H. This plot also shows that within the few data points taken, the taller fences generally have the same minimal variation in the force attenuation factors with distance from the model as the short fence. Still, the 4H and 8H ranges could be considered the optimal spacing for fences of any heights.

Figure 4.14c is the average of the two force attenuation factors for the two building models. As with the porosity tests, the shear force coefficient factor values are dominant, therefore the total forces plot is very similar to the side forces plot. In the normalized plot in Figure 4.15c the same shear force dominance is apparent.

4.5.3 Distance

The porosity test and the height tests also included the dependence of fence distance from the house model. Figures 4.13 and 4.15 show that for the shear force reduction the optimum range of spacing for fence placement is between 2H and 8H, and that for the uplift force the optimum locations are around 4H and 8H. Figure 4.16 is a plot of extended distances of fence

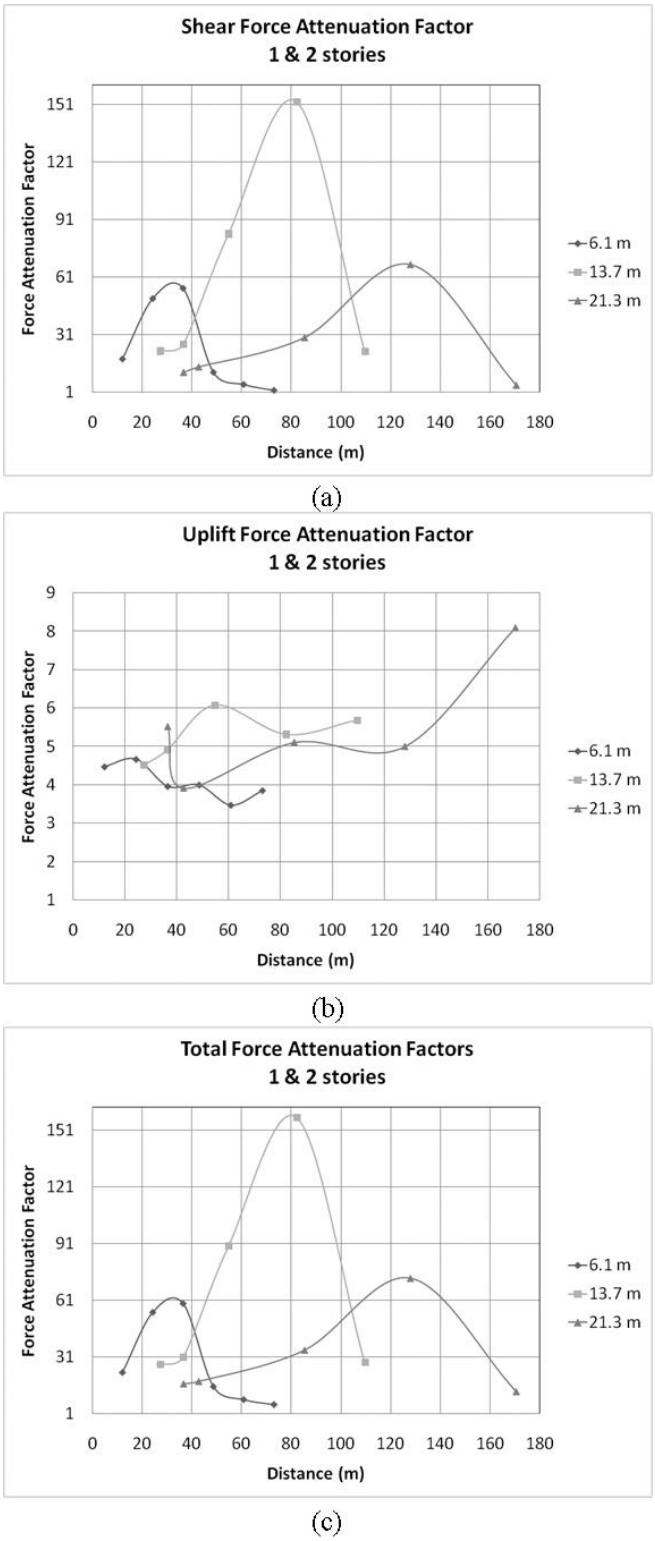

Figure 4.14 Force attenuation factors for different height fences

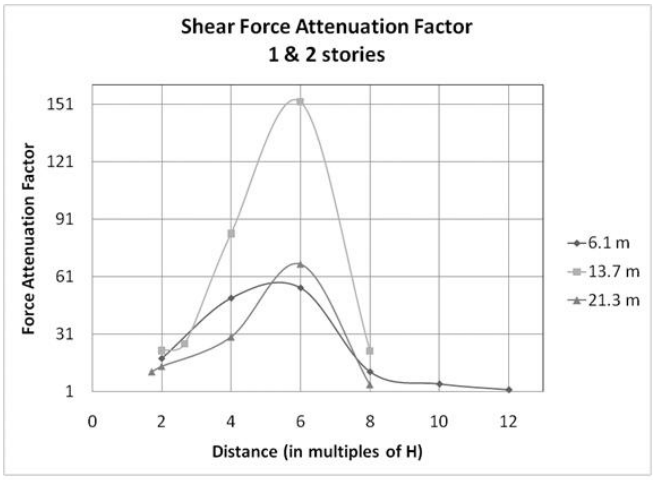

(a)

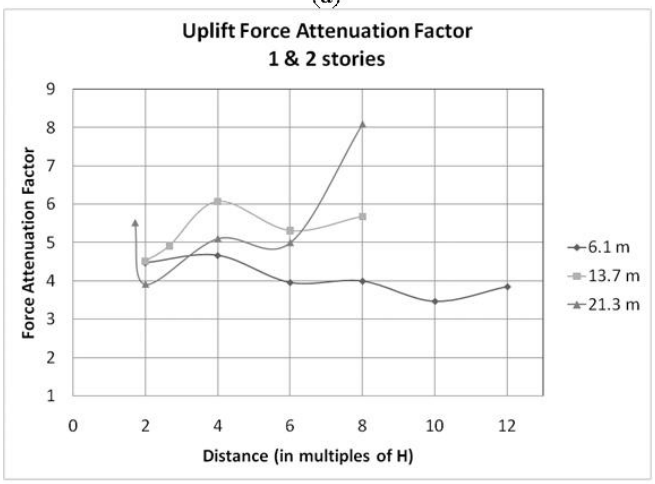

(b)

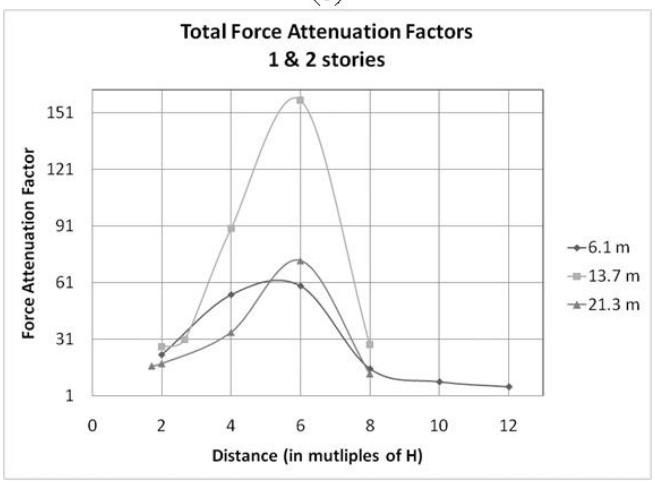

(c)

Figure 4.15 Force attenuation factors for different height fences

spacing. The plot shows that for a very long distance the fences are minimally effective.

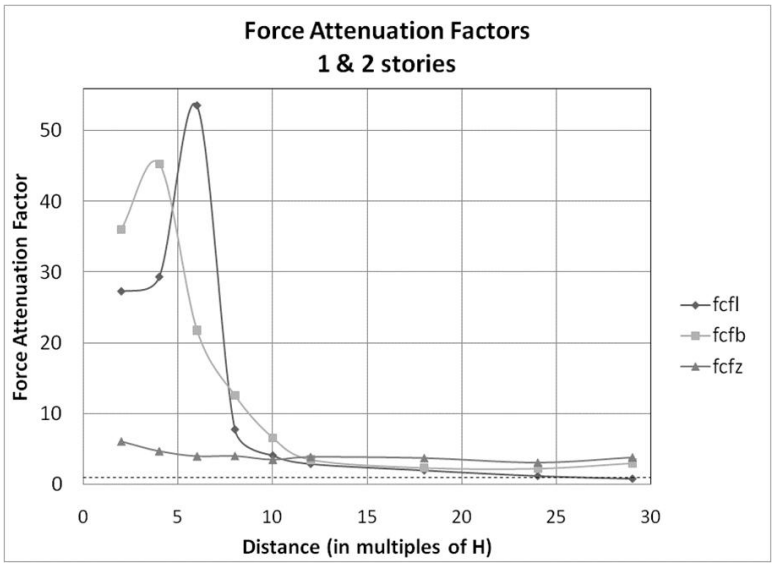

Figure 4.16 Force attenuation factors for extended spacings of the fence

Eventually, at 29H, the longitudinal force attenuation factor (fCf_l) (see Equation 4.2) goes below one, indicating an increase in the force. However, even at this distance the other two forces are still fairly reduced.

4.5.4 Deflector

Figure 4.17a shows the shear force attenuation factors for the cases with and without a deflector. While the fence was effective at reducing the loads even before the deflector was added, the addition of the deflector nearly doubles the protection in shear. However, the deflector is only effective in the 2H to nearly 8H range for the shear force. Figure 4.17b shows that for the uplift force the deflector is effective over the entire range tested, while becoming less effective as it approaches 12H. The effect on the uplift force attenuation factor is nearly a constant amount of improvement in force attenuation over the range through 10H. Figure 4.17c shows the total force attenuation factors, and as with the other tests the magnitude of the shear force attenuation factors dominate the lift's therefore the total trends the same as the shear.

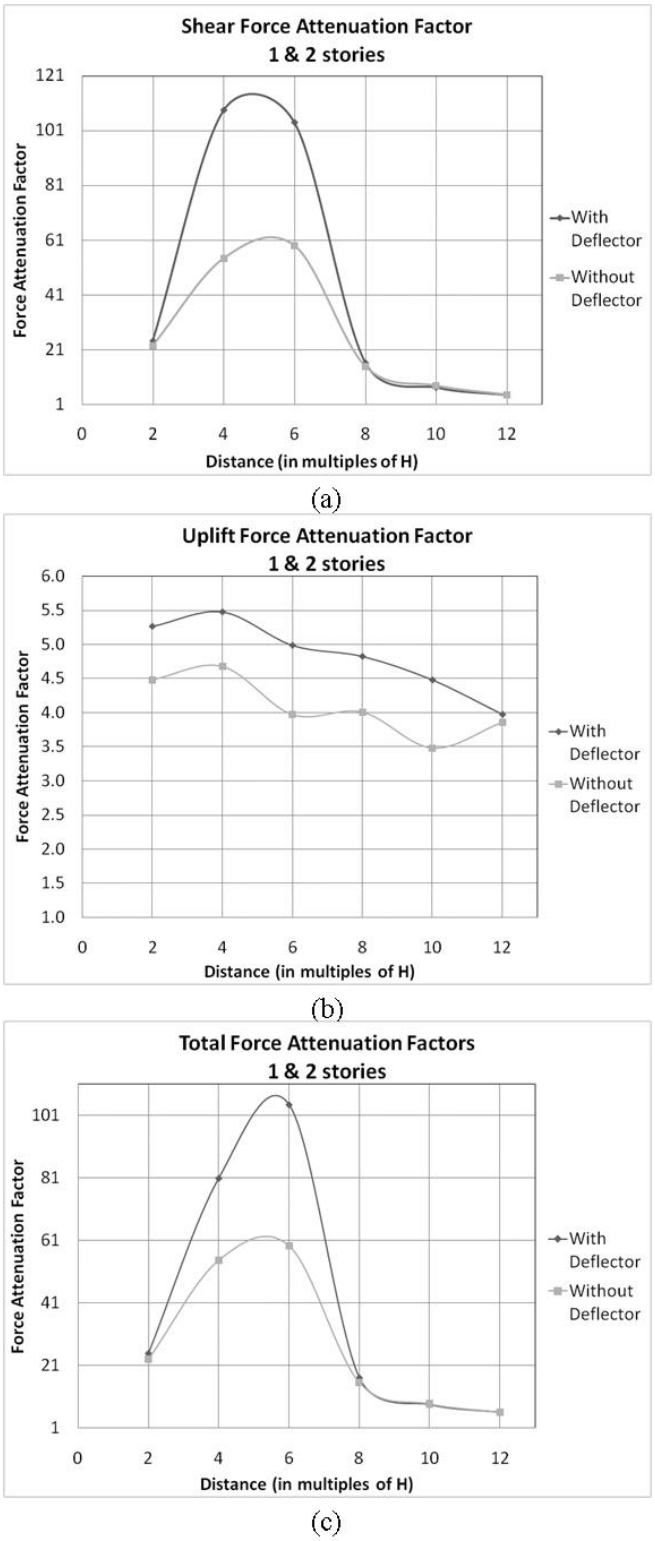

Figure 4.17 Force coefficients for the fence with and without the deflector

4.6 Summary and Conclusions

These studies found that the presence of a fence greatly decreases the shear and uplift forces on a house. The fences were found to reduce the shear forces much more than the uplift forces. However, the uplift force is not as dependent on the distance of the fence from the building like the shear force. When examining total force attenuation, the trends are similar to the shear force because of its greater magnitude than the uplift forces.

The study of effect of fence porosities found that all porosities resulted in reduced loads. However, the more porous the fences are the least effective these are. Also, the fence with lowest porosity was only most effective over all at the large distances from the building, but it was the most effective for uplift forces. In the mid-range distances from the building the fence with 30.3% porosity was much more effective than fences with any other porosity.

As with effect of the porosities, all fences of different heights but same porosity were found to be effective in reducing the forces. Previous studies have found a direct correlation between height of a fence and the distance over which it is effective downstream. In this study, the two taller fences were more effective than the shortest fence. However, the tallest fence was not as effective as the medium height fence.

While the fences were found to be effective for a long range of spacings, up to approximately 29H, the range over which the total forces are most reduced was between 2H and 8H, where H is the fence height. The porosity and distance tests plots had a semi-bimodal shape with local peaks of maximum reduction near 4H and 8H; however the overall range of effectiveness was between 2H and 8H. The fence height tests found a slightly smaller range of maximum effectiveness within the above range, between 3H and 7H. When determining the maximum distance over which the fences were effective, the location where the force attenuation factors become less than 1 is interpreted as the point where the separation bubble created by the barrier reattaches to the model.

The tests performed with the 45° deflector showed that such a device increases the effectiveness to reduce loads even further. The deflector doubles the peak shear force attenuation factor compared to the case without the deflector. While the deflector remains effective in

reducing uplift forces over the entire range of spacings tests (0-12H) its effectiveness to reduce shear forces reduces with increasing distance.

4.7 Numerical Comparison

For validation of the numerical model with wind tunnel results, a comparison of wind profiles was made between the numerical model and wind tunnel data. For this test the Bill James wind tunnel was used, which produces uniform and laminar flow in a 0.762 x 0.762m test section. The largest challenge for the comparison was the attempt to define the screen in the numerical model. The numerical model was not designed for such a thin obstacle, and the LAD (leaf area density), calculated from the porosity, is a function of the width of the obstacle, as seen in Equation 1.1. Also, the numerical model is designed to run with a boundary layer flow; while this was minimized, it was still not uniform and laminar.

Given that the wind tunnel setup and the numerical parameterizations were not exactly the same, the comparison between the numerical and experimental data is fairly good. Figure 4.18 shows the vertical velocity profiles at 1H behind the fence, where H is the height of the fence, in the wind tunnel (a) and the screen in the numerical model (b). The numerical results are more smoothed than the experimental results, and have a slightly narrower range of normalized velocity values. However, both plots show a nearly 15% reduction within the height of the screen. The numerical model does have the recovery starting at a lower height than the experimental data with a more gradual increase as compared to the jump at the shelter height in the experimental data. Also, the numerical data does not have the same amount of speed up above the screen that the experimental data does. The speed up in the wind tunnel may be due to the confined space of the wind tunnel that would increase the pressure within and cause the speed up, where as the numerical model is not similarly constrained at the top.

Figure 4.19 shows the horizontal wind speed profiles at many heights, from 1H to approximately 8H. As seen in the vertical profile, the wind tunnel (a) has a sharper jump at the top of the screen. However, there is still a noticeable separation in the numerical model (b) although not as drastic. The numerical model has more flow between the low levels and high levels, in

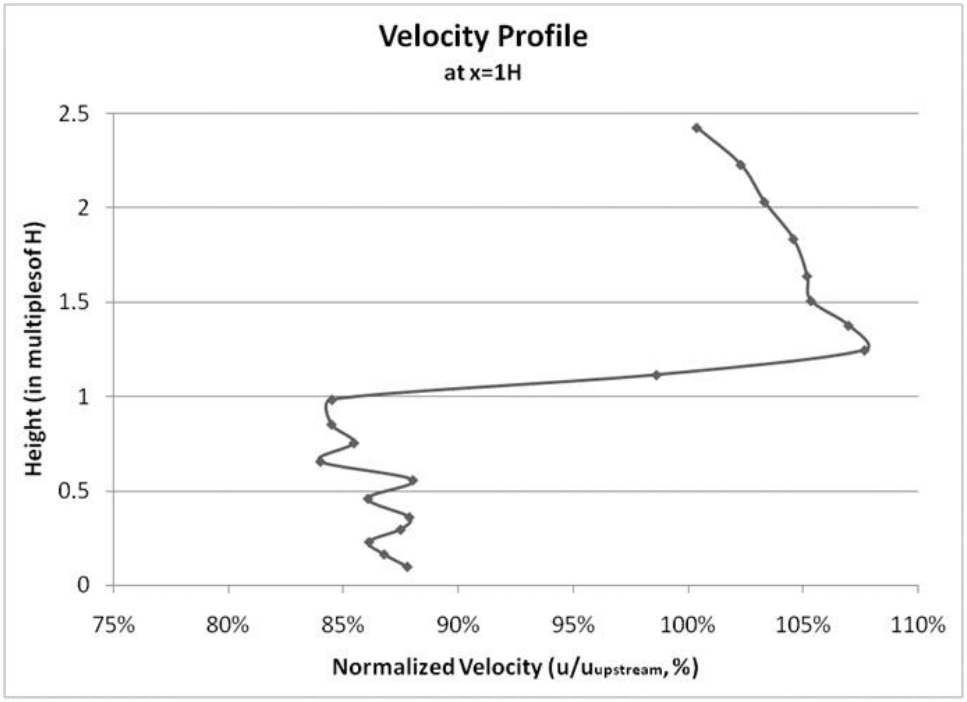

(a)

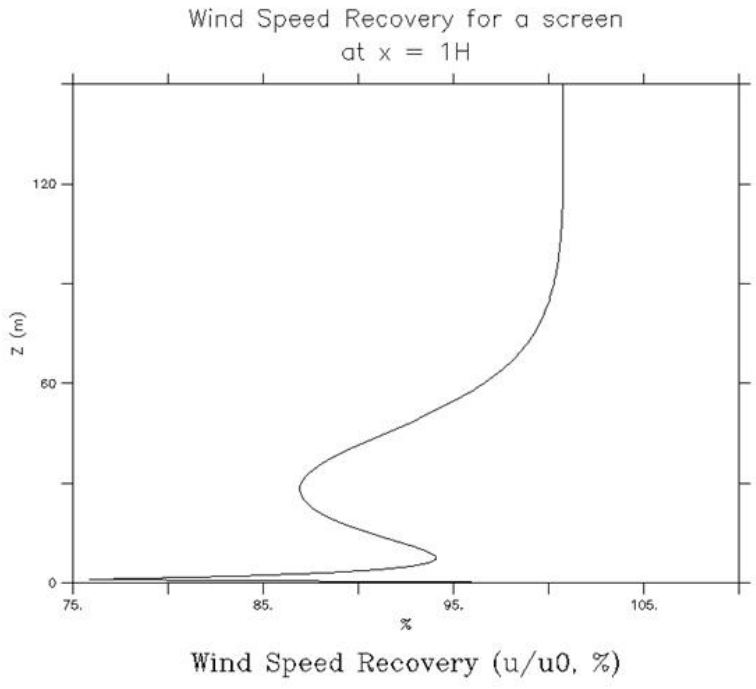

(b)

Figure 4.18 Vertical velocity profiles for experimental wind tunnel tests and numerical modeling tests

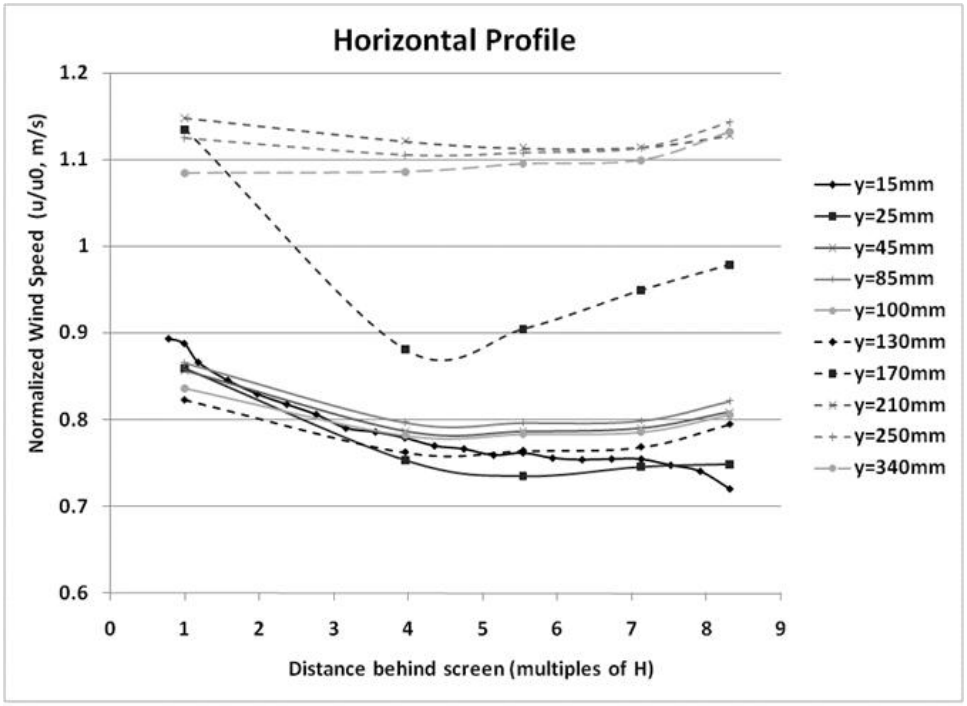

(a)

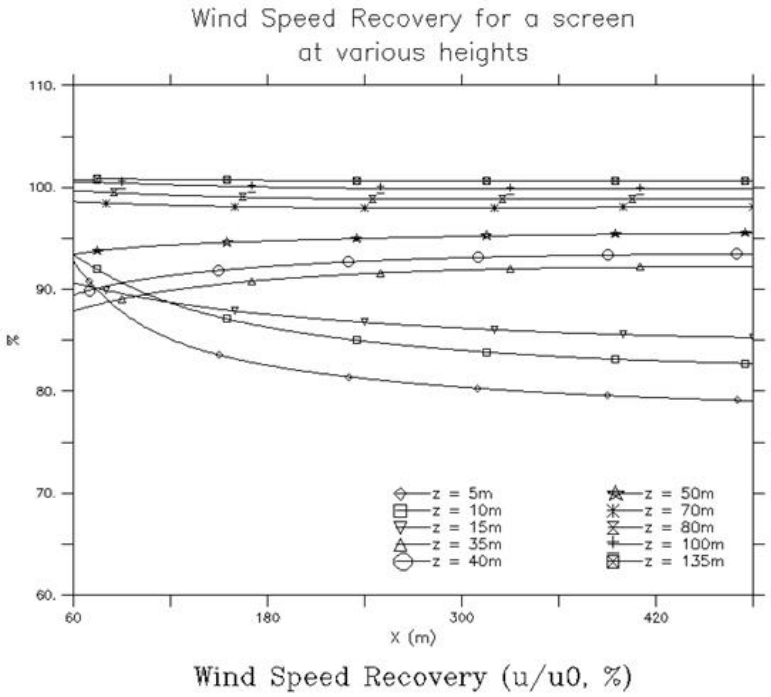

(b)

Figure 4.19 Horizontal velocity profiles for experimental wind tunnel tests and numerical modeling tests

the top half of the obstacle, than the wind tunnel does. This region is where the numerical model and the experimental data differ the most. The experimental data shows a consistent convex shape to the plots, first decreasing then slightly increasing. The numerical plots have this same convex shape at the low and high levels, but it does not have the same increase at the farther distances. Then in the mid-heights the plots are concave in shape, showing the increase in speed with distance. This difference may arise from the numerical model not being an extremely thin fence; therefore it has elements that would cause some vertical velocity, which would increase the velocity through the top of the shelter.

CHAPTER 5. SUMMARY AND CONCLUSIONS

5.1 Summary

Numerical and experimental tests were done to determine the optimum design parameters of a shelterbelt for wind damage mitigation to structures behind the shelterbelt. The Wang and Takle shelterbelt numerical model was used to study the shelterbelt cross-sectional shape, height, spacing/line tightness, density/density distribution, line width, number of lines, and wind speed parameters. These were studied parametrically, isolating each parameter to study the effect each had on the shelter effect. The numerical model was then used to study the effectiveness of more realistically shaped shelterbelt tree lines, rather than using the traditional blocks to represent each line of trees in the shelterbelt. These trees were studied individually as well as in arrangements that could represent possible scenarios in coastal areas where high winds from tropical storms and hurricanes as well as high speed water flows of tsunamis are a threat. Finally, experiments were conducted in a wind tunnel to test the effects of wind-induced load reduction on buildings with the implementation of a shelterbelt screen. The tests results were in the form of force attenuation factors, rather than wind speed reduction as has been done in the past.

5.2 Conclusions

The parametric numerical studies determined most effective shelterbelt configurations of shelterbelt cross-sectional shape, height, spacing/line tightness, density/density distribution, line width, number of lines and wind speed on sheltered distance near the surface based on wind speed sheltered distance. These studies found that height and density have the largest effect on shelter provided. The other shelter parameters tested showed very little variation

throughout the range of values tested. Cross-sectional shapes of all same height lines (blocks) or increasing height (wedge-up) windward to leeward were found to be optimal. It was also found that sheltered distance increases with the height of the shelter with no evidence of a limit to this trend. The density tests showed that denser shelters give better sheltered distances. For non-uniformly dense shelters, increasing density was found to be best. The spacing tests showed that any amount of spacing between the lines of the shelterbelt is better than none. It was found that less space with more lines is most effective. However, spacing plays a minimal role in shelter efficiency. Line width tests showed that thinner lines of the same porosity as wider lines have a more positive effect on the sheltered distance. However, line width was also found to have minimal effect on the shelter efficiency. For the number of line tests, it was found that any number of multiples lines in the shelterbelt was better than just one. Also, increasing the number of lines only slightly improves the shelter. The tests of different wind speeds showed that above approximately 50 m s^{-1} the shelter effect does not change much.

The tree parameterization studies focused on determining the best tree and tree arrangement characteristics for optimal shelter effect. It was found that arrangements that had low trees were found to be the most effective at completely eliminating the wind near the surface as well as reducing the TKE produced. Arrangements without low trees had increased wind speeds in the near lee suggesting that jetting below the trees' crowns is influencing the flow, where low trees would have reduced this jet. Also, having multiple low elements improved the length of protection for the wind speed as well as the TKE. It was also found that having the taller trees to the windward side, or the shorter trees to the leeward side, is better for both abruptness and magnitude of wind speed reduction as well as the reduction of TKE production. Combining trees did not lead to a linear combination of the protection that each individual tree provided. In all cases, having more than one tree improved the amount of protection from the wind speeds and the protected distance, as well as reducing the amount of TKE produced. Generally, it was found that arrangements with multiple dense trees had a protected zone that started closer to the leeward edge of the shelterbelt. It was also found that the added space between the lines did not appreciably improve the amount of protection.

Overall, the experimental studies found that the presence of a fence greatly decreases the shear and uplift loads on a house. The fences were found to reduce the shear forces much more than the uplift forces. However, the uplift force was found to be less dependent on the distance of the fence than the shear forces were. The study of the range of porosities found that all porosities resulted in reduced loads with the most porous being less effective than the more dense. In the mid-range spacings, the 30.3% porosity was found to be much more effective than any of the other porosities. All three fence height tests were found to be effective in reducing the forces. In this study, the two taller fences were more effective than the shortest fences. The fences were found to be effective for a long range, up to approximately 29H, and the range of distance over which the total forces are most reduced is between 2H and 8H. From the tests done with the deflector it was found that such a device is very effective. The deflector diverts enough flow so that the peak protection of the shear forces is nearly doubled. While the deflector becomes less effective over distance for the shear forces, it improves the uplift forces over the entire range tested.

5.3 Future Work

Future parametric numerical work could include a larger domain size to allow for taller trees. Using objective functions other than wind speed reduction, such as pressure perturbation, kinetic energy or momentum, to investigate these parameters may lead to more conclusions of the influences of each parameter. Future tree parameterization work can include further studies of the individual tree effects, as well as studying the effect of the height, span and density of the trees. Here also, using other objective function may also lead to more substantial conclusions. Future experimental work could include testing the effect of the fences on multiple houses at once, testing multiple lines of fences, and testing fences with distributed porosity that could represent trees.

APPENDIX A. ADDITIONAL FIGURES

Wind Speed Shapes

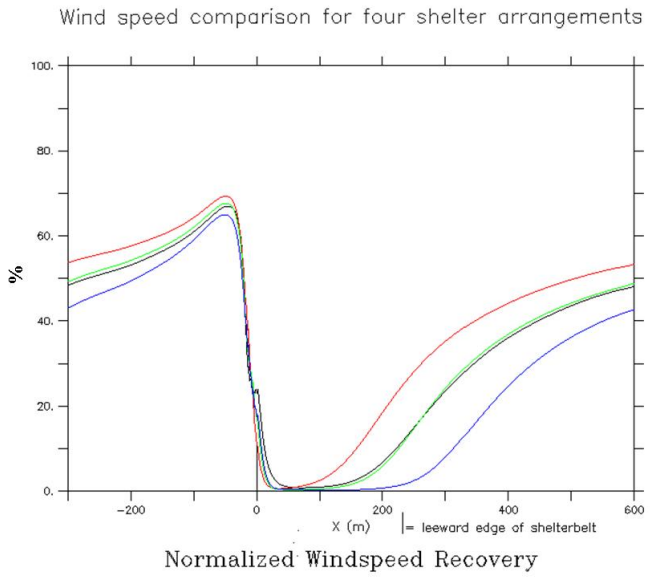

Figure A.1 Wind speed comparison for four shelter shape arrangements

For shelterbelts of tall height, increasing density, and medium spacing, at 2 m above the surface
black: wedge-up, red: wedge-down, green: triangle, blue: block

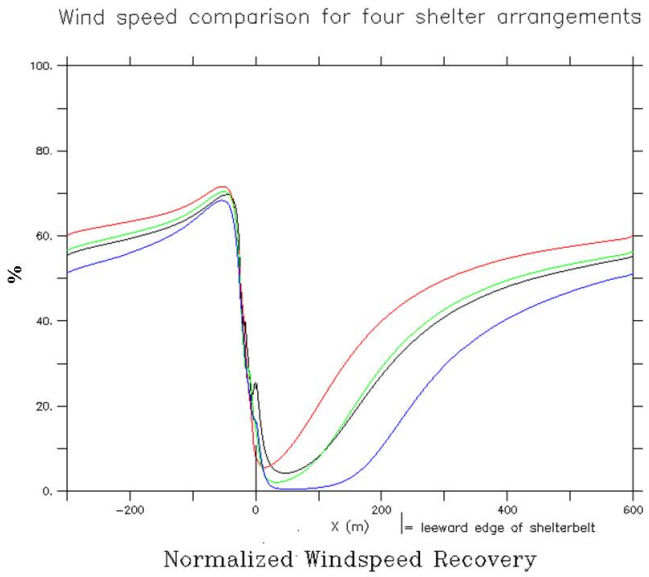

Figure A.2 Wind speed comparison for four shelter shape arrangements

For shelterbelts of medium height, increasing density, and wide spacing at, 2 m above the surface black: wedge-up, red: wedge-down, green: triangle, blue: block

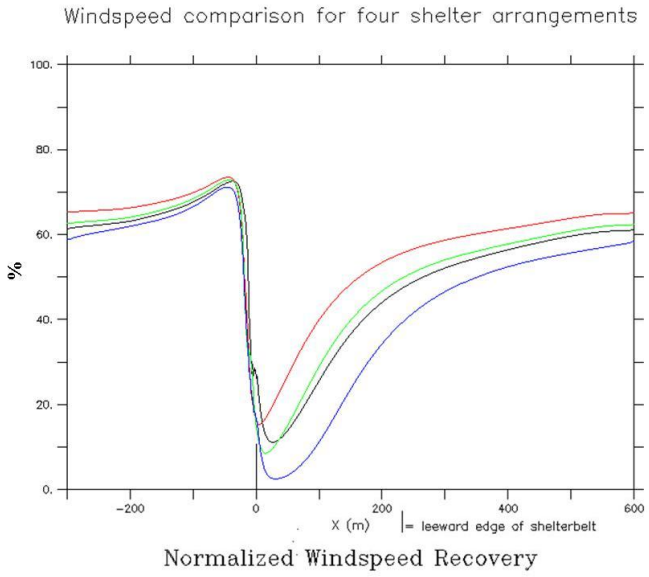

Figure A.3 Wind speed comparison for four shelter shape arrangements

For shelterbelts of short height, increasing density, and medium spacing, at 2 m above the surface black: wedge-up, red: wedge-down, green: triangle, blue: block

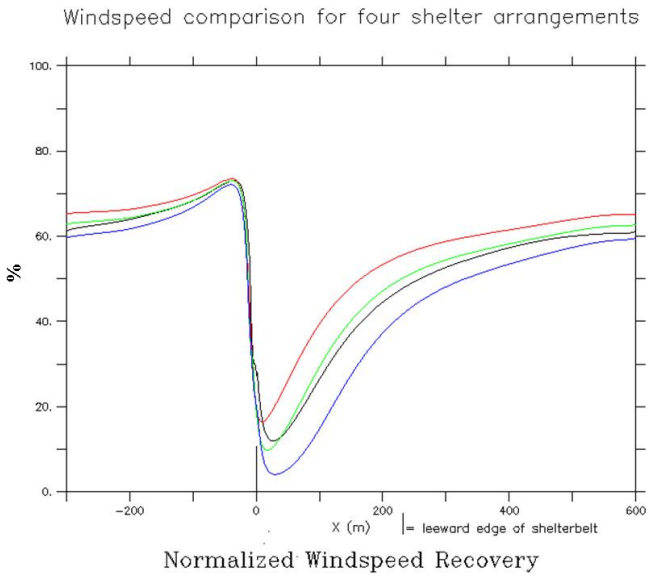

Figure A.4 Wind speed comparison for four shelter shape arrangements

For shelterbelts of short height, increasing density, and close spacing, at 2 m above the surface
black: wedge-up, red: wedge-down, green: triangle, blue: block

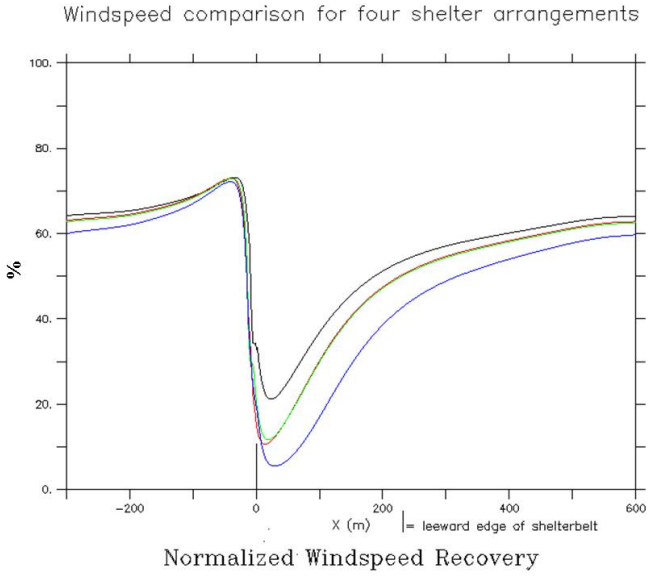

Figure A.5 Wind speed comparison for four shelter shape arrangements

For shelterbelts of short height, decreasing density, and close spacing, at 2 m above the surface
black: wedge-up, red: wedge-down, green: triangle, blue: block

Wind Speed Height

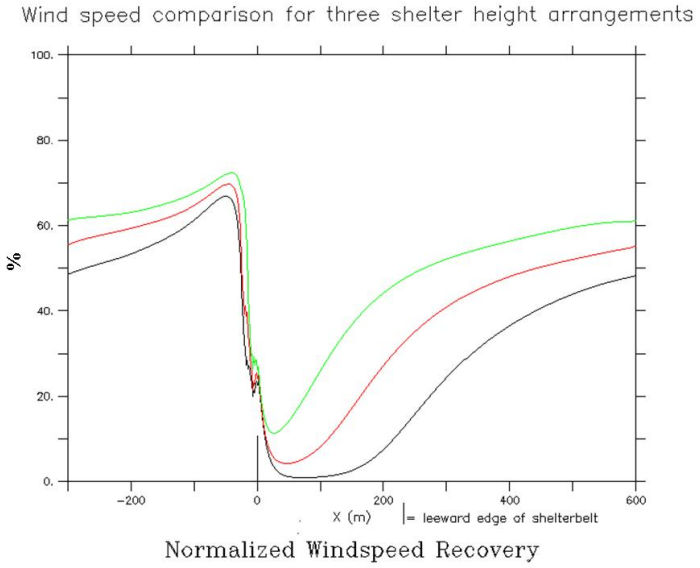

Figure A.6 Wind speed comparison for three shelter height arrangements

For shelterbelts of wedge-up shape, increasing density, and wide spacing, at 2 m above the surface
black: tall, red: medium, green: short

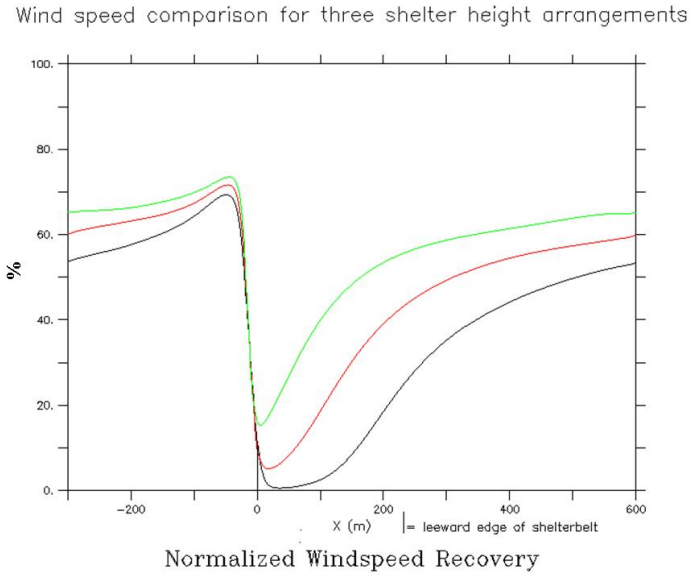

Figure A.7 Wind speed comparison for three shelter height arrangements

For shelterbelts of wedge-down shape, increasing density, and medium spacing, at 2 m above the surface

black: tall, red: medium, green: short

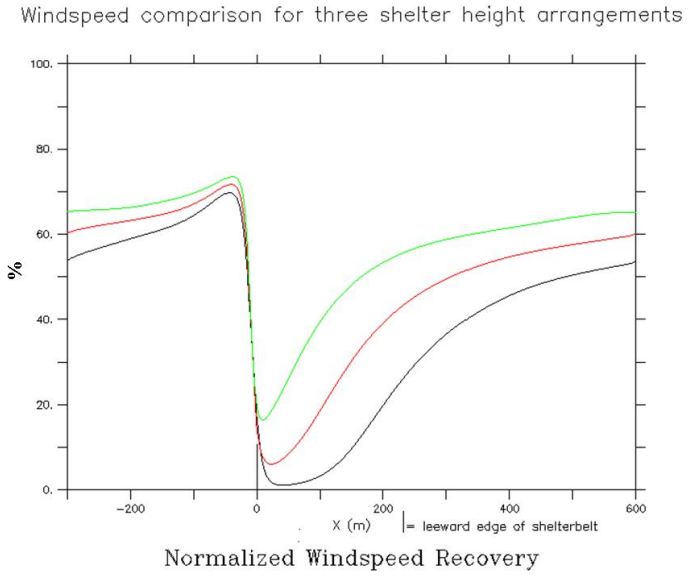

Figure A.8 Wind speed comparison for three shelter height arrangements

For shelterbelts of wedge-down shape, increasing density, and close spacing, at 2 m above the surface

black: tall, red: medium, green: short

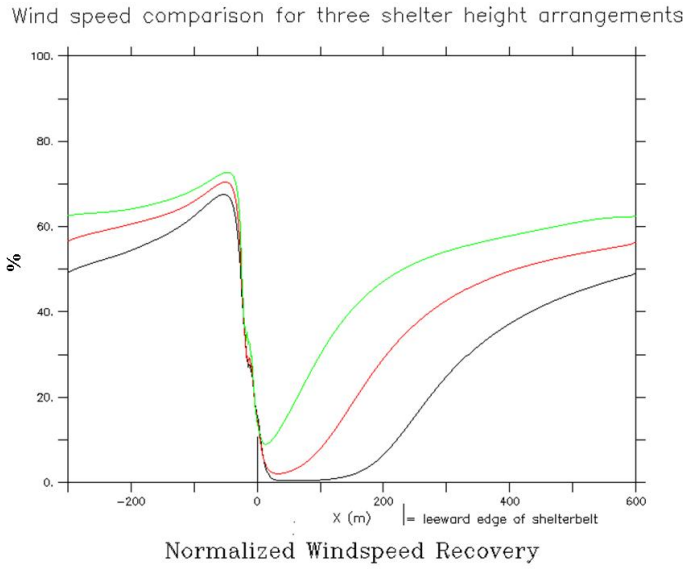

Figure A.9 Wind speed comparison for three shelter height arrangements

For shelterbelts of triangle shape, increasing density, and wide spacing, at 2 m above the surface
black: tall, red: medium, green: short

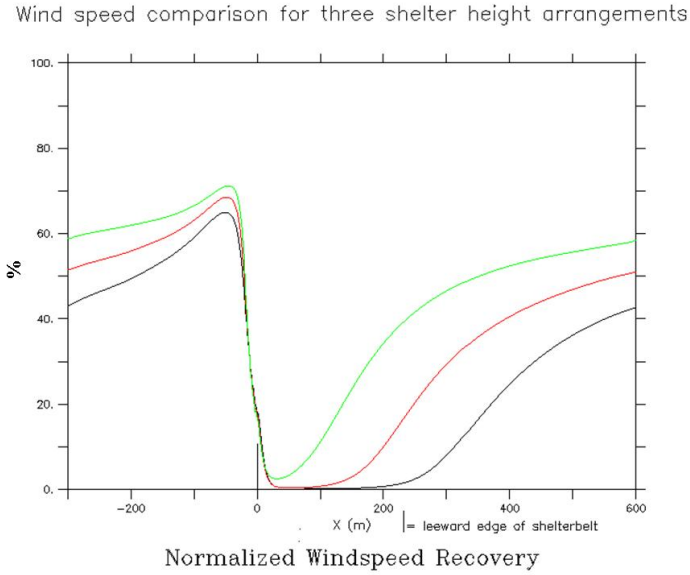

Figure A.10 Wind speed comparison for three shelter height arrangements

For shelterbelts of block shape, increasing density, and medium spacing, at 2 m above the surface
black: tall, red: medium, green: short

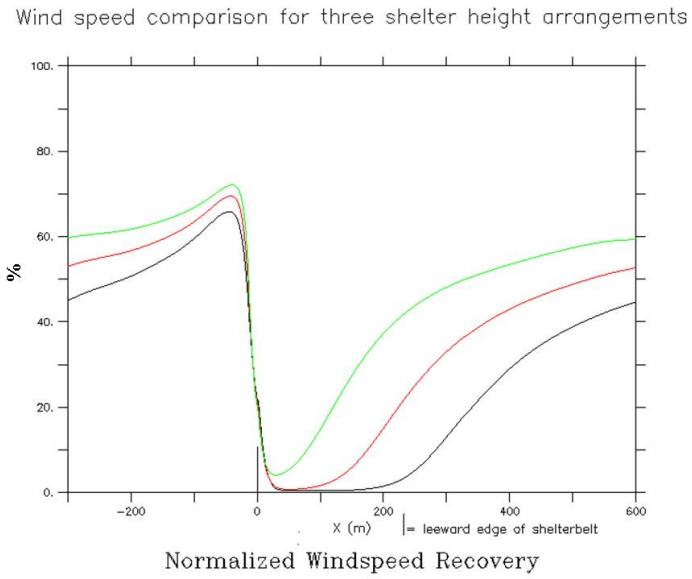

Figure A.11 Wind speed comparison for three shelter height arrangements

For shelterbelts of block shape, increasing density, and close spacing, at 2 m above the surface
black: tall, red: medium, green: short

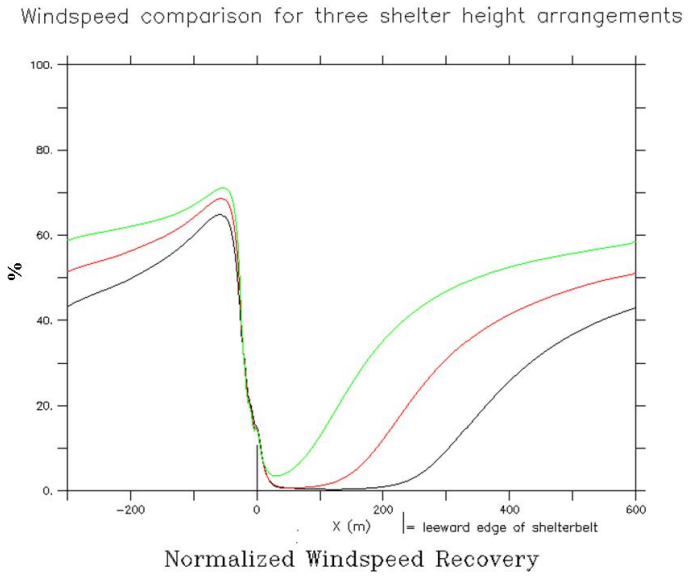

Figure A.12 Wind speed comparison for three shelter height arrangements

For shelterbelts of block shape, decreasing density, and wide spacing, at 2 m above the surface
black: tall, red: medium, green: short

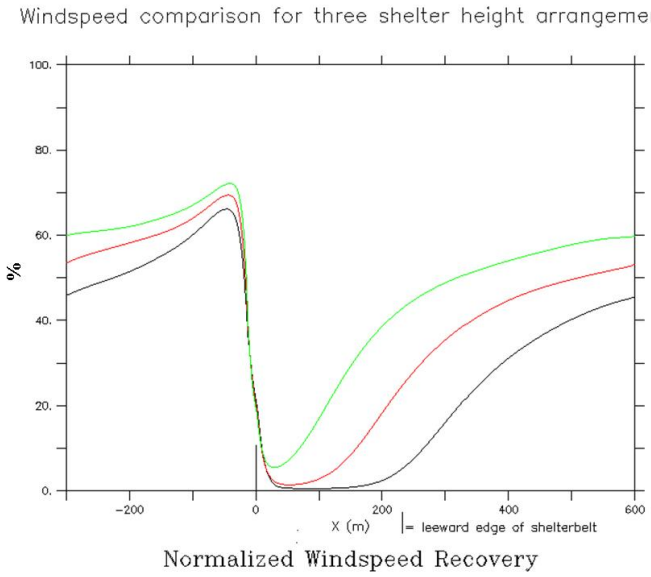

Figure A.13 Wind speed comparison for three shelter height arrangements

For shelterbelts of block shape, decreasing density, and close spacing, at 2 m above the surface
black: tall, red: medium, green: short

Wind Speed Spacing

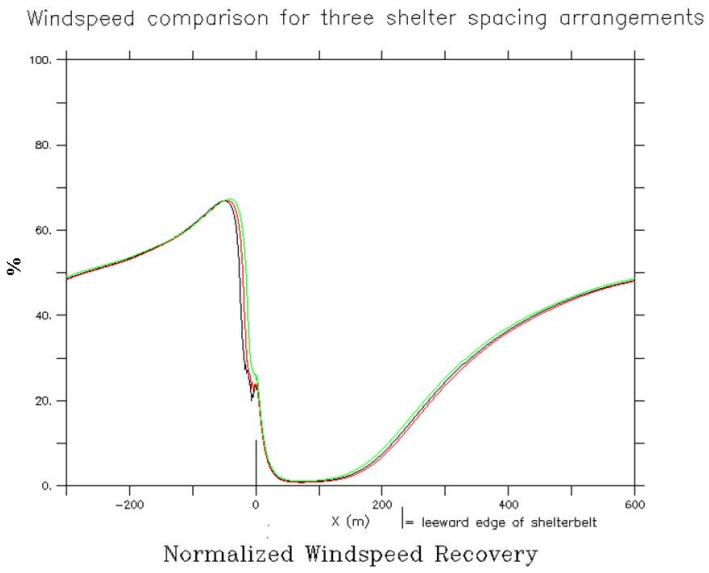

Figure A.14 Wind speed comparison for three shelter spacing arrangements

For shelterbelts of wedge-up shape, increasing density, and tall height, at 2 m above the surface
black: wide, red: medium, green: close

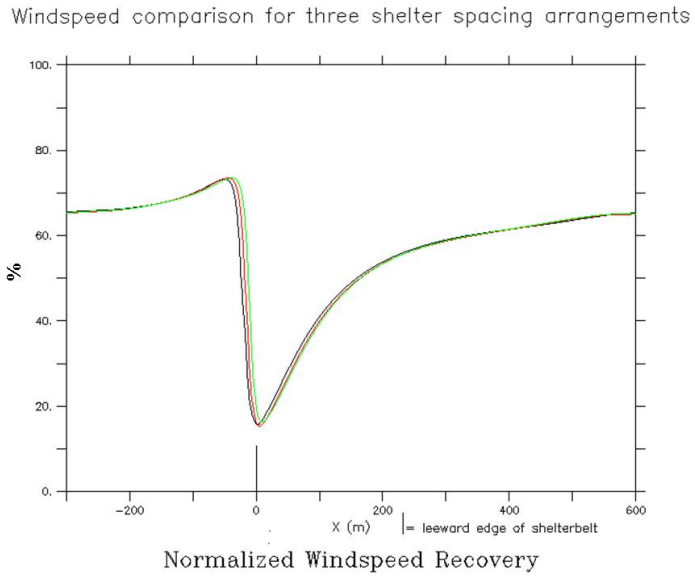

Figure A.15 Wind speed comparison for three shelter spacing arrangements

For shelterbelts of wedge-down shape, increasing density, and short height, at 2 m above the surface
black: wide, red: medium, green: close

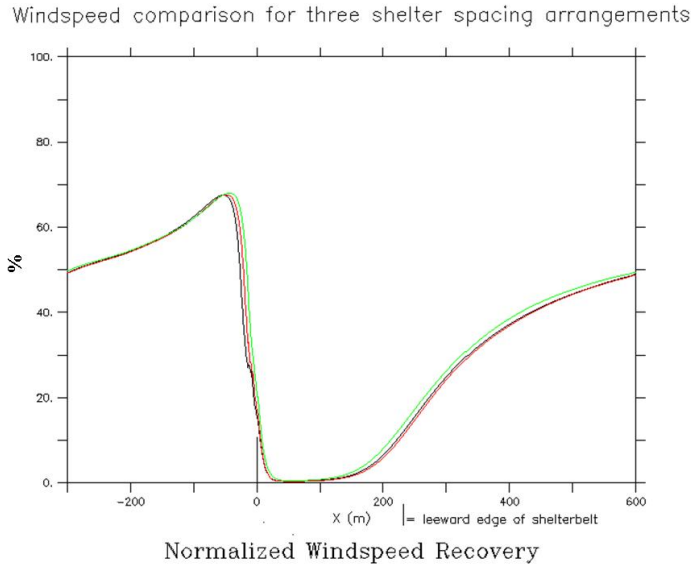

Figure A.16 Wind speed comparison for three shelter spacing arrangements

For shelterbelts of triangle shape, increasing density, and tall height, at 2 m above the surface
black: wide, red: medium, green: close

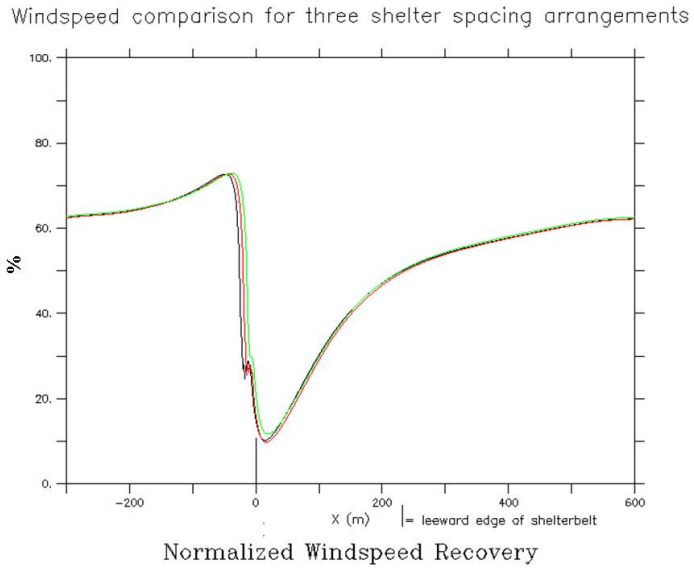

Figure A.17 Wind speed comparison for three shelter spacing arrangements

For shelterbelts of triangle shape, decreasing density, and short height, at 2 m above the surface
black: wide, red: medium, green: close

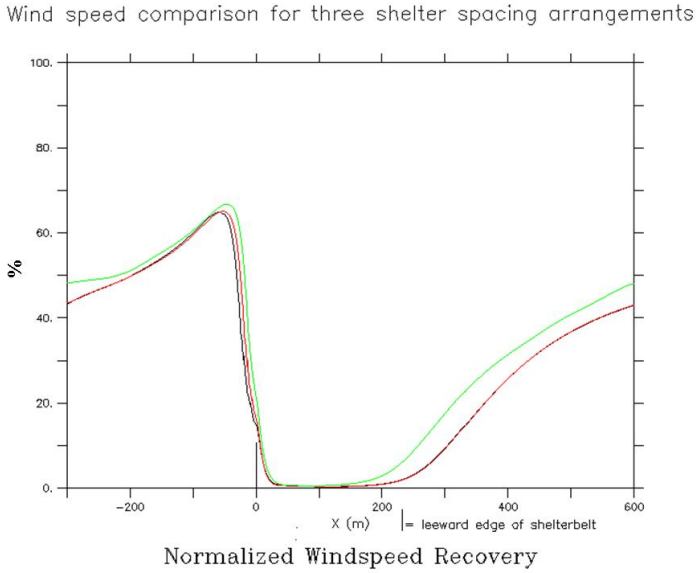

Figure A.18 Wind speed comparison for three shelter spacing arrangements

For shelterbelts of block shape, decreasing density, and tall height, at 2 m above the surface
black: wide, red: medium, green: close

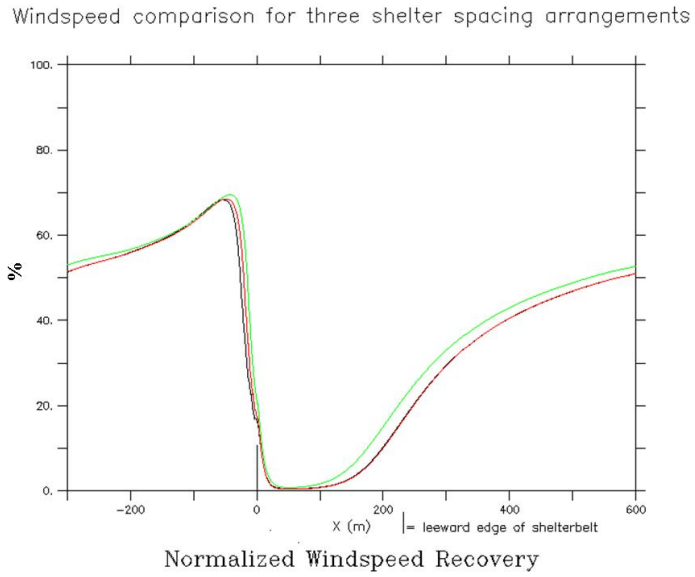

Figure A.19 Wind speed comparison for three shelter spacing arrangements

For shelterbelts of block shape, increasing density, and medium height, at 2 m above the surface
black: wide, red: medium, green: close

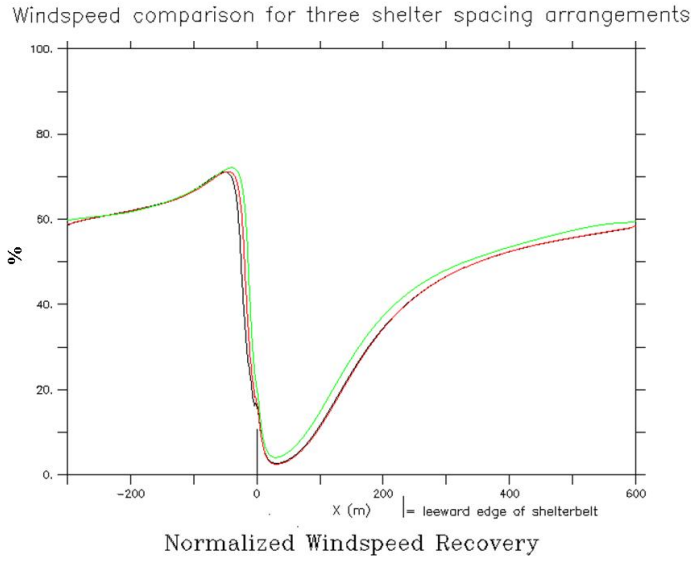

Figure A.20 Wind speed comparison for three shelter spacing arrangements

For shelterbelts of block shape, increasing density, and short height, at 2 m above the surface
black: wide, red: medium, green: close

Wind Speed Density

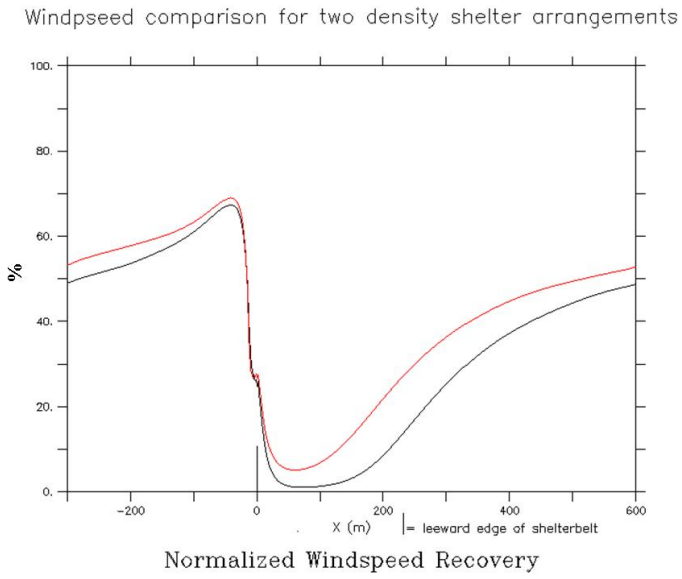

Figure A.21 Wind speed comparison for two shelter density arrangements

For shelterbelts of wedge-up shape, tall height, and close spacing, at 2 m above the surface
black: black: increasing, red: decreasing

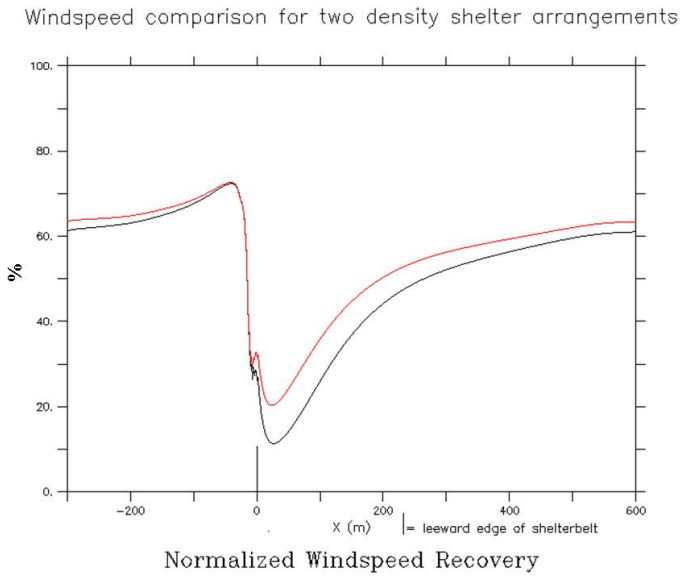

Figure A.22 Wind speed comparison for two shelter density arrangements

For shelterbelts of wedge-up shape, short height, and wide spacing, at 2 m above the surface
black: increasing, red: decreasing

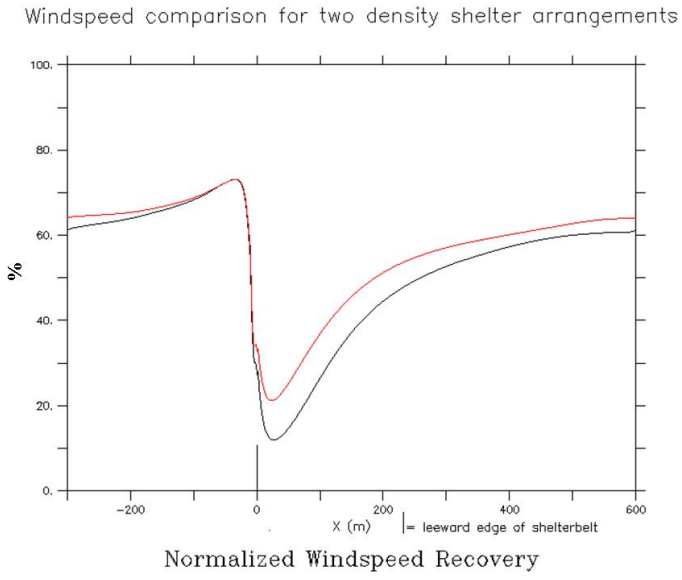

Figure A.23 Wind speed comparison for two shelter density arrangements

For shelterbelts of wedge-up shape, short height, and close spacing, at 2 m above the surface
black: increasing, red: decreasing

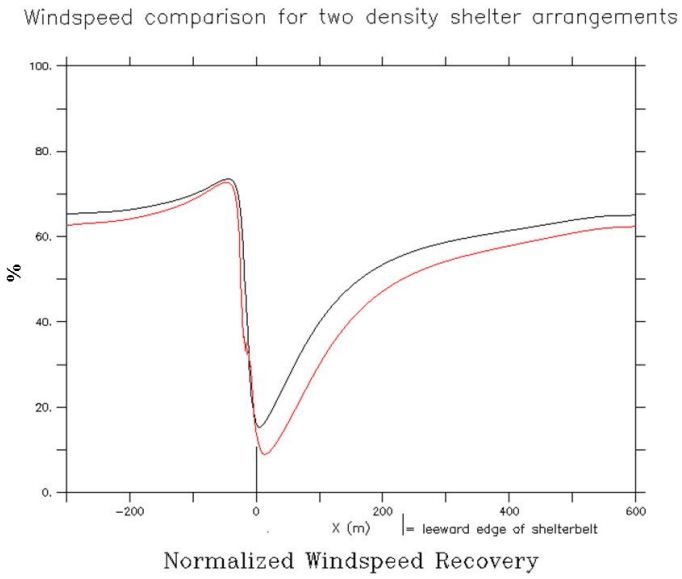

Figure A.24 Wind speed comparison for two shelter density arrangements

For shelterbelts of wedge-down shape, tall height, and close spacing, at 2 m above the surface
black: increasing, red: decreasing

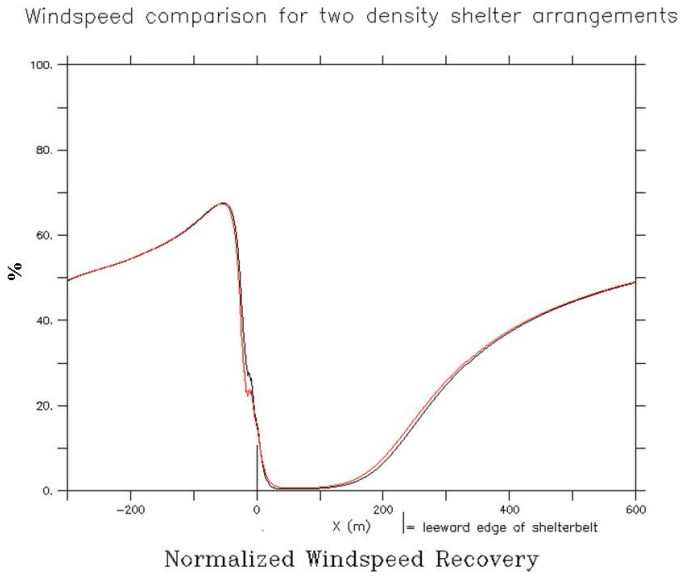

Figure A.25 Wind speed comparison for two shelter density arrangements

For shelterbelts of triangle shape, tall height, and wide spacing, at 2 m above the surface
black: increasing, red: decreasing

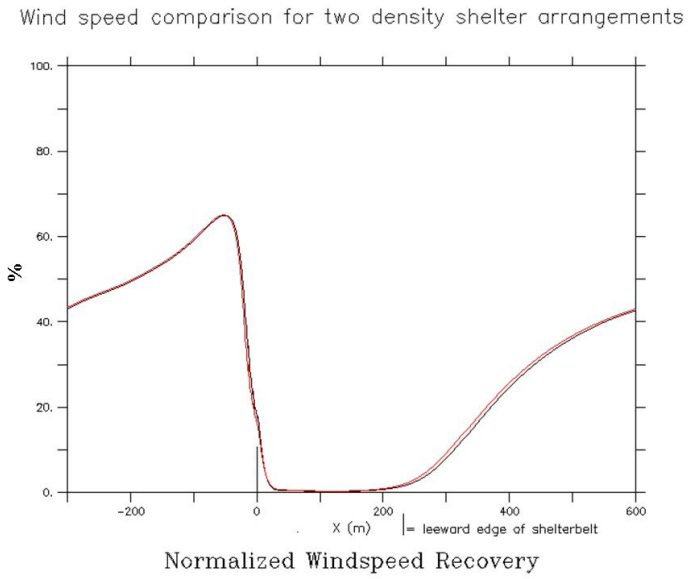

Figure A.26 Wind speed comparison for two shelter density arrangements

For shelterbelts of block shape, tall height, and medium spacing, at 2 m above the surface
black: increasing, red: decreasing

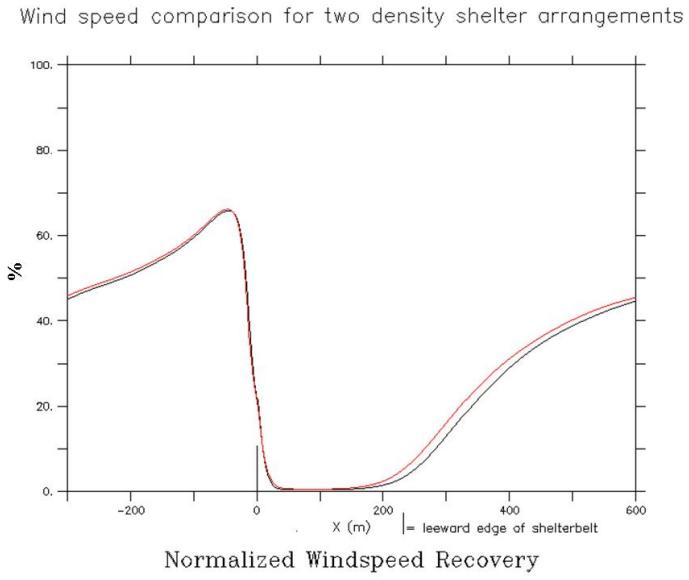

Figure A.27 Wind speed comparison for two shelter density arrangements

For shelterbelts of block shape, tall height, and close spacing, at 2 m above the surface
black: increasing, red: decreasing

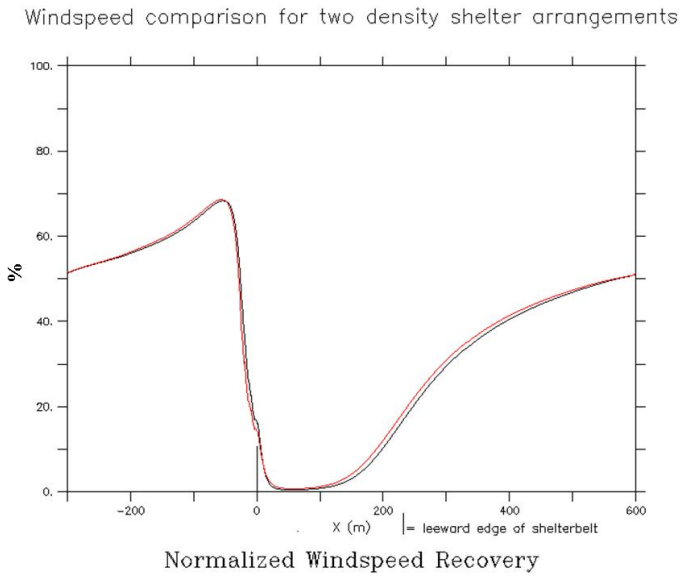

Figure A.28 Wind speed comparison for two shelter density arrangements

For shelterbelts of block shap, medium height, and wide spacing, at 2 m above the surface
black: increasing, red: decreasing

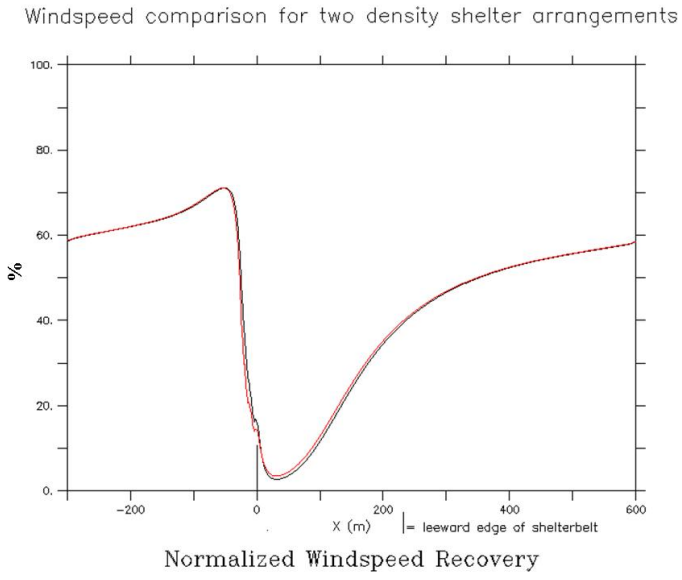

Figure A.29 Wind speed comparison for two shelter density arrangements

For shelterbelts of block shape, short height, and wide spacing, at 2 m above the surface
black: increasing, red: decreasing

TKE Shape

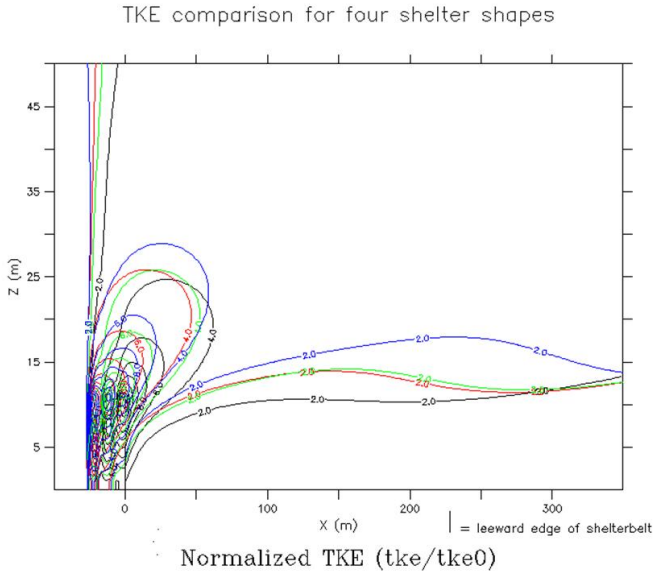

Figure A.30 TKE comparison for four shelter shape arrangements

For shelterbelts of tall height, density configuration, and wide spacing, at 2 m above the surface
black: wedge-up, red: wedge-down, green: triangle, blue: block

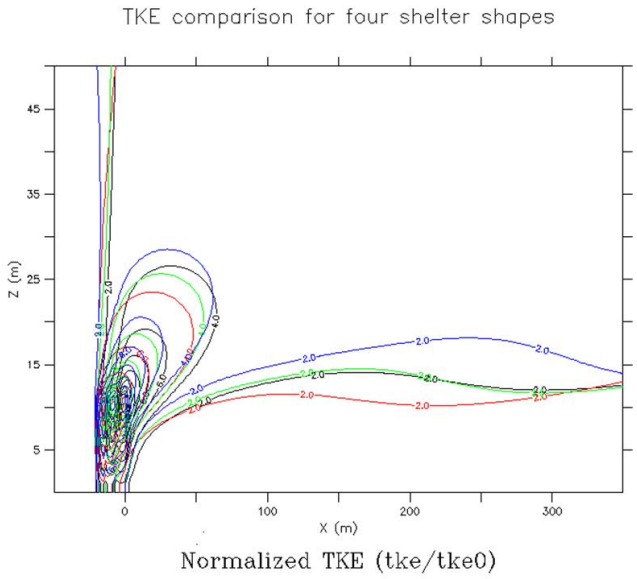

Figure A.31 TKE comparison for four shelter shape arrangements

For shelterbelts of tall height, increasing density, and medium spacing, at 2 m above the surface
black: wedge-up, red: wedge-down, green: triangle, blue: block

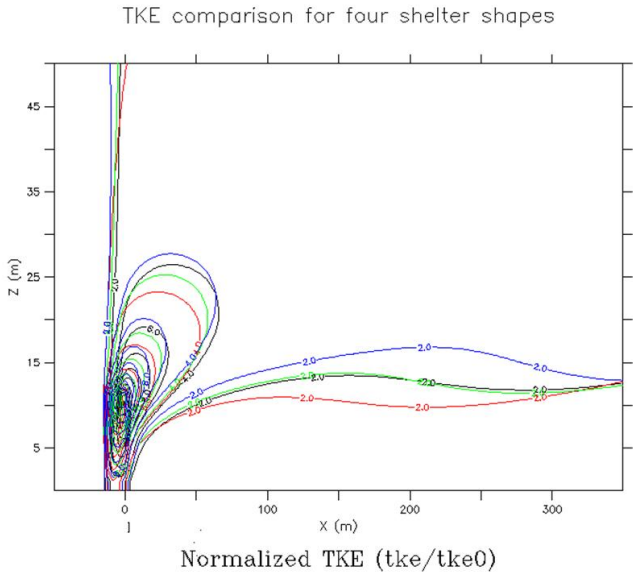

Figure A.32 TKE comparison for four shelter shape arrangements

For shelterbelts of tall height, increasing density, and close spacing, at 2 m above the surface
black: wedge-up, red: wedge-down, green: triangle, blue: block

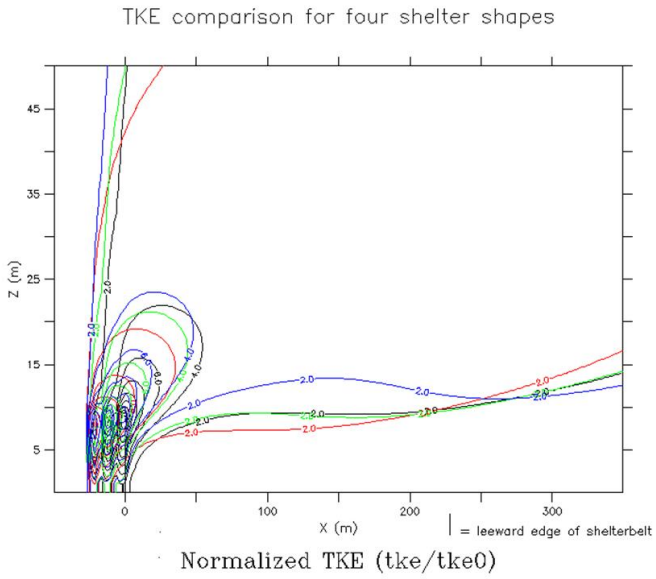

Figure A.33 TKE comparison for four shelter shape arrangements

For shelterbelts of medium height, increasing density, and wide spacing, at 2 m above the surface
black: wedge-up, red: wedge-down, green: triangle, blue: block

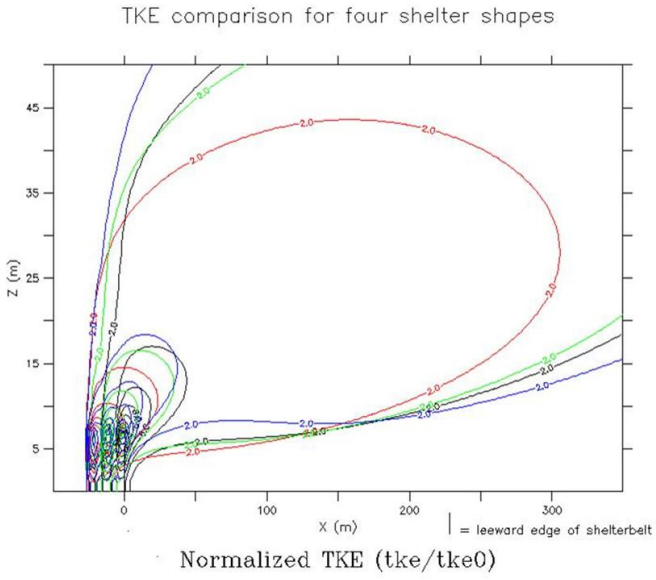

Figure A.34 TKE comparison for four shelter shape arrangements

For shelterbelts of short height, increasing density, and wide spacing, at 2 m above the surface
black: wedge-up, red: wedge-down, green: triangle, blue: block

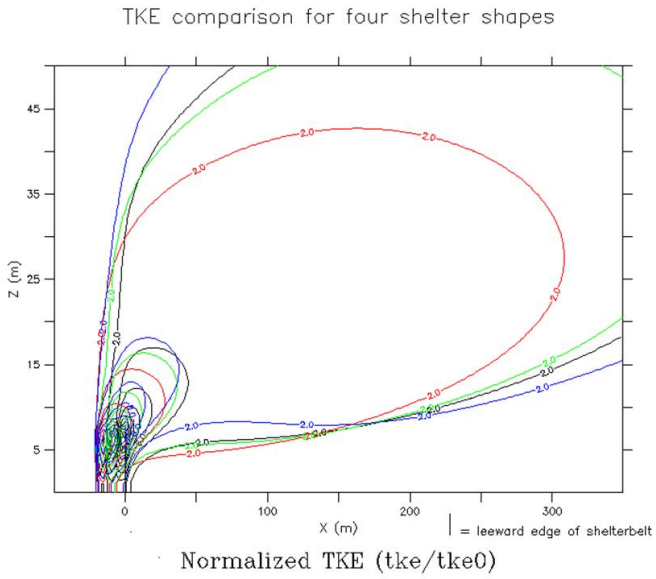

Figure A.35 TKE comparison for four shelter shape arrangements

For shelterbelts of short height, increasing density, and medium spacing, at 2 m above the surface
black: wedge-up, red: wedge-down, green: triangle, blue: block

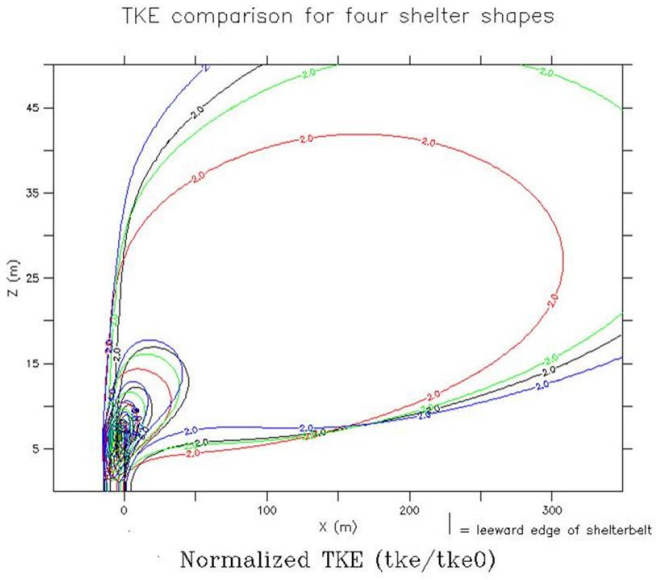

Figure A.36 TKE comparison for four shelter shape arrangements

For shelterbelts of short height, increasing density, and close spacing, at 2 m above the surface
black: wedge-up, red: wedge-down, green: triangle, blue: block

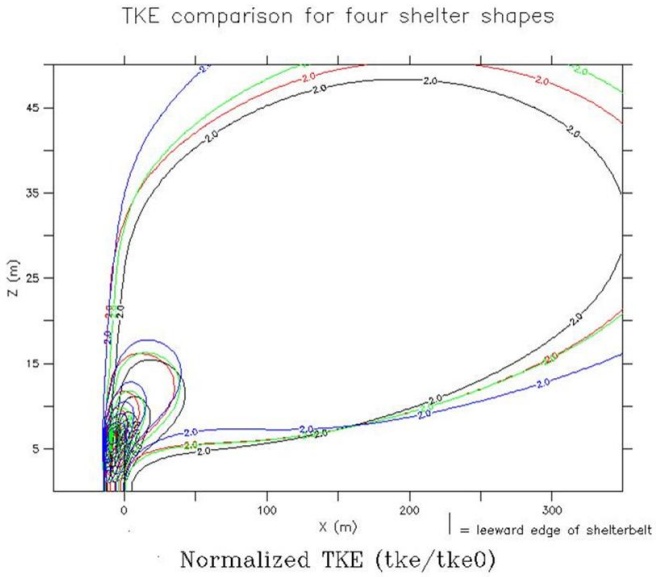

Figure A.37 TKE comparison for four shelter shape arrangements

For shelterbelts of short height, decreasing density, and close spacing, at 2 m above the surface
black: wedge-up, red: wedge-down, green: triangle, blue: block

TKE Height

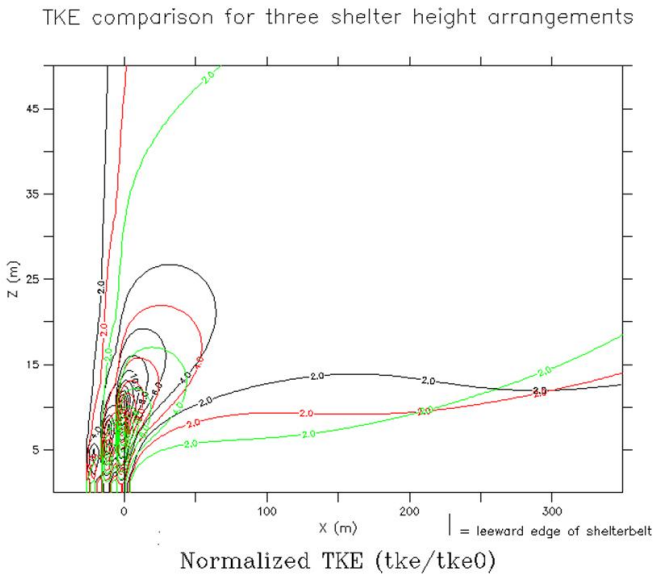

Figure A.38 TKE comparison for three shelter height arrangements

For shelterbelts of wedge-up shape, increasing density, and wide spacing, at 2 m above the surface
black: tall, red: medium, green: short

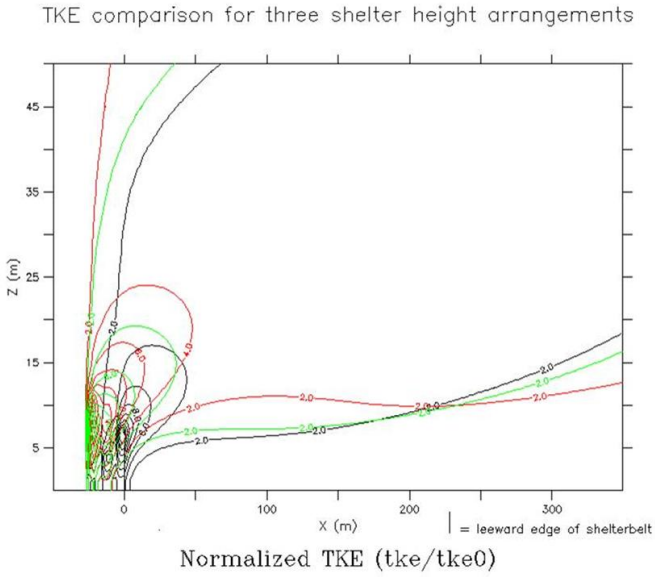

Figure A.39 TKE comparison for three shelter height arrangements

For shelterbelts of wedge-down shape, increasing density, and wide spacing, at 2 m above the surface
black: tall, red: medium, green: short

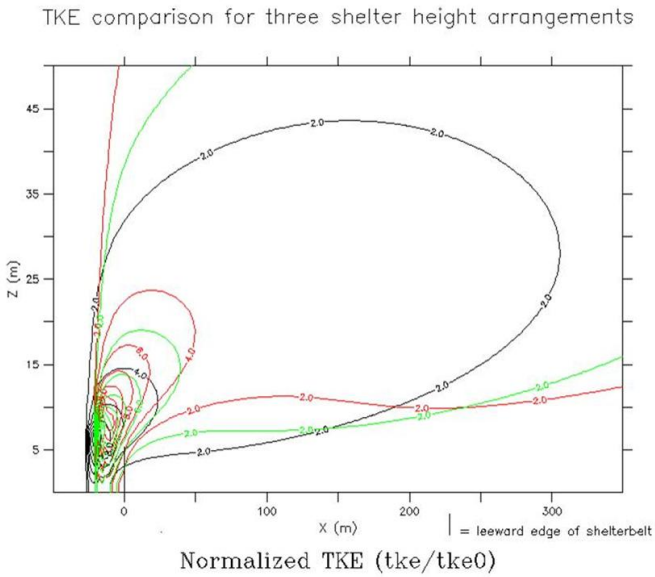

Figure A.40 TKE comparison for three shelter height arrangements

For shelterbelts of wedge-down shape, increasing density, and medium spacing, at 2 m above the surface
black: tall, red: medium, green: short

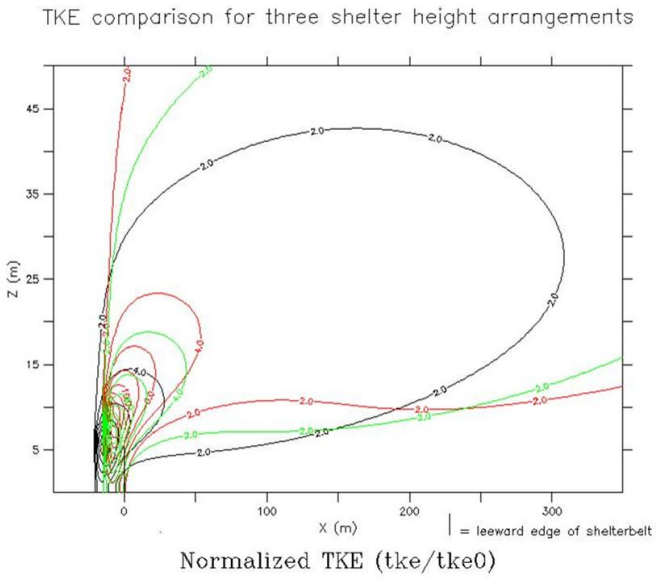

Figure A.41 TKE comparison for three shelter height arrangements

For shelterbelts of wedge-down shape, increasing density, and close spacing, at 2 m above the surface
black: tall, red: medium, green: short

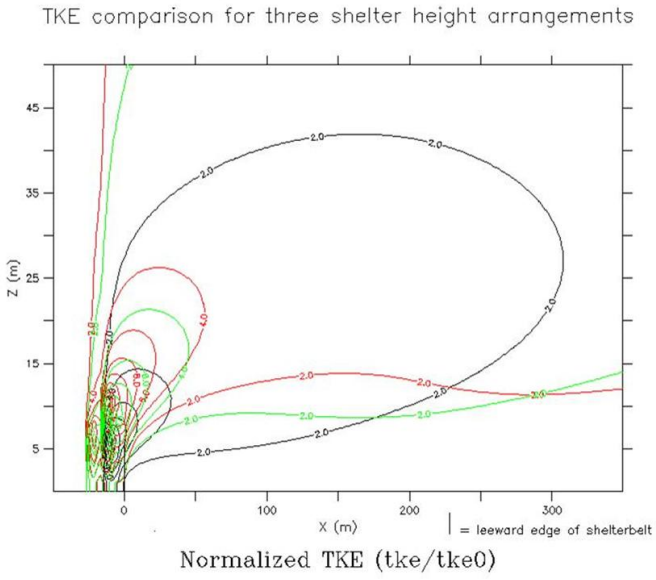

Figure A.42 TKE comparison for three shelter height arrangements

For shelterbelts of triangle shape, increasing density, and wide spacing, at 2 m above the surface
black: tall, red: medium, green: short

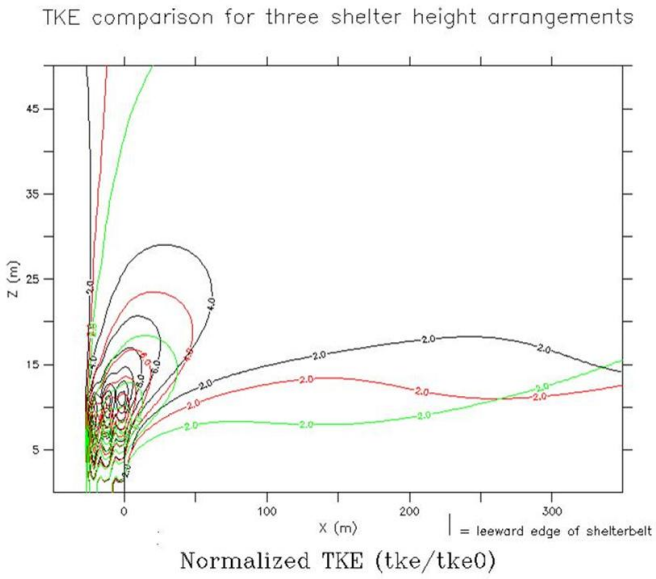

Figure A.43 TKE comparison for three shelter height arrangements

For shelterbelts of block shape, increasing density, and wide spacing, at 2 m above the surface
black: tall, red: medium, green: short

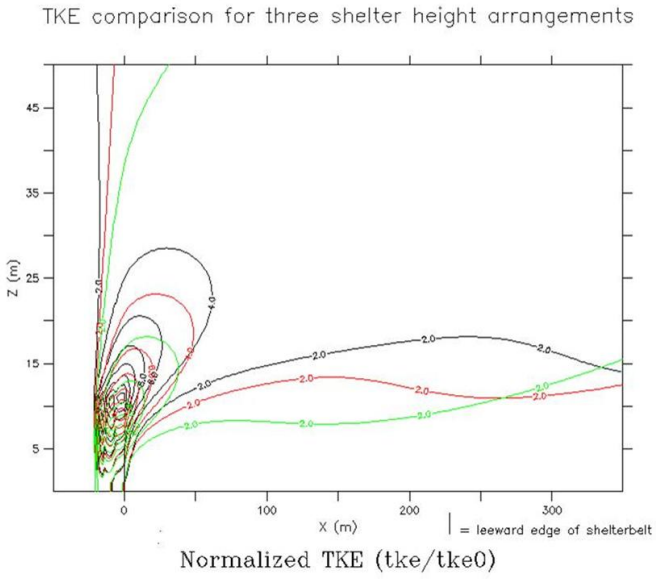

Figure A.44 TKE comparison for three shelter height arrangements

For shelterbelts of block shape, increasing density, and medium spacing, at 2 m above the surface
black: tall, red: medium, green: short

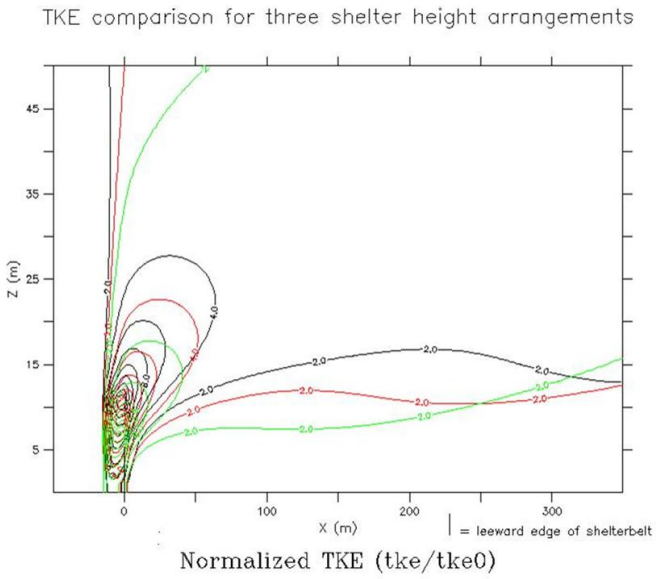

Figure A.45 TKE comparison for three shelter height arrangements

For shelterbelts of block shape, increasing density, and close spacing, at 2 m above the surface
black: tall, red: medium, green: short

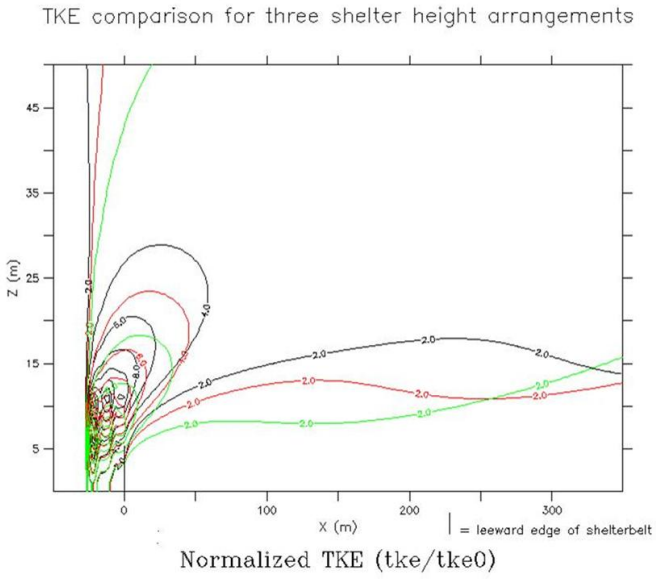

Figure A.46 TKE comparison for three shelter height arrangements

For shelterbelts of block shape, decreasing density, and wide spacing, at 2 m above the surface
black: tall, red: medium, green: short

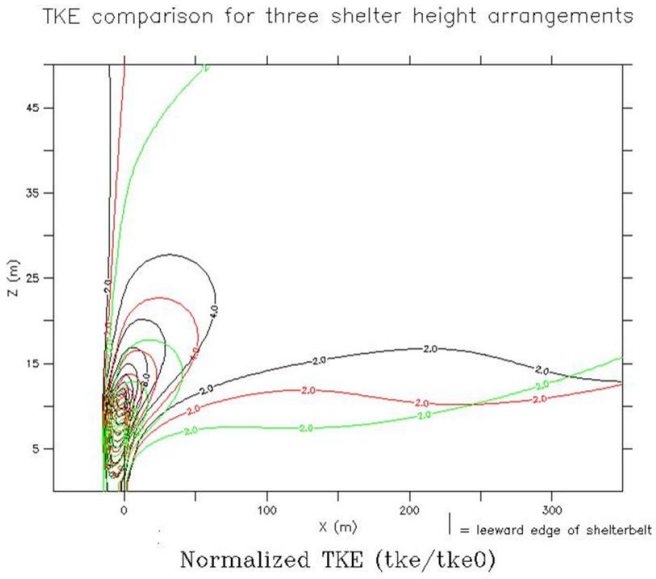

Figure A.47 TKE comparison for three shelter height arrangements

For shelterbelts of block shape, decreasing density, and close spacing, at 2 m above the surface
black: tall, red: medium, green: short

TKE Spacing

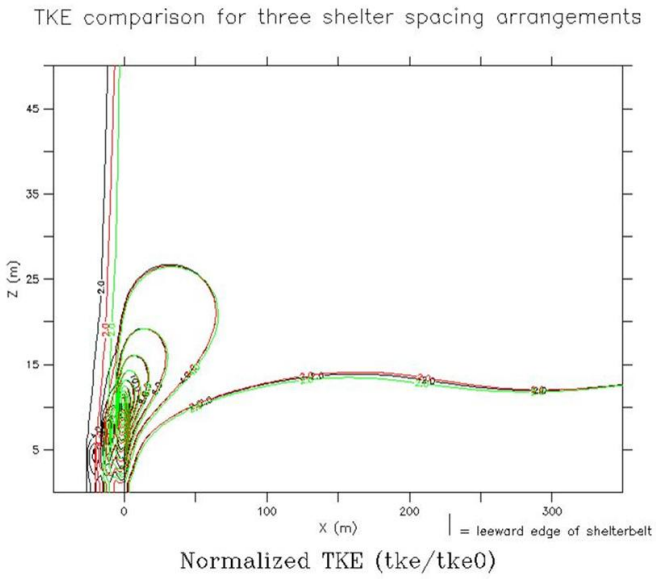

Figure A.48 TKE comparison for three shelter spacing arrangements

For shelterbelts of wedge-up shape, increasing density, and tall height, at 2 m above the surface
black: wide, red: medium, green: close

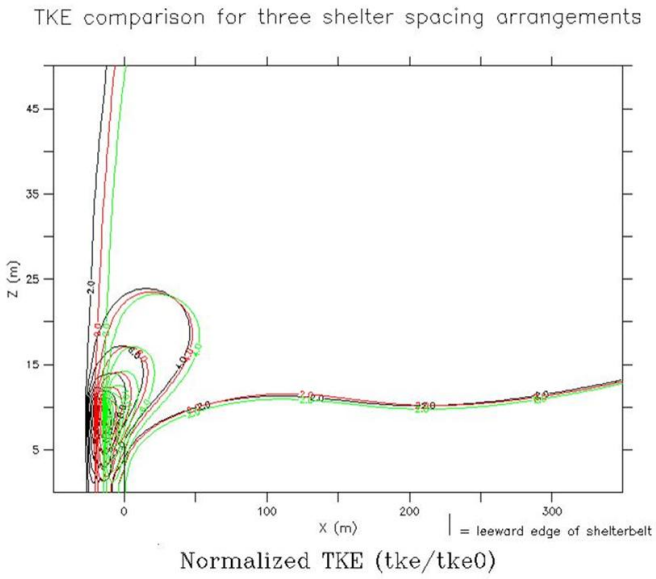

Figure A.49 TKE comparison for three shelter spacing arrangements

For shelterbelts of wedge-down shape, increasing density, and tall height, at 2 m above the surface
black: wide, red: medium, green: close

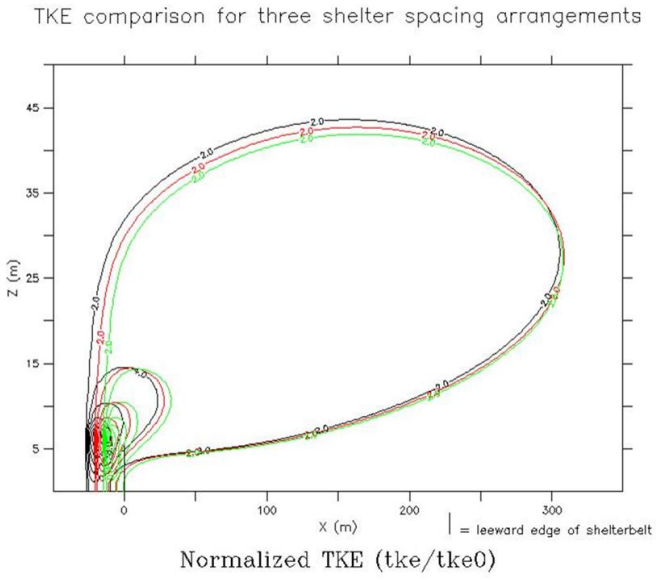

Figure A.50 TKE comparison for three shelter spacing arrangements

For shelterbelts of wedge-down shape, increasing density, and short height, at 2 m above the surface
black: wide, red: medium, green: close

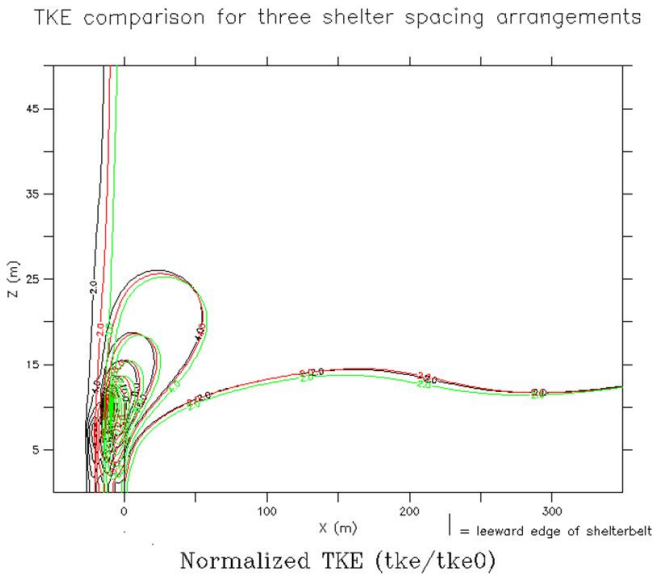

Figure A.51 TKE comparison for three shelter spacing arrangements

For shelterbelts of triangle shape, increasing density, and tall height, at 2 m above the surface
black: wide, red: medium, green: close

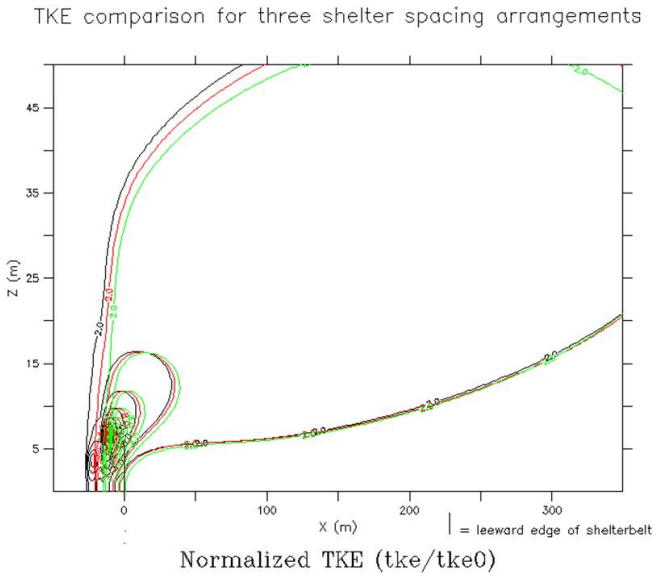

Figure A.52 TKE comparison for three shelter spacing arrangements

For shelterbelts of triangle shape, decreasing density, and short height, at 2 m above the surface
black: wide, red: medium, green: close

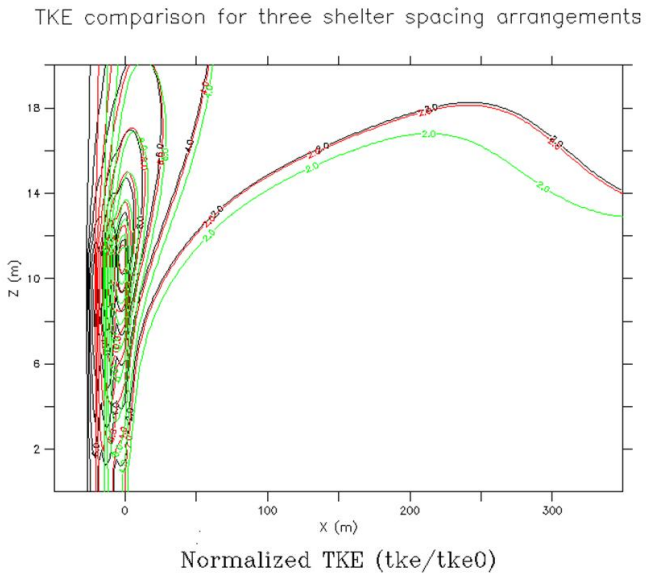

Figure A.53 TKE comparison for three shelter spacing arrangements

For shelterbelts of block shape, increasing density, and tall height, at 2 m above the surface
black: wide, red: medium, green: close

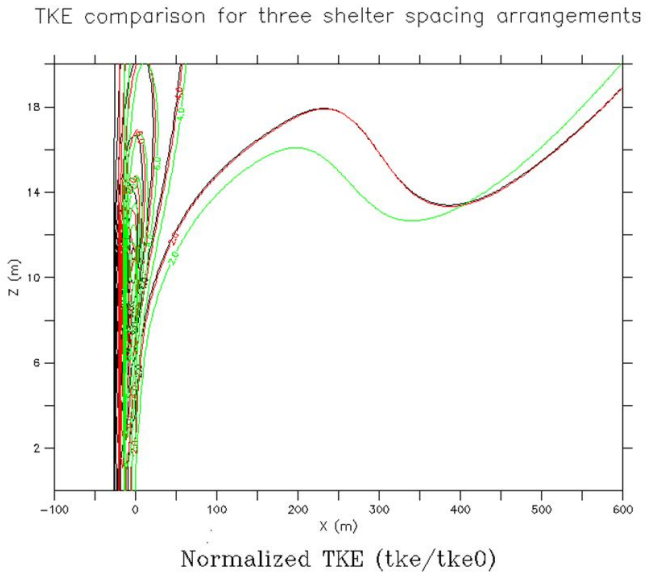

Figure A.54 TKE comparison for three shelter spacing arrangements

For shelterbelts of block shape, decreasing density, and tall height, at 2 m above the surface
black: wide, red: medium, green: close

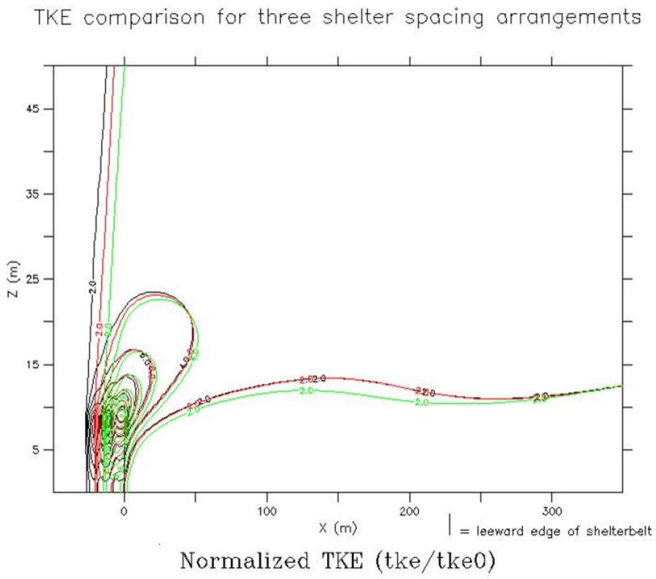

Figure A.55 TKE comparison for three shelter spacing arrangements

For shelterbelts of block shape, increasing density, and medium height, at 2 m above the surface
black: wide, red: medium, green: close

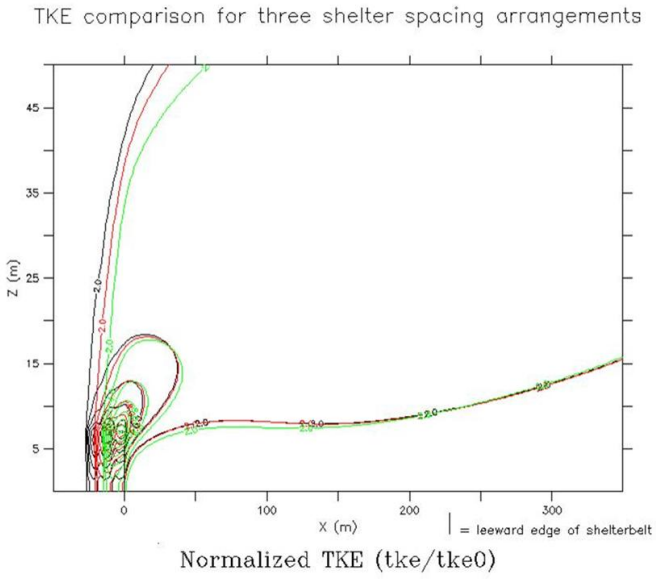

Figure A.56 TKE comparison for three shelter spacing arrangements

For shelterbelts of the block shape, increasing density, and short height, at 2 m above the surface
black: wide, red: medium, green: close

TKE Density

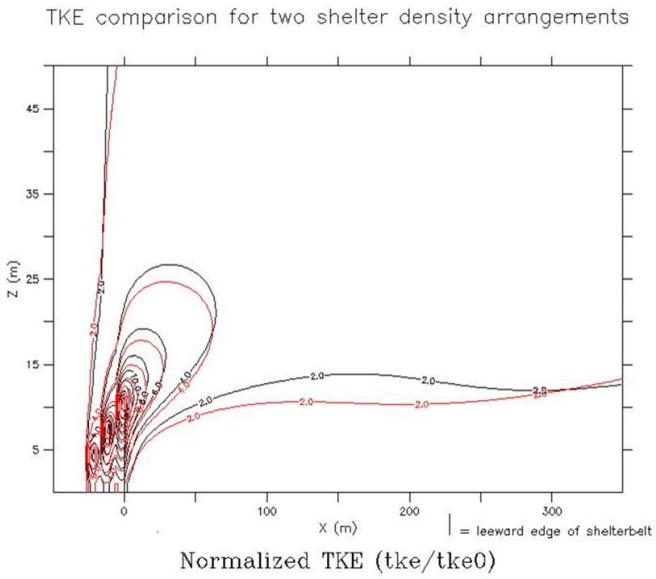

Figure A.57 TKE comparison for two shelter density arrangements

For shelterbelts of wedge-up shape, tall height, and wide spacing, at 2 m above the surface
black: black: increasing, red: decreasing

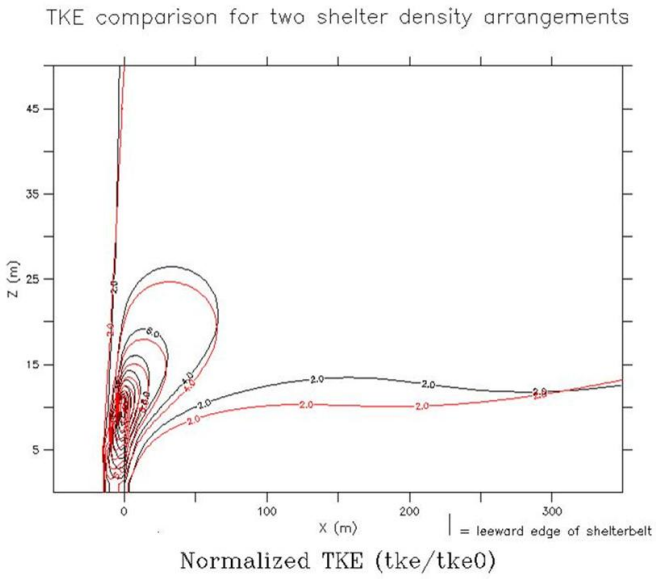

Figure A.58 TKE comparison for two shelter density arrangements

For shelterbelts of wedge-up shape, tall height, and close spacing, at 2 m above the surface
black: black: increasing, red: decreasing

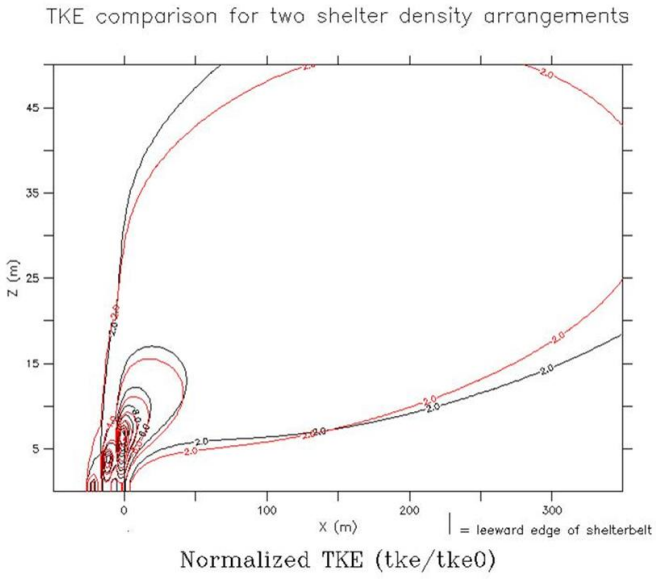

Figure A.59 TKE comparison for two shelter density arrangements

For shelterbelts of wedge-up shape, short height, and wide spacing, at 2 m above the surface
black: black: increasing, red: decreasing

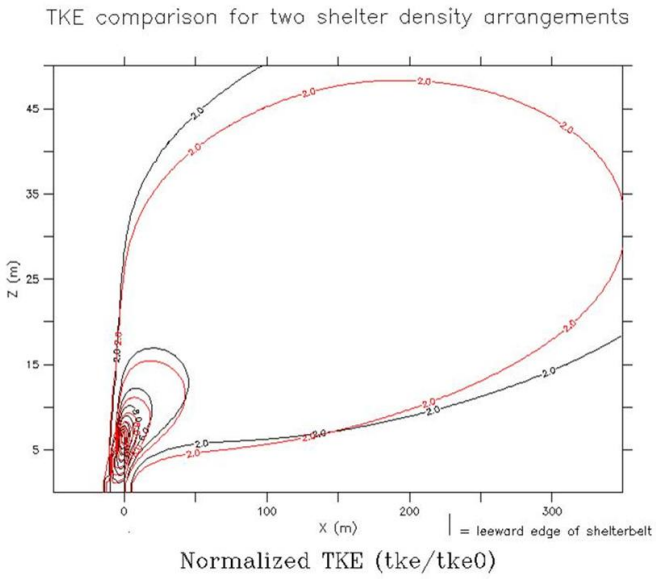

Figure A.60 TKE comparison for two shelter density arrangements

For shelterbelts of wedge-up shape, short height, and close spacing, at 2 m above the surface
black: black: increasing, red: decreasing

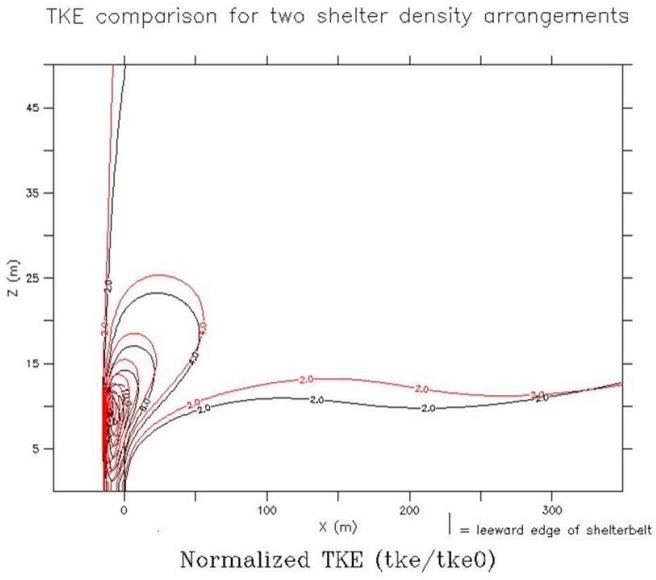

Figure A.61 TKE comparison for two shelter density arrangements

For shelterbelts of wedge-down shape, tall height, and close spacing, at 2 m above the surface
black: black: increasing, red: decreasing

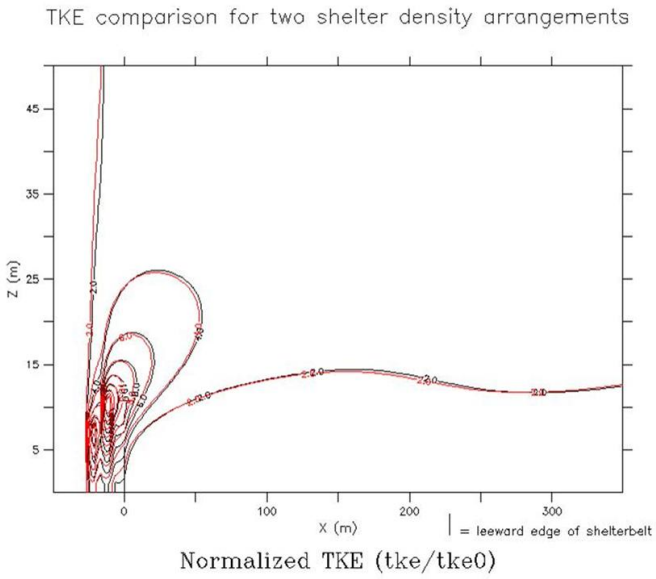

Figure A.62 TKE comparison for two shelter density arrangements

For shelterbelts of triangle shape, tall height, and wide spacing, at 2 m above the surface
black: black: increasing, red: decreasing

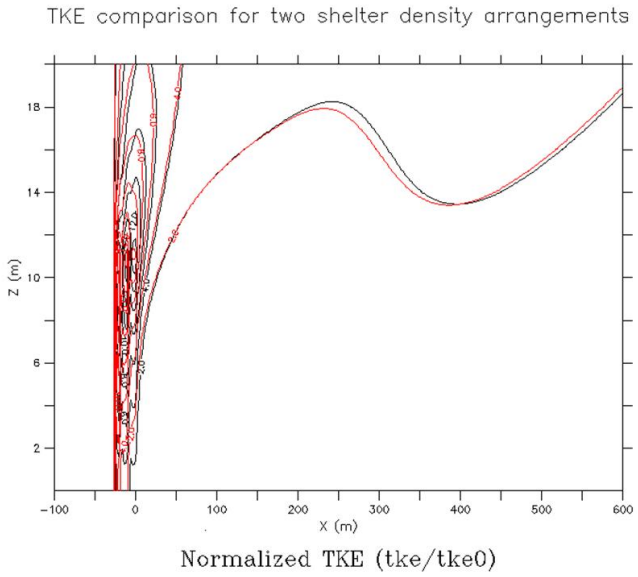

Figure A.63 TKE comparison for two shelter density arrangements

For shelterbelts of block shape, tall height, and wide spacing, at 2 m above the surface
black: black: increasing, red: decreasing

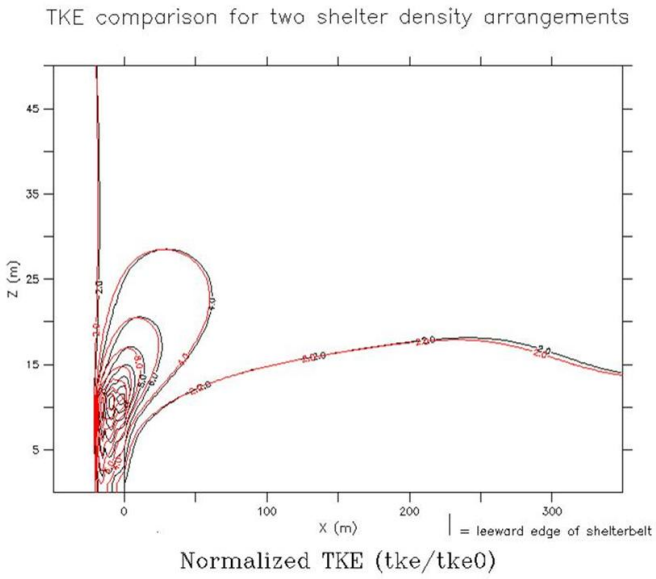

Figure A.64 TKE comparison for two shelter density arrangements

For shelterbelts of block shape, tall height, and medium spacing, at 2 m above the surface
black: black: increasing, red: decreasing

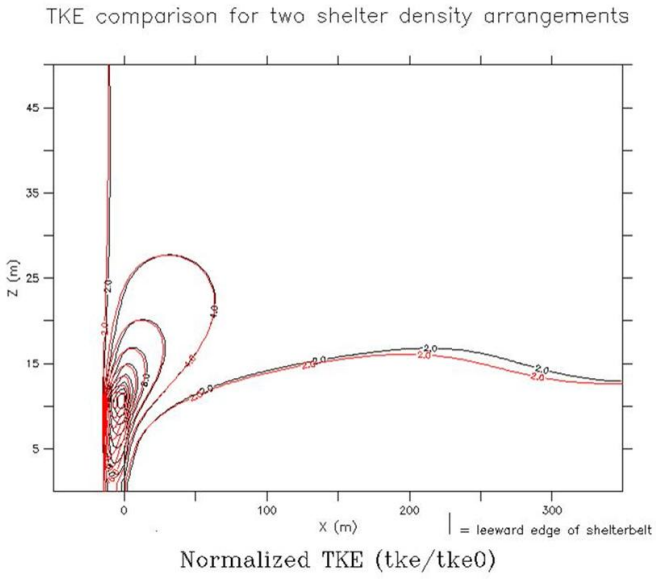

Figure A.65 TKE comparison for two shelter density arrangements

For shelterbelts of block shape, tall height, and close spacing, at 2 m above the surface
black: black: increasing, red: decreasing

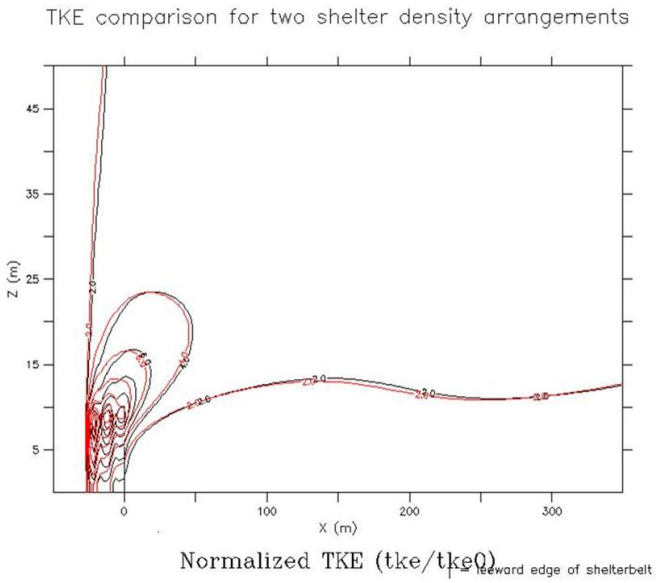

Figure A.66 TKE comparison for two shelter density arrangements

For shelterbelts of block shape, medium height, and wide spacing, at 2 m above the surface
black: black: increasing, red: decreasing

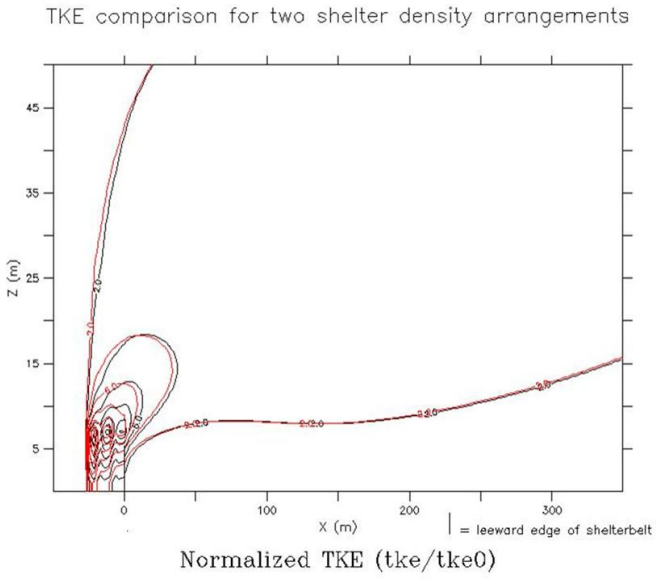

Figure A.67 TKE comparison for two shelter density arrangements

For shelterbelts of block shape, short height, and wide spacing, at 2 m above the surface
black: black: increasing, red: decreasing

BIBLIOGRAPHY

Architectural Institute of Japan (AIJ), 1996. *Recommendations for loads on buildings.* AIJ.

American Society of Civil Engineers (ASCE), 2005. *Minimum design loads for buildings and other structures.* ASCE 7-05, ASCE.

Blenk, H., and H. Trienes, 1956. *Strömungstechnische Beiträge zum Windschutz. Grundlagen der Landtechnik*, **8**,V.D.I. Verlag, Düsseldorf.

Blenk, H., and H. Trienes, 1956. Field study of the flow behind single and double row herbaceous windbreaks. *J. Wind Eng. and Ind. Aerody.*, **89**, 665–687.

Bolton, D., 1980. The computation of equivalent potential temperature. *J. Monthly Weather Review*, **108**, 1046–1053.

Caborn, J. M., 1957. Shelterbelts and microclimate. *For. Comm. Bull. (Edinburgh)*, **29**, 1–129.

Caborn, J. M., 1965. *Shelterbelts and Windbreaks*, Faber & Faber, 288 pp.

Cao, S. S., Q. D. Lei, and F. Q. Jiang, 1981. Field determination of optimum porosity and cross-sectional shape of a shelterbelt. *Bull. of the Inst. of For. Res. and Pedo.*, **5**, 9–19.

Cornelis, W. M., and D. Gabriels, 2005. Optimal windbreak design for wind-erosion control. *J. of Arid Environ.*, **61**, 315–332.

Dierickx, W., D. Gabriels, and W. M. Cornelis, 2001. Wind Tunnel Study on Wind Speed Reduction through Successive Synthetic Windscreens. *J. Agric. Eng. Res.*, **79**, 117–123.

Dirr, M. A., 1990. *Manual of Woody landscape plats: their identification, ornamental characteristics, culture, propagation, and uses*. Stipes Publishing, Champaign, IL., 1007 pp.

Finney, E. A., 1934. Snow control on the highways. *Mich. St. Eng. Expt. Sta. Bull.*, **57**, 1–62.

Frank, C., and B. Ruck, 2005. Double-arranged mound-mounted shelterbelts: influence of porosity on wind reduction between the shelters. *Environ. Fluid Mech.*, **5**, 267–292.

Gandemer, J., 1979. Wind Shelters. *J. Ind. Aerodyn.*, **4**, 371–389.

Hagen, L. J., and E. L. Skidmore, 1971. Windbreak drag as influenced by porosity. *Trans. ASAE*, 464–465.

Harlow, W. M., and E. S. Harrar, 1969. *Textbook of Dendrology: Covering the Important Forest Trees of the United States & Canada*. McGraw-Hill, 512 pp.

Heisler, G. M., and D. R. Dewalle, 1988. Effects of windbreak structure on wind flow. *Agri. Ecosyst. Environ.*, **22/23**, 41–69.

Herman, D. E., C. M. Stange, and V. C. Quam, 1996. *North Dakota Tree Handbook*. USDA NRCS ND State Soil Conservation Committee; NDSU Extension and Western Area Power Admin., Bismarck, ND.

Jensen, M., 1954. *Shelter Effect: Investigations into Aerodynamics of Shelter and its Effects on Climate and Crops*. Danish Tech. Press, Copenhagen.

Jensen, M., 1974. The aerodynamics of the shelter. *FAO/DEN/TF Rep.*, **123**, 132–145. [Available from Food and Agricultural Organization of the United Nations, Rome, Italy.]

Jones, E. C., 2008. Experimental simulation of atmospheric boundary layers and extreme gust events. Master's Thesis. Iowa State University. Ames, IA.

Kershner, D., 1977. A suspended anemometer system for measuring true airspeed on low-speed airplanes. *NASA Technical Note*, **TND-8523**. National Aeronautics and Space Administration. Washington, D.C.

Loeffler, A. E., A. M. Gordon, and T. J. Gillespie, 1992. Optical porosity and windspeed reduction by coniferous windbreaks in Southern Ontario. *Agroforestry Systems*, **17**, 119–133.

Marshall, J. K., 1967. The effect of shelter on the productivity of grass lands and field crops. *Field Crop Abstracts*, **20**, 1–14.

Mazda, Y., E. Wolanski, B. King, A. Sase, D. Ohtsuka, and M. Magi, 1997. Drag force due to vegetation in mangrove swamps. *Mangroves and Salt Marshes*, **1**, 193–199.

Mellor, G. L., and T. Yamada, 1982. Development of a turbulent closure model for geophysical fluid problems. *Rev. Geophys. Space Sci.*, **20**, 851–875.

Nägeli, W., 1946. Weitere Untersuchungen über die Windverhltnisse im Bereich von Windschutzstreife. *Mitteilungen/Schweizerische Anstalt fur das forstliche Versuchswesen*, **24**, 659–737.

Nökkentved, C., 1938. Laevirkningsundersögelser og Typebestemmelser af Laehegn. *Hedeselsk. Tidsskr.*, **59**, 80–136.

Raine, J. K., and D. C. Stevenson, 1977. Wind protection by model fences in simulated atmospheric boundary layer. *J. of Ind. Aerody.*, **2**, 159–180.

Rudnicki, M., S. J. Mitchell, and M. D. Novak, 2004. Wind tunnel measurements of crown streamlining and drag relationships for three conifer species. *Can. J. For. Res.*, **34**, 666–676.

Schultz, H. B., and C. F. Kelly, 1960. Studies on wind protection efficiency of slatted fence windbreaks. *California Agriculture*, **14**, 3–11.

Silvics of North America: 1. Conifers, 2. Hardwoods. Agriculture Handbook 654, 1990. U.S. Department of Agriculture, Forest Service, Washington, DC., **2**, 877 pp.

Simiu, E., and R. H. Scanlan, 1996. *Wind Effects on Structures: Fundamentals and Applications to Design*, Third Edition, John-Wiley and Sons, Inc., New York.

Skidmore, E. L., and L. J. Hagen, 1970a. Evapotranspiration and the aerial environment as influenced by windbreaks. *Proceedings of Great Plains Evapotranspiration Seminar*, Bushland, TX, Great Plains Agricultural Council, **50**, 339–369.

Skidmore, E. L., and L. J. Hagen, 1970b. Evaporation in sheltered areas as influenced by windbreak porosity. *Agricultural Meteorology*, **7**, 363–374.

Stull, R. B., 1988. *An Introduction to Boundary Layer Meteorology*. Kluwer Academic Publishers, Dordrecht, The Netherlands.

Sydnor, T. D., and W. F. Cowen, 1994. *Ohio Trees*. The University of Ohio Extension Bulletin 700-00. Department of Natural Resources at The Ohio State University.

Takle, E. S., T. C. Chen, and X. Wu, 2006. The role of coastal forests and trees for protecting against wind and salt spray. *Workshop on Coastal Protection in the Aftermath of the Indian Ocean Tsunami: What Role for Forests and Trees?*. The University of Ohio Extension Bulletin 700-00. United Nations Food and Agricultural Organization (Rome). Khao Lak Thailand 28-31 August 2006. [Invited] [http://www.fao.org/forestry/site/coastalprotection/en/]

Tani, N., 1958. On the wind tunnel test of the model shelter hedge. *Bulletin of the National Institute for Agricultural Sciences*, **A.6**, 1–80.

Tillie, M., 1992. Ambiance dans les batiments d'élevage bovin. *Session Institut de l'Elevage*, **222**, Paris.

Tree Fact Sheet Series, 1993. Environmental Horticulture Department, Florida Cooperative Extension Service, Institute of Food and Agricultural Sciences, University of Florida.

Wang, H., and E. S. Takle, 1995. A numerical simulation of boundary-layer flows near shelterbelts. *Boundary-Layer Meteorol.*, **75**, 145–173.

Wang, H., and E. S. Takle, 1997. Model-simulated influences of shelterbelt shape on windshearing efficiency. *J. Appl. Meteor.*, **36**, 695–704.

Wang, H., E. S. Takle, and J. Shen, 2001. Shelterbelts and Windbreaks: Mathematical modeling and computer simulations of turbulent flows. *Annu. Rev. Fluid Mech.*, **33**, 549–586.

Wilson, J. D., 1985. Numerical studies of flow through a windbreak. *J. Wind Eng. Ind. Aerodyn.*, **21**, 119–154.

Wilson, J. D., 1987. On the choice of windbreak porosity profile. *J. Boundary-Layer Meteor.*, **38**, 37–49.

Woodruff, N. P., and A. W. Zingg, 1952. Wind-tunnel studies of fundamental problems related to windbreaks. *Soil Conser. Service (USDA)*, **SCS-TP-112**, 1–25.

Woodruff, N. P., and A. W. Zingg, 1953. Wind tunnel studies of shelterbelt models. *J. For.*, **51**, 173–178.

van Eimern, J., R. Karschon, L. A. Razumova, and G. W. Robertson, 1964. Windbreaks and Shelterbelts. *World Meteor. Organ., Tech. Note* , **59**, 188 pp.

Vogel, S., 1989. Drag and reconfiguration of broad leaves in high winds. *J. Exp. Botany*, **40**, 941–948.

Vozzo, J. A., 2003. *Tropical Tree Seed Manual*. United States Department of Agriculture Forest Service, 874 pp.

Yamada, T., 1982. A numerical model study of turbulent airflow in and above a forest canopy. *J. Meteorol. Soc. Japan*, **60**, 438–454.

Zhang, H., J. R. Brandle, G. E. Meyer, and L. Hodges, 1992. A model to evaluate windbreak protection efficiency. *Agroforestry Systems*, **29**, 191–200.